DISSERTATION

TRACKING AMMONIA VOLATILIZATION AND FATE FROM EMISSION SOURCE TO PRISTINE ECOSYSTEM

Submitted by

Joshua James Stratton

Department of Chemistry

In partial fulfillment of the requirements

For the Degree of Doctor of Philosophy

Colorado State University

Fort Collins, Colorado

Spring 2014

Doctoral Committee:

Advisor: Thomas Borch

Amy Prieto
Elliott Bernstein
Ellen R. Fisher
Jeffrey L. Collett, Jr.

ABSTRACT

TRACKING AMMONIA VOLATILIZATION AND FATE FROM EMISSION SOURCE TO PRISTINE ECOSYSTEM

Ammonia has been widely documented as a contributor to negative impacts on natural ecosystems. Agricultural related management has been closely tied to ammonia emission and therefore negative impacts of ammonia pollution. The aim of this research is to improve our current understanding of how ammonia is lost from native and agricultural soils and if nitrogen isotopes can be used to elucidate what sources of ammonia pollution affect native ecosystems the most.

Rocky Mountain National Park (RMNP) has undergone ecosystem changes due to excessive nitrogen deposition in the forms of ammonium, nitrate and organic nitrogen. Due to uncertainty in source apportionment; the efficacy of nitrogen isotopes of ammonia to distinguish sources of ammonia deposited in RMNP was investigated. This study shows average $\delta^{15}N$ isotopes of certain sources (beef cattle, dairy cattle production, wastewater treatment, cropland, urban) were distinguishable at this study's emission sites; however, the average $\delta^{15}N$ isotope values measured at a RMNP site were not useful for identification of specific ammonia sources. Supplemental information (weekly integrations of gaseous and particulate reduced nitrogen, oxidized nitrogen, sulfur measurements, and HYSPLIT modeling) was needed to help pinpoint the likely sources of ammonia, such as agriculture and biomass burning, affecting RMNP. Moreover, this supplemental information was used to support the most likely reasons $\delta^{15}N$ isotope values observed in gaseous ammonia and wet deposition were indistinguishable compared to emission sources.

Little is known about the potential local contribution of ammonia from soils within RMNP. Thus, the goal of this study was also to develop a method for analysis of ammonia emissions from intact soil cores sampled from a sub-alpine grassland and forest within RMNP. Nitrogen wet deposition was monitored at the sampling location to investigate possible impacts on soil emissions of ammonia. Lastly, method development and analysis of formation of ammonia (urea hydrolysis), pH speciation (ammonia and ammonium), and vapor pressure (Henry constant) were investigated in beef and dairy feedlots to reveal important controls on ammonia emission.

This research provides new information on the importance of post emission physical and chemical processes, such as source mixing, isotopic fractionation, and dry deposition, preventing the use of $\delta^{15}N$ isotopes for source tracking without the use of complementary techniques, such as atmospheric modeling. Moreover this work provides further evidence indicating that natural emissions within RMNP are not major sources of reduced nitrogen in the RMNP airshed. Lastly, this work provides new chemical values for the Henry constant, acid dissociation constant, and urea hydrolysis rate constants in animal production systems and can be used to better estimate ammonia emissions from animal production to improve our current emission inventories.

ACKNOWLEDGEMENTS

First and foremost, I would like to thank my advisor, Dr. Thomas Borch, who started a project much to my personal liking. Dr. Borch has been a great mentor for my professional development. I am thankful for his invaluable guidance and support throughout my time at Colorado State University I am thankful for all the opportunities he has provided to me and I have grown from having worked with him.

A special thanks to Dr Jay Ham for his guidance, support, and creative thought throughout my Ph. D. research. Thanks to Dr Jeffrey Collett, Jr. for access to equipment, research sites, and invaluable input on research design and interpretation. Thanks to Dr. Jill Baron for access to National Atmospheric Deposition Program's samples for our research. Thanks to Dr. Emily Elliott for her open communication and distribution of knowledge in chemical analysis. Thanks to my committee members who have played an important role in the completion of this dissertation.

I am indebted to all the members of the Borch group for all their assistance, friendship, and knowledge. Special thanks go to Lyndsay Troyer for her help during my research. Thanks also to Dr. Masayuki Shimizu and Dr. Gina McKee for their time and assistance with research and GIS. Thanks to Dr. Katie Benedict and Dr. Doris Chen for their help with work at Rocky Mountain National Park. Special thanks to Christina Williams for her never-ending help with the work presented in this dissertation.

I would also like to acknowledge and thank the International Plant Nutrition Institute, Denver Wastewater Reclamation District, Rocky Mountain Agribusiness Association, United States Department of Agriculture AFRI project (COLO-2009-04554) and the U.S. EPA STAR

grant (834551) for the financial support. I would like to thank all of our cooperators for assess to research sites, materials, and knowledge at all of our field sites.

Finally, I am greatly indebted to my mother, father, and family for their love and encouragement during my time as a graduate student and for allowing me to pursue my goals. Much thanks to my friend, Jamie Frederick, for her patience, fortitude, and emotional support through the most difficult time of my graduate work. I could not have done this work alone, and it would not be the same without the contributions and influences of all of the aforementioned people. My deepest thanks to you all!

TABLE OF CONTENTS

LIST OF TABLES

LIST OF FIGURES

CHAPTER ONE

Introduction to Reactive Nitrogen, Isotopic Tracers, and Ammonia Emissions

1.1 Nitrogen Cycling

Nitrogen (N) is most commonly found as N_2 gas in the atmosphere. N_2 is fairly inert in the atmosphere; however, it can be converted to more reactive forms of N through N fixation

$$N_2 + 8H^+ + 8e^- \rightarrow 2NH_3 + 2H_2$$

(*24*). Moreover, ammonium can be formed through breakdown of organic matter in the soil (mineralization) (*1*). Once fixation or mineralization to ammonia has occurred, the N becomes more bio-available. Ammonia can be readily converted to ammonium through acid base chemistry, as well as, undergo nitrification to nitrate (*24*). Nitrification occurs under aerobic

$$NH_4^+ + 2O_2 + H_2O \rightarrow NO_3^- + 2H_3O^+$$

conditions. Both ammonium and nitrate serve as the base N source for amino acid production for bacteria and plants (*25*). Nitrate can be converted to N_2O and N_2 through denitrification thus completing the cycle back to N_2 in the atmosphere (Figure 1.1).

1.1.1 Terrestrial and Anthropogenic Sources, and Sinks of Reactive Nitrogen

Terrestrial formation of reactive N occurs through biological fixation of N_2 (discussed above) and production of NO by lightning. Biological fixation can occur in both soils (107 Tg N yr^{-1}) and estuarine (121 Tg N yr^{-1}) systems. Ultimately, NO produced by lightning (5.4 Tg N yr^{-1}) is more common near the equator and is converted to HNO_3 in the atmosphere. Estimates of fixation and lighting produced NO totaled 233 Tg N yr^{-1} in the early 1990s (*26*). Anthropogenic

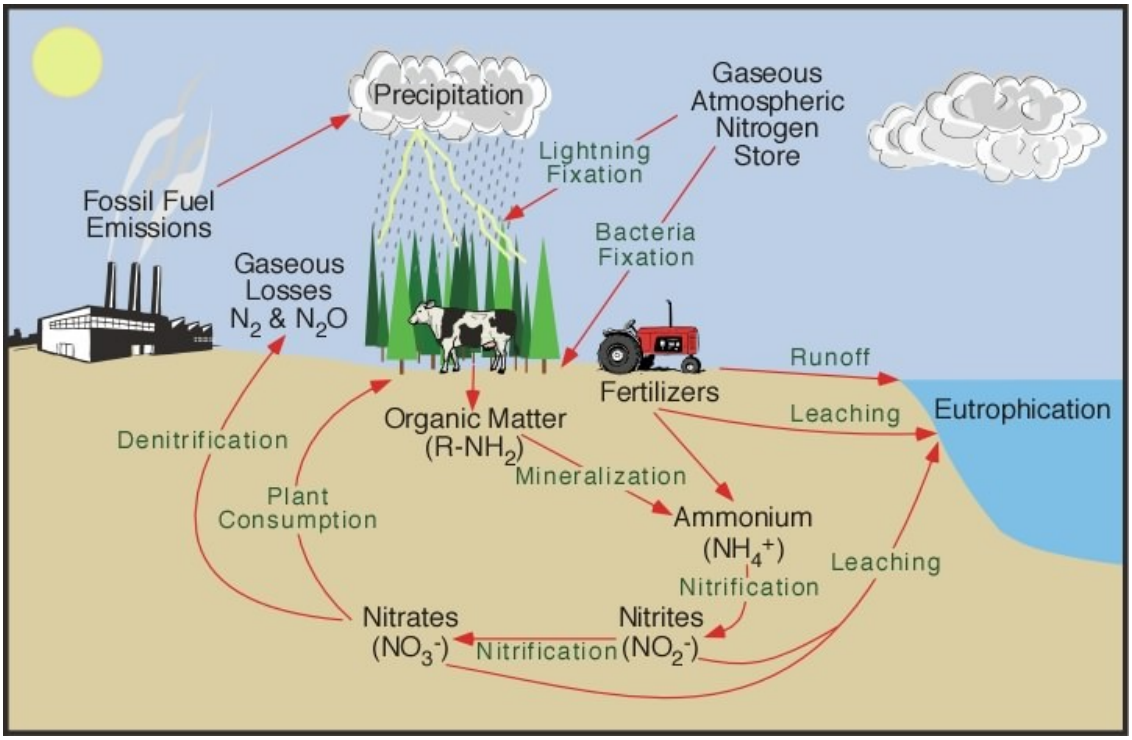

Figure 1.1 . A conceptual depiction of the N cycling in soils. Adapted from reference (*1*).

reactive N formation has increased from 15 to 156 Tg N yr^{-1} from 1860 to the early 1990s to 187 Tg N yr^{-1} in 2005; while reactive N creation is estimated to be as high as 267 Tg N yr^{-1} by 2050 (*26, 27*). The two most common pathways for increases in anthropogenic created reactive N are food production and energy consumption.

NH_3 accounts for most of the reactive N created for food production. The most commonly cited anthropogenic process converting N_2 to reactive N is the Haber-Bosch process, contributing 100 Tg N yr^{-1} in the 1990s (*26*). However, 20% of reactive N created by the Haber-Bosch is for industrial use (*28*). This industrial based process converts N_2 to NH_3 primarily for fertilizer use to meet food production demands.

$$N_2 + 3H_2 \xrightarrow{T,P,Fe\ catalyst} 2NH_3$$

Due to increase in population, reactive N created through the Haber-Bosch process has exponentially increased since the 1940s and it is estimated that 40% of the world's population is supported through the Haber Bosch (*29*).

Reactive N is created with intent for food production; however, it is not the intended result of energy consumption. Most common sources are mobile sources, electrical generation, and industrial production contributing 24.5 Tg N yr^{-1} to reactive N production (*26*). These processes result in the creation and release of NO_x ($NO + NO_2$), typically through oxidation of fuel. NO_x continues to form HNO_3 which contributes to aerosol creation and acid rain (*24, 30*).

1.1.2 Sources of Ammonia and Ammonium

Ammonia is an important constituent in the atmosphere because it is the most common basic gas in the atmosphere (*30*). Currently, NH_3 is an unregulated pollutant and ecological ramifications have been associated with excess ammonia and ammonium pollution. Largely, ammonia production is governed by three pathways: 1) biological fixation, 2) breakdown of organic matter (mineralization), and 3) the Haber-Bosch process. However, a small percent of ammonia can be produced from three way catalytic converters, and from human breath and perspiration (*31*). Overall, ammonia is strongly tied to agriculture, in particular, to synthetic fertilizer and animal waste. Ammonia production in agriculture is most commonly formed from the breakdown of urea (urea hydrolysis), whether through chemical or enzymatic processes and breakdown of natural organic matter ($R\text{-}NH_2$).

$$(NH_2)_2CO_{(aq)} + H_2O_{(l)} \rightarrow NH_{3\,(aq)} + H_2NCOOH_{(aq)} \rightarrow 2NH_{3\,(aq)} + CO_{2\,(aq)}$$

Three-way catalytic converters were introduced to meet emission standards for NO_x from vehicles. The process converts, NO_x to N_2 and O_2, followed by combustion for carbon monoxide

to carbon dioxide. Gasoline engines operate at stoichiometric ratios of fuel to air, but limitations in fuel injection mixing can result in incomplete combustion. An undesired byproduct of incomplete oxidation is carbon monoxide. Carbon monoxide and water vapor are in equilibrium with CO_2 and H_2. At this state, N_2 and H_2 are both present and can react over the catalyst to create NH_3 very similar to the Haber-Bosch processes.

$$2NO_x \rightarrow N_2 + xO_2$$

$$2CO + O_2 \rightarrow 2CO_2$$

$$CO + H_2O \leftrightarrow CO_2 + H_2$$

1.1.3 Dynamics of Ammonia and Ammonium

Ammonia and ammonium can exist in a number of phases and forms. Ammonia and ammonium speciation is dependent on pH through the acid dissociation constant (K_a; Eq. 1.1). $[NH_{3(aq)}]$ represents ammonia concentration in solution, $[NH^+_{4(aq)}]$ represents ammonium concentration in solution, $[H^+_{(aq)}]$ is the hydronium concentration, and γ represents the activity coefficient for each species (*18*). Moreover, ammonium has the ability to sorb onto soil

$$NH_4^+{}_{(aq)} \leftrightarrow NH_{3\,(aq)} + H^+_{(aq)} \qquad K_a = \frac{\gamma_{NH_3}[NH_{3\,(aq)}]\gamma_{H^+}[H^+]}{\gamma_{NH_4^+}\left[NH_4^+{}_{(aq)}\right]} \text{ (Eq. 1.1)}$$

constituents depending on soil surface charge. Depending on the concentration difference between ammonia in the soil solution and the air, ammonia can be lost to the air as described by the Henry constant (K_h; Eq. 1.2). $[NH_{3(g)}]$ represents ammonia concentration in the gas phase. Several units (dimensionless, M atm^{-1}, MPa mg^{-1} L^{-1}, etc.) have been used in the literature. The various forms and phases which ammonium and ammonia can partition between and within create great difficulty in studying transformations.

$$NH_{3\,(aq)} \leftrightarrow NH_{3\,(g)} \qquad K_h = \frac{[NH_{3\,(g)}]}{\gamma_{NH_{3(aq)}}[NH_{3\,(aq)}]} \text{ (Eq. 1.2)}$$

1.1.4 Emissions of Reactive Nitrogen

Both natural and anthropogenic processes contribute to N (NO_x, NH_3, and N_2O) emissions into the atmosphere. Natural processes include soil emission and biomass burning (e.g., forest fires). Biomass burning releases high amount of NO_x in the early stages of a burn, while NH_3 is released in later stages (smoldering phase) where oxidation is incomplete (*32, 33*). Also, NH_3 is emitted from native soil surfaces, but to a smaller extent compared to anthropogenic emissions (discussed below). Soils create N_2O under reducing conditions and account for 67% of N_2O emissions, however, roughly 50% of these emissions are associated with fertilization (both natural and synthetic), animal grazing, and cultivation of N-fixing crops (*26, 34, 35*).

Anthropogenic emissions of NO_x, NH_3, and N_2O totaled 88.0 Tg N yr^{-1} in the early 1990s (*26*). As mentioned above, NO_x created from combustion is the primary pathway for NO_x formation. On (29.6-32%) and off-road (20.1-30%) vehicles account for 49.7-62% of nitric oxide emissions (*3, 34*). Electricity and power generators account for most of the remaining emissions (27-34.6%) (*3, 34*). Also, production of fuel, metals, and waste water account for small amounts of US NO_x emissions (*34*). N_2O is primarily emitted from soils (67%), but contributions from fossil fuel combustion (12%) and industrial processes (8%) contribute to N_2O emissions in the US (*34*).

Crop and animal production totaled roughly 45% of worldwide anthropogenic ammonia emissions (39.4 Tg N yr^{-1}) in the 1990s (*26*). 59-80% of the ammonia emission inventories in the US are related to fertilizer use and animal production (*3, 34*). Large uncertainty exists within

these inventories for agricultural sources due to the difficulty of measuring ammonia emission and incomplete data information (*34*). A small portion (7%) of ammonia emissions are created in mobile sources by three way catalytic converters (*3, 34*). Industrial processes, biomass burning, wild animals, and waste management are sources of ammonia, however their contribution to emission inventories remains small and uncertain (*3*). Other work has provided emission estimates for non-agricultural sources, including human sweat, perspiration, domesticated animals, biomass burning, landfill, etc (*31*). This work identified critical uncertainties for sources like biomass burning (*31*). However, these non-agricultural sources only comprised 19% of N emissions in the United Kingdom (*31*). The work presented here will focus on ammonia and ammonium analysis.

1.1.5 Transformation and Transport of Reactive Nitrogen

Reactive N released into the atmosphere can undergo numerous chemical transformations which may allow it to travel long distances from the emission source (*36, 37*). NO_x and NH_3 are more reactive than N_2O in the atmosphere and thus N_2O will not be discussed further. NO_x can readily react with common atmospheric compounds to ultimately form HNO_3.

Dominant pathway during the day:

$$NO^{\cdot} + O_3 \rightarrow NO_2^{\cdot} + O_2$$

$$NO^{\cdot} + RO^{\cdot}\ (VOC\ mediated) \rightarrow NO_2^{\cdot} + RO_2^{\cdot}$$

$$NO_2^{\cdot} + OH^{\cdot} + M\ (O_2, N_2, etc.) \rightarrow HNO_3 + M$$

Important pathways in absence of daylight:

$$NO_2^{\cdot} + O_3 \rightarrow NO_3^{\cdot} + O_2$$

$$NO_{3(g)}^{\cdot} + H_2O_{(\ell)} \rightarrow HNO_{3\,(aq)} + OH_{(aq)}^{\cdot}$$

$$NO_3^{\cdot} + RH \quad (VOC\ mediated) \rightarrow HNO_3 + R^{\cdot}$$

$$NO_{3(g)}^{\cdot} + NO_2 \rightarrow N_2O_5$$

$$N_2O_5 + H_2O \rightarrow 2HNO_3$$

Ammonia is not generally produced in the atmosphere like nitric acid and is not readily oxidized in the atmosphere. NH_3 has a relatively short lifetime and is more important near a source (*38*). Ammonia plays an important role in aerosol formation with acidic gases (HNO_3 and H_2SO_4). Ammonium aerosol formation drastically increases the lifetime of N and thus increases

$$NH_3\,(g) + HNO_3\,(g) \quad \leftrightarrow \quad NH_4NO_3\,(p)$$

$$NH_3\,(g) + H_2SO_4\,(g) \quad \rightarrow \quad (NH_4)HSO_4\,(p)$$

the possible transport distance before deposited back to the surface. Ammonium nitrate formation reaction is shown with a bi-directional arrow since this equilibrium is highly dependent on temperature and humidity (*39*). Ammonium sulfate does not demonstrate the same sensitivity to changes in temperature and humidity and is more accurately depicted as a unidirectional reaction at atmospheric temperatures (*40*).

1.1.6 Deposition and Impacts of Reactive Nitrogen

Reactive N can be deposited back to the earth's surface through wet deposition (with the aid of precipitation) or dry deposition (without the aid of precipitation) (Figure 1.2). Wet deposition can occur within cloud droplets (in-cloud scavenging) or below a cloud by incorporation of species into falling precipitation (below-cloud scavenging). Dry deposition is largely dependent on the species' deposition velocity (V_d). V_d is highly dependent on

environmental variables such as temperature, humidity, surface resistances, and particle size (*30*).

Most reactive N species are water soluble and thus wet deposition tends to dominate compared to dry deposition but is variable across the US. Drier regions tend to have higher fractions of dry deposition, such as the Western US (*41*). Dry deposition is much more difficult to monitor than wet deposition. Dry deposition monitoring requires more instrumentation than wet deposition. Wet deposition has traditionally been monitored at various sites in the US for over 30 years.

With the demand of N increasing worldwide, anthropogenic processes have led to a rapid increase of reactive N in soils, water, and the atmosphere. Soils are generally N-limited, thus, increases in N result in increased productivity until N is no longer the limiting nutrient. Once this occurs nitrogen saturation has been reached and excess nitrogen is lost to the air by volatilization (NH_3, N_2O, N_2), transferred to surface waters by runoff, or transported into a new

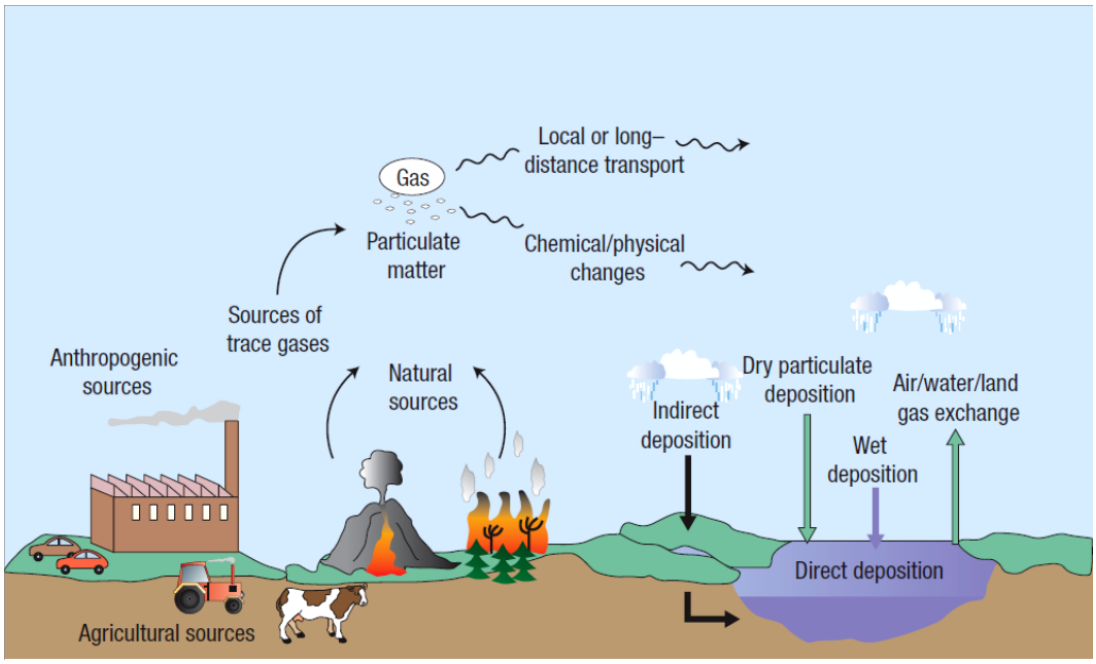

Figure 1.2. Conceptual lifecycle of ammonia from emission, transport, transformation, and deposition. Adopted from reference (*2*).

ecosystem. If excess nitrogen is introduced into surface waters, eutrophication (over-fertilization) can result in rapid growth of algae resulting in hypoxia thus endangering aquatic life(*2, 42, 43*). Both soils and surface water can become acidified by introduction of HNO_3 leading to shifts in soil fertility and diatom populations in surface water (*44-46*). N_2O plays an important role in global warming (298 CO_2 equivalents) and is currently the 4th largest contributor to global warming (*47*). NH_3 and NO_x engage in aerosol creation contributing to deterioration of human health and regional haze.

1.2 Current Understanding of Nitrogen Deposition in the Front Range (Colorado, USA)

The Front Range is defined as the area between Cheyenne, WY and Colorado Springs, CO. The Front Range has a rapidly expanding human population (*48, 49*) that adjoins a productive agricultural region (*50*) and lies below the eastern flank of the Rocky Mountains. This creates a unique union consisting of metropolitan, agricultural, and pristine sectors (Figure 1.3). Previous studies have suggested a connection between human population, head of cattle, and sales of synthetic fertilizer with N deposition observed in RMNP (*44*).

Estimates of N deposition (wet and dry) in the Rocky Mountains range from 1-7 kg N ha^{-1} yr^{-1} (*51*). Long term wet deposition monitoring of N in RMNP has demonstrated increases in concentrations of N (Figure 1.4 a) and elevated levels of N deposition (Figure 1.4 b, c, d) compared to the park's critical load, 1.5 kg N ha^{-1} yr^{-1} (*46*). Subalpine mountain ecosystems bordering the Front Range are vulnerable to small increases in N deposition leading to negative effects at rates as low as 1.5 to 5 kg N ha^{-1} yr^{-1} (*44, 45, 52*). Negative impacts have been documented in form of changes of lake diatom communities and decreased biodiversity (*53, 54*). These studies were critical in the development of the Rocky Mountain National Park Initiative.

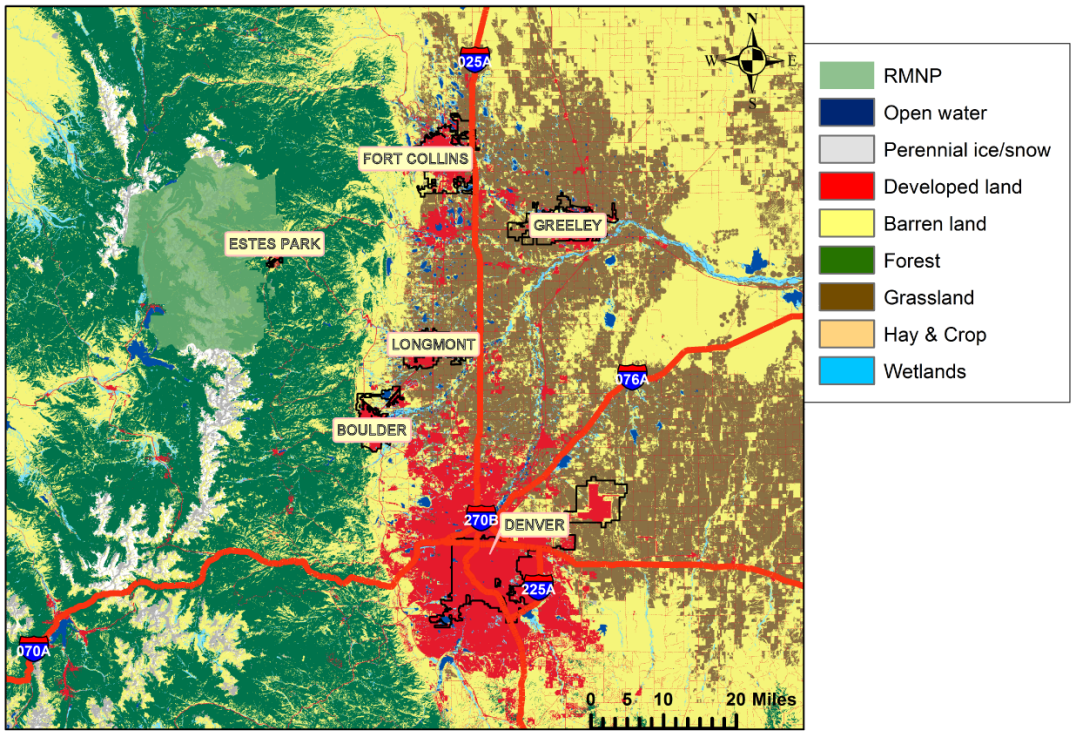

Figure 1.3 Topographical map of the Front Range from Denver, CO to Wyoming border. Green areas represent native forests of the Front Range, with RMNP being shown in pale green. Brown and light brown loosely represent agricultural sectors of the Front Range, while red represents populated areas in the Front Range. The area from Denver, CO to Fort Collins is referred to as the urban corridor. Figure shown with permission of Dr. Gina Mckee.

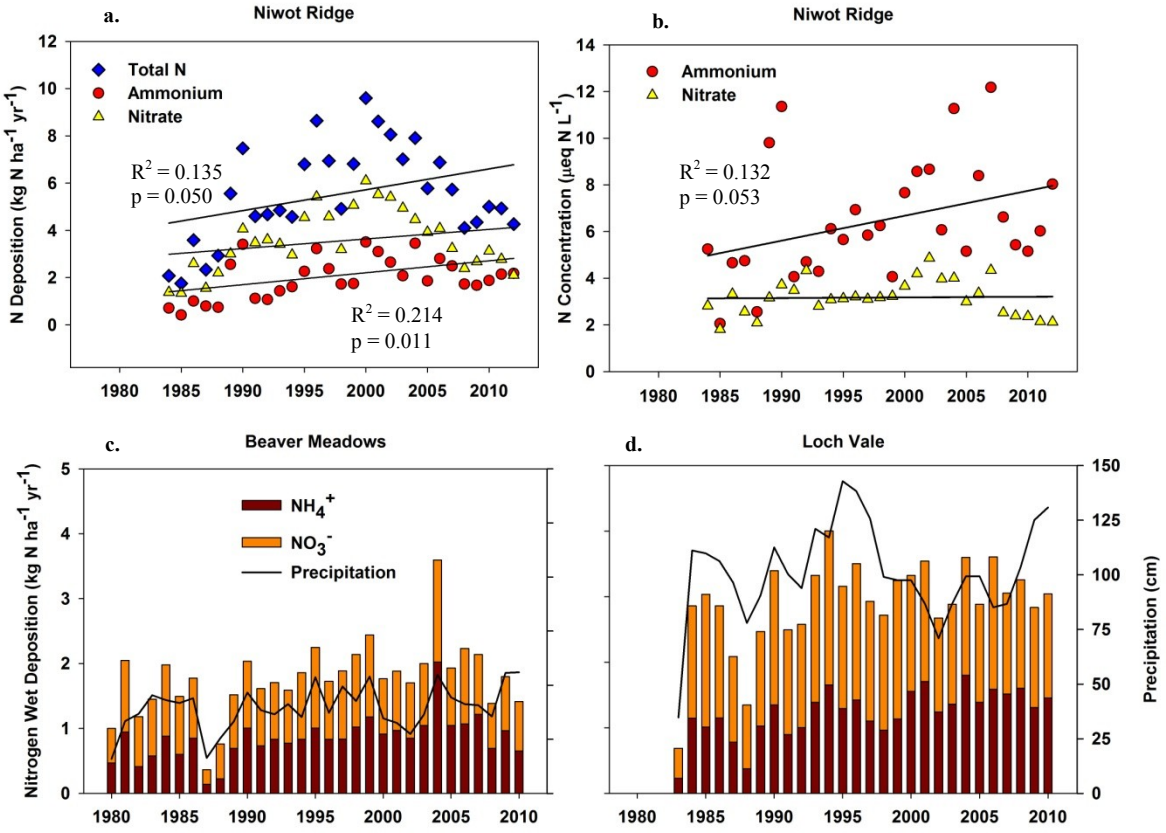

Figure 1.4. Historical inorganic N deposition (a,c,d) and concentration (b) at three NTN sites in the Rocky Mountains. Beaver Meadows (c) has been studied slightly longer than the Niwot Ridge (a, b) and Loch Vale Watershed (d). An increase in total N deposition at Niwot Ridge has been witnessed over nearly 30 years (1984-2012). Data provided by National Trends Network.

With the introduction of this initiative, inventories provided information about current N emission knowledge. Statewide anthropogenic NO_x emissions in Colorado were dominated by on and off-road vehicles (50.1%) and point sources (37.2%) such as energy generators, while ammonia emission were dominated by livestock (39.9-46.8%), fertilizer (22.0-25.8%), on-road mobile sources (5.2-10.8%) (*3, 55*). Front Range estimates of ammonia emissions differed from statewide emissions with livestock (37.3%) and fertilizer (18.9%) contributing slightly less and mobile sources (11.9%) and waste water treatment (18.6%) contributed more to ammonia emissions (*55*).

The Rocky Mountain airborne nitrogen and sulfur (RoMANS I) study was conducted in 2006 to improve the understanding of N and sulfur deposition, their forms, and their sources (*3*). This study occurred over two five weeks periods in the spring and summer (*56*). This study demonstrated the importance of easterly influence on N deposition in RMNP. N deposition was dominated in the spring and summer by wet deposition of ammonium (34%, 34%) and dry deposition of ammonia (14%, 16%), respectively. RoMANS I demonstrated that a single precipitation event or rainfall can contribute significant amounts of N (*3, 56*). Furthermore, northeastern CO and local source areas were the majority (62%) and plurality (32%) of ammonium deposition in the spring and summer period, respectively (Figure 1.5 & 1.6) (*3*).

RoMANS I demonstrated that anthropogenic sources contribute to N deposition in areas near RMNP. However, this study was conducted over 10 weeks. A new study, RoMANS II, was conducted for 1 year to fully understand annual N and sulfur deposition in RMNP (*4, 57*). RoMANS II showed larger deposition during the late spring to the late fall (Figure 1.7). The window is often referred to as deposition season in RMNP Furthermore ammonia and ammonium were two of the top three forms in which N was deposited in RMNP (Figure 1.8) (*4*).

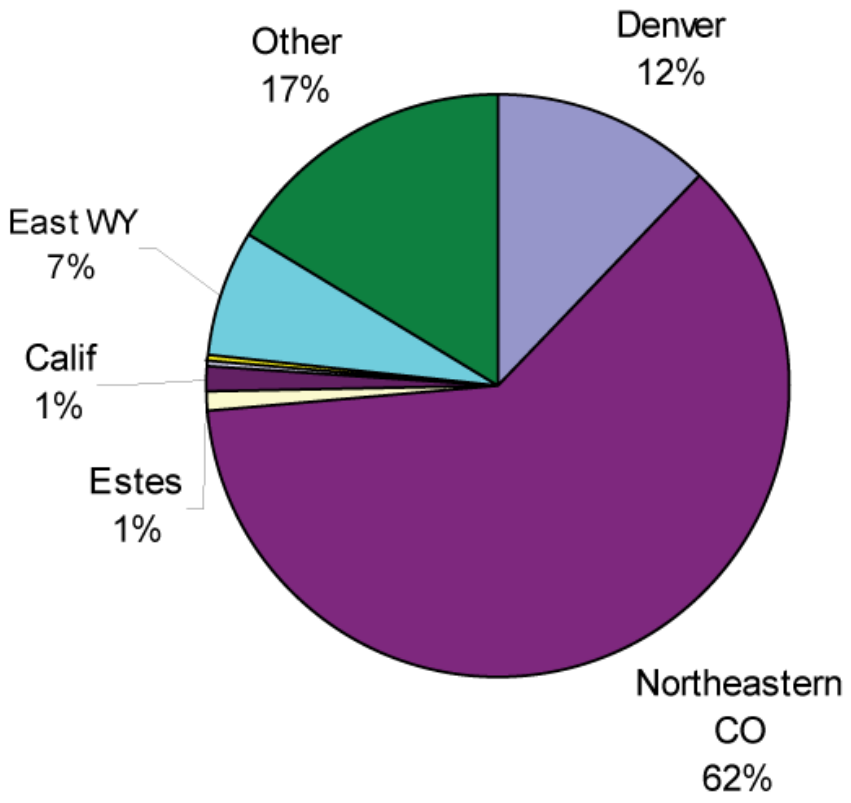

Figure 1.5. Spring source apportionment of ammonium wet deposition from RoMANS I. This study period was dominated by a single precipitation event in late April identified from northeastern CO. Adopted from reference (*3*).

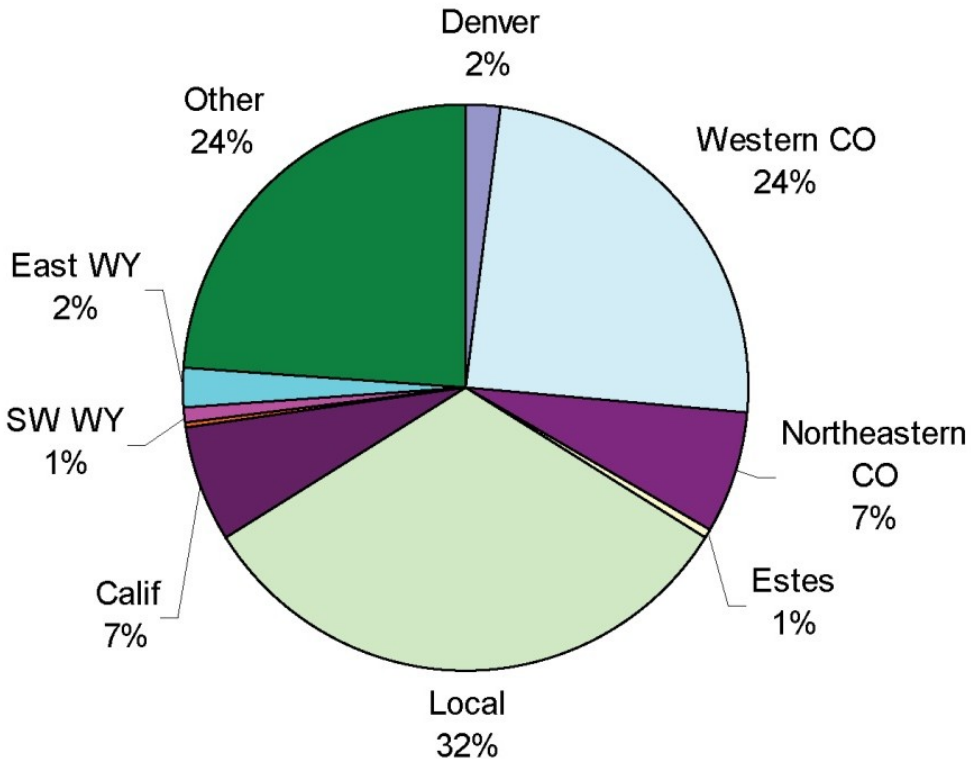

Figure 1.6. Source apportionment of ammonium wet deposition from RoMANS I. Each apportionment is associated with an area of Colorado of the United States. Adopted from reference (*3*).

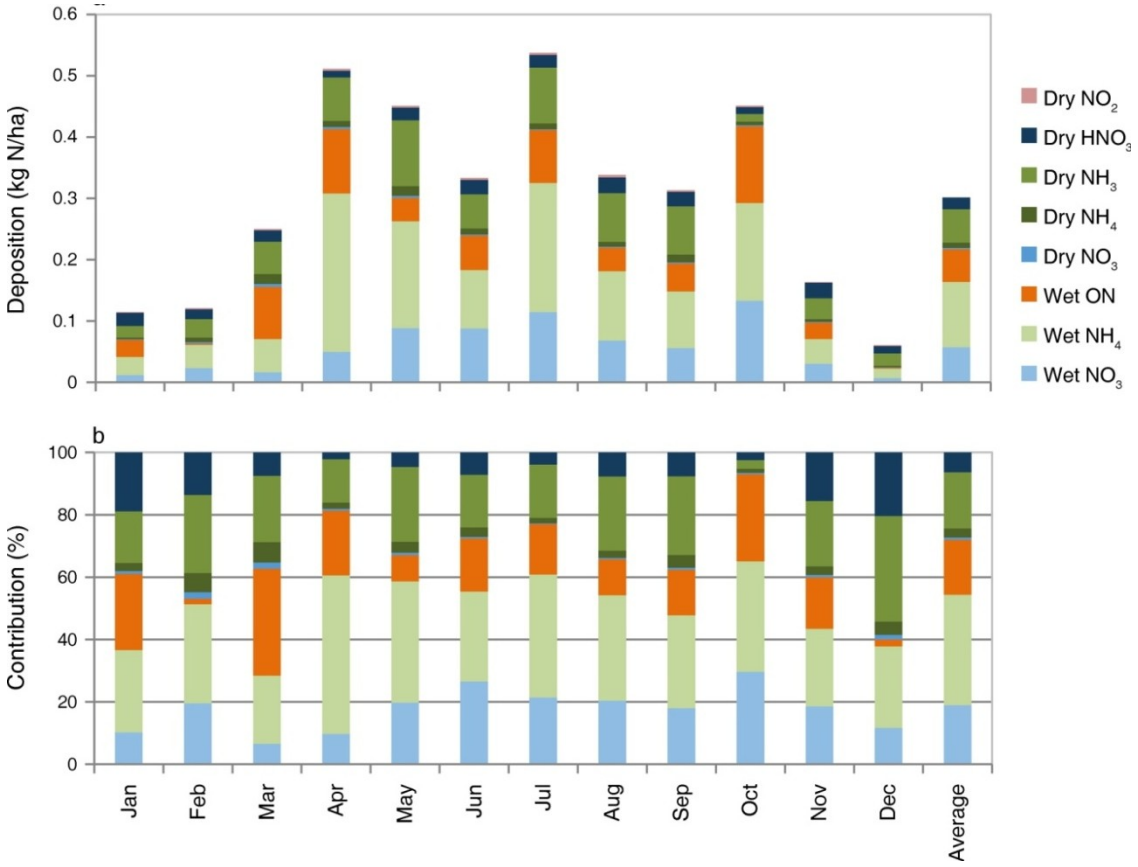

Figure 1.7. Total N deposition (dry and wet deposition) by month observed during RoMANS II study. The spring and summer period is often referred to as deposition season and coincides with easterly flow regimes. Adopted and shown with permission from reference (*4*).

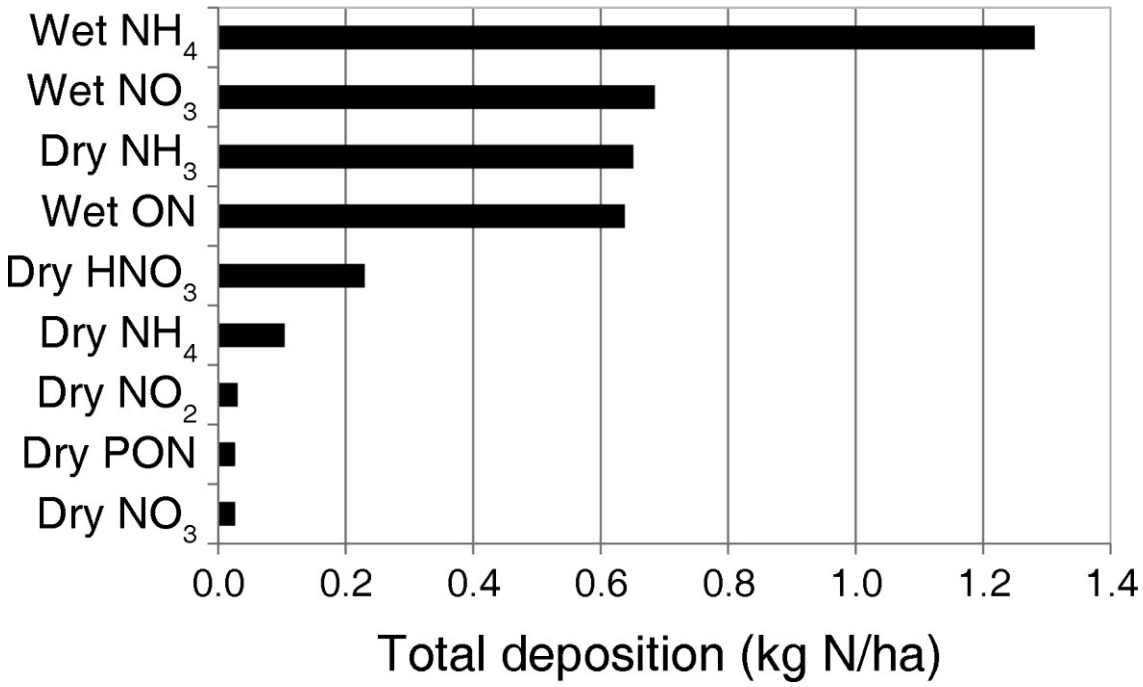

Figure 1.8. Annual apportionment of N deposition observed in RoMANS II. Wet deposition remains the primary pathway of N deposition. Wet deposition of ammonium was the dominant form, while dry deposition of gaseous ammonia was third. Adopted and shown with permission from reference (*4*)

$$\delta^{15}N\ (‰) = \frac{(^{15}N/^{14}N)_{sample} - (^{15}N/^{14}N)_{standard}}{(^{15}N/^{14}N)_{standard}} \times 1000 \qquad \text{(Eq. 1.3)}$$

However, it remained uncertain as to what specific emission sources (e.g. livestock, fertilizer, mobile sources, etc.) of ammonia and ammonium contributed to N deposition in RMNP. According to the ammonia emission inventories discussed above, agriculture was assumed to be a major contributor to ammonia and ammonium deposition (*3, 55*). However, no direct chemical or physical evidence has connected N deposition observed in RMNP to agricultural sources.

1.3 Nitrogen Isotope Tracers and Indicators

1.3.1 Isotope Notation

Nitrogen has two stable isotopes (^{14}N and ^{15}N) (*58*). The heavier isotope (^{15}N) is referred to as the rare isotope and its natural occurrence is 0.365% in the atmospheric N_2 pool (*59, 60*). It is a stable percentage among the N_2 pool and is used as a reference for all natural abundance isotopic measurements according to the equation 1.3 below (*61*). Isotopes near natural abundance are reported in $\delta^{15}N$ (‰, denoted per mil) and are calculated relative to the N_2 standard ratio ($^{15}N/^{14}N_{standard} = 3.6765 \times 10^{-3}$). $(^{15}N/^{14}N)_{sample}$ is the isotopic ratio of the sample. The ratio of the isotopes in atmospheric NH_3 will depend primarily on the N source. Different chemicalreaction or processes can result in different isotopic ratios; for examples, agricultural practices can produce significantly different $\delta^{15}N$ values than non-agricultural sources (*8*) (Figure 1.9). Ammonia lost from animal waste is typically strongly depleted in ^{15}N (*7, 10, 62*). This is due to differences rate of reaction, diffusion, and volatilization of the different isotope causing isotopic fractionation.

Typical $\delta^{15}N$ values observed in nature range from -50 to +50‰ (*60*). Total $\delta^{15}N$ (nitrate and ammonium) in synthetic fertilizers are usually derived by industrial fixation of atmospheric N_2 by the Haber-Bosch process, resulting in $\delta^{15}N$ values close to zero (*12*). Ammonia derived from the combustion of coal typically has $\delta^{15}N$ values in the range -4 to -8‰ (*10*). Animal waste is generally depleted in ^{15}N. The only animal waste study showing enriched values used a series of filters (*8*). Collection of ammonium aerosol on filters has been shown to cause artifacts with temperature changes possibly affecting these results (*63*). Generally, ammonium aerosol is enriched in comparison to its parent gas, ammonia (*64*). Figure 1.10 provides some insight

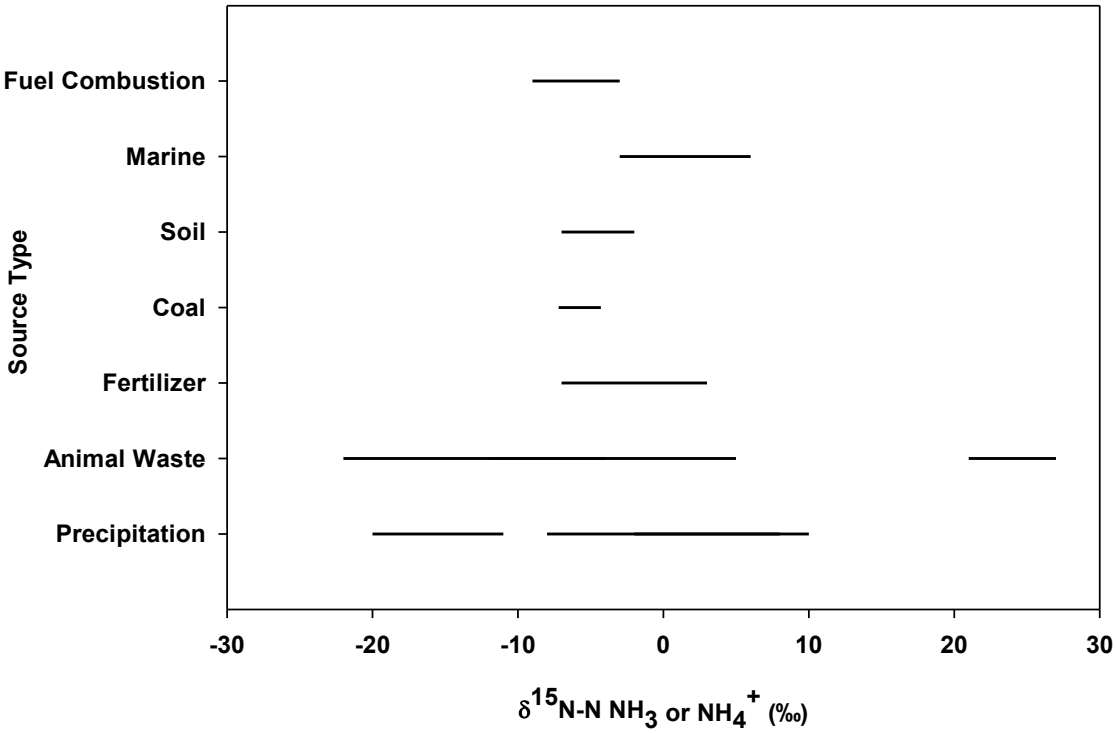

Figure 1.9 . Comparison of N isotopes from ammonia or ammonium measured in source material (marine, soil, fertilizer), emissions (coal, animal waste), and in precipitation from various literature sources over the last 50 years. Modified from (*5-15*).

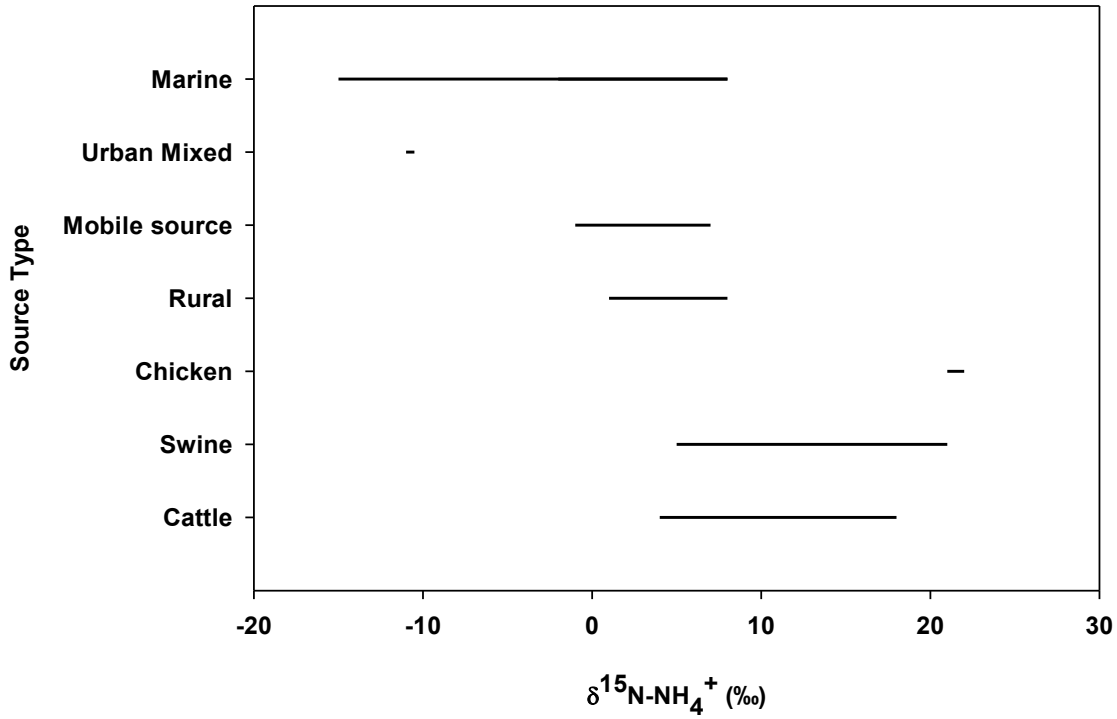

Figure 1.10. Comparison of N isotopes of ammonium aerosol measured from known sources (poultry, cattle, swine, mobile sources, and marine) and rural and urban locations (either no known sources or mixed). Modified from (*16*).

from previously measured ammonium aerosols from various agricultural and urban sources. In comparing Figures 1.9 and 1.10, ^{15}N compounds tend to favor denser substances such as aerosol and liquid phases over gas phases. Ultimately these differences in isotopic ratios may allow for source apportionment of ammonia pollutants.

1.3.2 Isotopic Fractionation

Differences in isotope fractionation are a result of physical, kinetic, and equilibrium process. Physical fractionation results from differences in diffusion rates. Kinetic fractionation results from small differences in bond energies between differing isotopes of N. This can be related to the vibrational energy, more specifically the difference in the zero point energy

(n=0) between isotopes. Where E is energy, h is Planck's constant, n is energy level, k is the force constant, υ is the harmonic frequency, and μ is the reduced mass of the heavy isotope (μ_H) and light isotope (μ_L). Ultimately, the heavier isotope has a slightly lower zero point energy vibrational level, (n=0),resulting in a slightly stronger bond. Another common depiction is the

$$E_{vibrational} = h\upsilon\left(n+\frac{1}{2}\right); \qquad \upsilon = \frac{1}{2\pi}\left(\frac{k}{\mu}\right)^{\frac{1}{2}} \quad \rightarrow \quad \Delta E_{vibrational} = \frac{1}{4\pi}h\left(\frac{k}{\mu_H} - \frac{k}{\mu_L}\right)^{\frac{1}{2}}$$

differences in activation energy between two like bonds with different N isotopes (Figure 1.11). This small difference in energy results in slightly different reaction rates generally resulting in discrimination of the heavier isotope leaving the substrate with slightly higher amount of ^{15}N and products with less ^{15}N. The increase in ^{15}N in the substrate and decrease in ^{15}N in the products is called enrichment and depletion, respectively.

Equilibrium fractionation refers to a preferential separation of isotopes between two well-mixed phases. This fractionation is governed by quantum mechanics and the total energy of a molecule (E_{Total}). Differences in mass effect translational ($E_{translational}$), vibrational ($E_{vibrational}$),

$$E_{Total} = E_{translation} + E_{vibrational} + E_{rotational} + E_{electronic} + E_{nuclear}$$

and rotation ($E_{rotational}$) motion result in equilibrium fractionation. For simplicity, a diatomic N_2 molecule is considered, where $^{15}N^{15}N$ is excluded due to the low probability of its occurrence. The equilibrium constant (K) can be written as concentrations or by their partition functions (q).

$$^{14}N^{14}N\ (g) + {}^{15}N^{14}N\ (aq) \leftrightarrow {}^{14}N^{14}N\ (aq) + {}^{15}N^{14}N\ (g)$$

$$K = \frac{\left[^{14}N^{14}N\ (aq)\right]\left[^{15}N^{14}N\ (g)\right]}{\left[^{14}N^{14}N\ (g)\right]\left[^{15}N^{14}N\ (aq)\right]} \quad \rightarrow \quad K = \frac{q^{14}N^{14}N\ (aq)\ q^{15}N^{14}N\ (g)}{q^{14}N^{14}N\ (g)\ q^{15}N^{14}N\ (aq)}$$

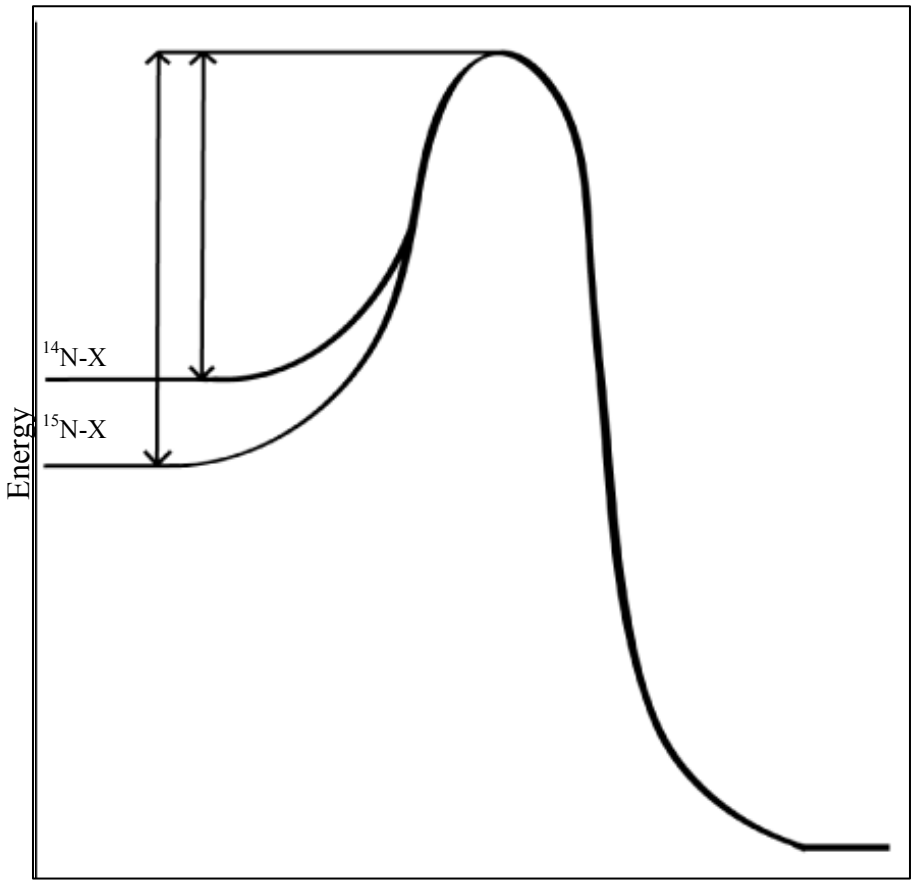

Figure 1.11. Reaction coordinate demonstrating the difference in bond strength due to differences in zero point energy. This illustrates that more energy is required to break like bonds containing heavier isotopes.

Where q is the product of each type of motion, we can substitute q in for each concentration.

$$q = (q_{translational})(q_{rotational})(q_{vibrational})$$

$$K = \frac{\mathrm{q^{14}N^{14}N\ (aq)}\ \ \mathrm{q^{15}N^{14}N\ (g)}}{\mathrm{q^{14}N^{14}N\ (g)}\ \ \mathrm{q^{15}N^{14}N\ (aq)}} = \frac{\mathrm{q_1}\ \ \mathrm{q_2}}{\mathrm{q_3}\ \ \mathrm{q_4}}$$

Translational motion can be described by a particle in a box (*65*). Where k is the Boltzmann constant and T is temperature. Ultimately, when applied to the equilibrium between two isotopes (or ratios of their energetic states) translational motion reduces to the ratio of the reduced masses (*66*). Much of the same mathematical reduction occurs when discussing rotational energy and vibrational energy. Rotational motion is described by the rigid rotor, where I is the moment

$$q_{translational} = \frac{(2\pi\mu kT)^{\frac{3}{2}}}{h}V \quad \rightarrow \quad K_{translational} = \Pi\left(\frac{\mu_1\ \mu_2}{\mu_3\ \mu_4}\right)^{\frac{3}{2}}$$

of inertia, and σ is the symmetry factor (*66*). When applied to isotopes of the same configuration; the equilibrium reduces to a ratio of the moments of inertia (I) since their σ are the same (*66*).

$$q_{rotational} = \frac{8\pi^2 I\ kT}{\sigma h^2} \quad \rightarrow \quad K_{rotational} = \left(\frac{I_1\ I_2}{I_3\ I_4}\right)$$

When applying the harmonic oscillator to model vibrational motion, the equilibrium constant demonstrates how vibrational frequencies (ν), which are mass dependent, affect isotopic

$$q_{vibrational} = \frac{e^{\left(\frac{-h\nu}{2kT}\right)}}{1-e^{\left(\frac{-h\nu}{2kT}\right)}} \quad \rightarrow \quad K_{vibrational} = \left(\frac{1-e^{\frac{-h(\upsilon_1+\upsilon_2)}{2kT}}}{1-e^{\frac{-h(\upsilon_3+\upsilon_4)}{2kT}}}\right) e^{\left(\frac{-h(\upsilon_1+\upsilon_2-\upsilon_3-\upsilon_4)}{2kT}\right)}$$

speciation (*66*). Multiplying these three partition functions, it would be possible to calculate isotopic equilibrium constants (*67*). These quantum mechanical explanations constitute the fundamental basis of kinetic and equilibrium isotopic fractionation.

$$K_{trans}\ K_{rot} K_{vib} = \left[\Pi \left(\frac{\mu_1\ \mu_2}{\mu_3\ \mu_4} \right)^{\frac{3}{2}} \right] \left[\left(\frac{I_1\ I_2}{I_3\ I_4} \right) \right] \prod \left[\left(\frac{1 - e^{\frac{-h(v_1 - v_2)}{2kT}}}{1 - e^{\frac{-h(v_3 - v_4)}{2kT}}} \right) e^{\left(\frac{-h(v_1 + v_2 - v_3 - v_4)}{2kT} \right)} \right]$$

1.3.3 Environmental Application of Nitrogen Isotopes

The use of N isotopes (natural abundance or labeling) has shown promise in its ability to distinguish N sources (*8, 62, 68*). Isotopic labeling is commonplace and has been used previously for tracing soil processes and other gaseous emissions such as N_2O (*69-73*). However, the use of natural abundance N isotopes exhibited a difficult start in terms of use as an environmental indicator. One of the first natural abundance N isotope tracer studies of notoriety was published in Science (*74*). This study claimed to quantify the amount of nitrate in surface water associated with run-off from nearby fertilizer application. Rebuttals soon followed and warned about the quantitative use of natural abundance isotopes in soil processes, as well as, criticized the methodology and interpretation (*75-78*). However within the same decade the use of natural abundance N isotopes was used to specify environmental impacts between synthetic fertilizer and animal waste (*79*).

Natural abundance isotopic tracers of N measured in precipitation, surface water, and gas samples have shown promise in identifying emission source contributions, transport, transformation, deposition, and/or ecosystem shifts (*7-11, 14, 16, 59, 64, 80-90*). Russell 1998 reported the range of $\delta^{15}N‰$ for various forms of N in wet deposition on a seasonal basis, as well as, reported trends between seasonal isotopic values and back trajectory models (*14*). More recently, Elliott 2007 demonstrated ^{15}N-nitrate deposited in wet deposition was strongly correlated with stationary NO_x emissions based on source area emission data (*80*). Occhipinti 2008 demonstrated that ^{15}N-nitrate in wet deposition was correlated to agricultural versus non-

agricultural back trajectory models (*91*). N isotopes have become useful indicators for source influence and environmental change. The use of $\delta^{15}N$ isotopes has been limited in use as a source tracking tool. To my knowledge, only a handful of studies have been conducted with simultaneous collection of ammonia at sources and a receptor site (*7, 16, 62, 91*) with limited success. Numerous studies have been conducted only on source characterization or receptor studies (*8, 9, 14, 15, 90, 92*).

1.4 Measuring Ammonia Emission

1.4.1 Emission Techniques

Measuring ammonia emissions rely on concentration measurements, thus accurate measurement of ammonia are crucial. Methodology includes acid scrubbers or traps, filter measurement, denuder measurement, or optical measurements to measure ammonia concentrations (*93*). Emission measurements include mass balance, enclosure studies, and micrometeorological methods. Mass balance studies are inherently subject to large uncertainty when numerous measurements are propagated for the unknown value. Micrometeorological methods are the best suited for accurate measurements of ammonia emission; unfortunately, these studies require a large amount of equipment and cost. Enclosure or chamber offer a more reliable measurement compared to mass balance methods without the cost of micrometeorological methods.

1.4.2 Chamber Methods

Due to the complexity of determining the ammonia flux (emission or deposition) in natural systems, several chamber approaches to measuring ammonia emission have been used

(*94-101*). Using a chamber approach for field measurements of ammonia is often challenging due to low concentrations and ammonia is highly adsorptive, water soluble, and sensitive to fluctuations in temperature further complicated by condensation at elevated humidity levels. Moreover, enclosures can perturb convective heat transfer, light transmission, and aerodynamic conductance (*93*). Therefore, care must be taken when considering chamber design and material for studying ammonia emissions. Shah 2006 provides a review on field and laboratory measurements of ammonia flux (*102*). To address these limitations of field applications, a dynamic flow-through laboratory apparatus was designed for our study to assess the magnitude of ammonia emission from intact soil cores (Chapter 2).

1.5 Difficulty and Complexity of Analyzing Ammonia and Ammonium in Animal Waste

As stated above, agricultural ammonia emissions are the highest among all inventories, but are subject to much uncertainty (*3, 34, 55*). One area of uncertainty is in the understanding of what chemical and physical properties control ammonia emission. Specifically, the production of ammonia through urea hydrolysis and the Henry and acid dissociation constants dictate the total ammoniacal N (TAN) and the fraction of ammonia within the soil and ammonia above the soil surface (*13*). Few studies have explored urea hydrolysis in soils (*103*) or animal waste (*104*). However, these studies may not applicable to feedlot soils, thus understanding the rate and ultimately the amount of TAN in feedlots systems within Colorado is important.

Previous studies have explored Henry and acid dissociation constants in aqueous ammonium solutions (*19, 105*). However, these studies are not applicable to animal waste due to high ionic strengths causing activities to deviate from unity. Numerous studies have been conducted in animal waste matrices, however, differences in sample matrix (poultry, beef, dairy, swine lagoon, anaerobic digester, etc.) with varying methodological approach (headspace

measurements, flux measurements, porous tubing, etc.), or both have not revealed a singular value for feedlots (Figure 1.12 & 1.13) (*17, 21, 22, 106-109*).

Equilibrium constants dependence on temperature can be described by the Van't Hoff equation with the assumption that enthalpy (ΔH) does not change over the temperature (T) range (0-40 °C). It remain unclear why previous work shown above use both ln and log functions

$$ln\frac{K_2}{K_1} = -\frac{\Delta H}{R}\left(\frac{1}{T_2} - \frac{1}{T_1}\right)$$

to describe equilibrium constant's dependence on temperature. With a wide variety of methodologies and environmental matrices, it is imperative to use values applicable to the waste matrix of choice (poultry, cattle, swine, etc.) and environmental conditions experienced here in Colorado.

1.6 Knowledge Gaps and Research Objectives

Connecting ammonia emissions from outside RMNP and ammonia deposition in RMNP has been an area of high importance in the Colorado Front Range. Current ammonia emission inventories are complicated by uncertainty. In particular, ammonia emissions from animal waste, agricultural soils and native soils are poorly understood. Moreover, the complex meteorology in the Colorado Front Range does not allow for a direct translation of ammonia emission inventories to apportionments of ammonium deposition in RMNP. New evidence is needed to connect ammonia emissions from different source types (agriculture, urban, native, etc.) to ammonium deposition in RMNP. Therefore, the objectives of my research are as follows:

.

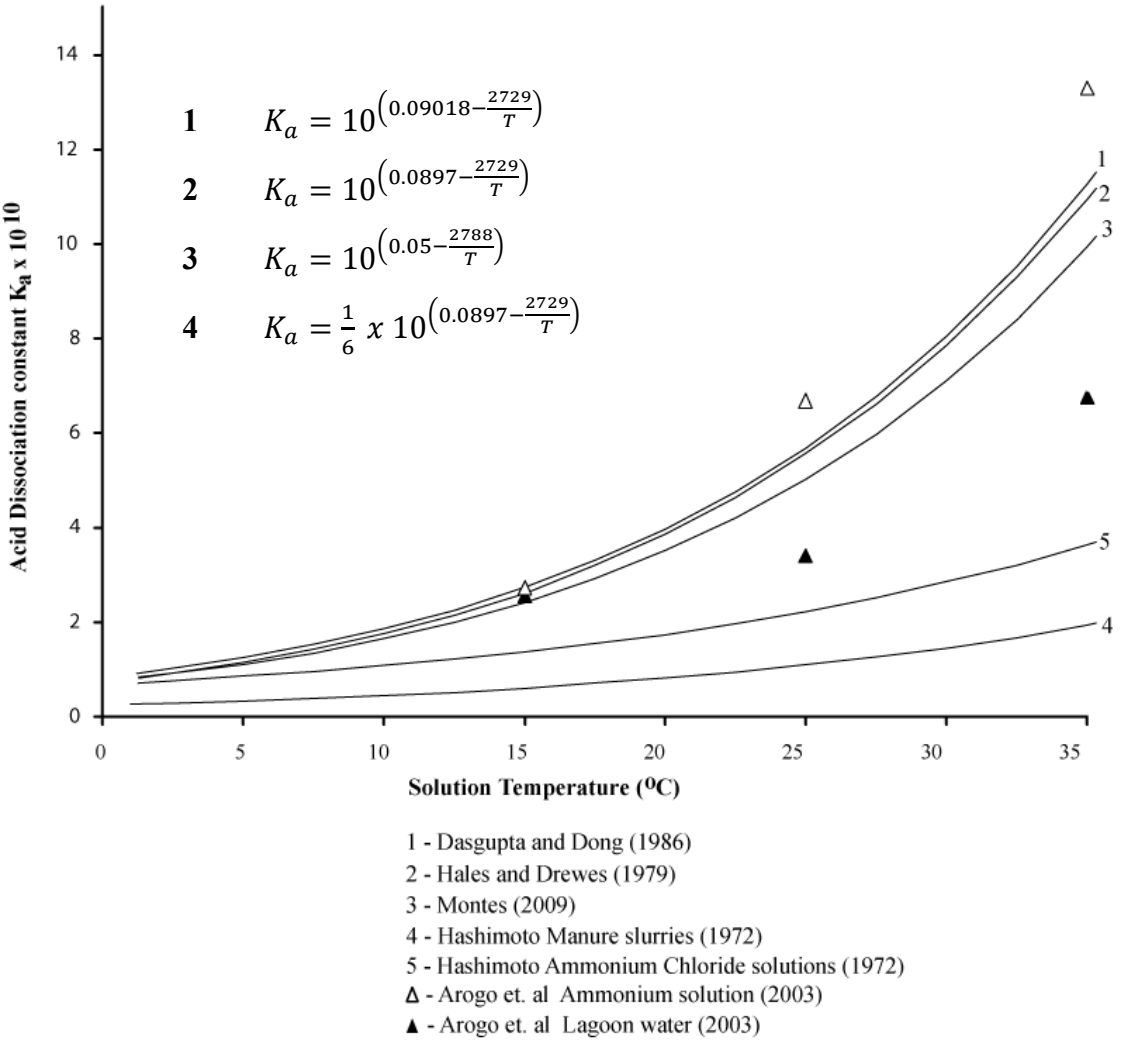

Figure 1.12. Comparison of literature values for acid dissociation constants for aqueous and animal waste slurries. Modified and shown with permission from reference (*17*).

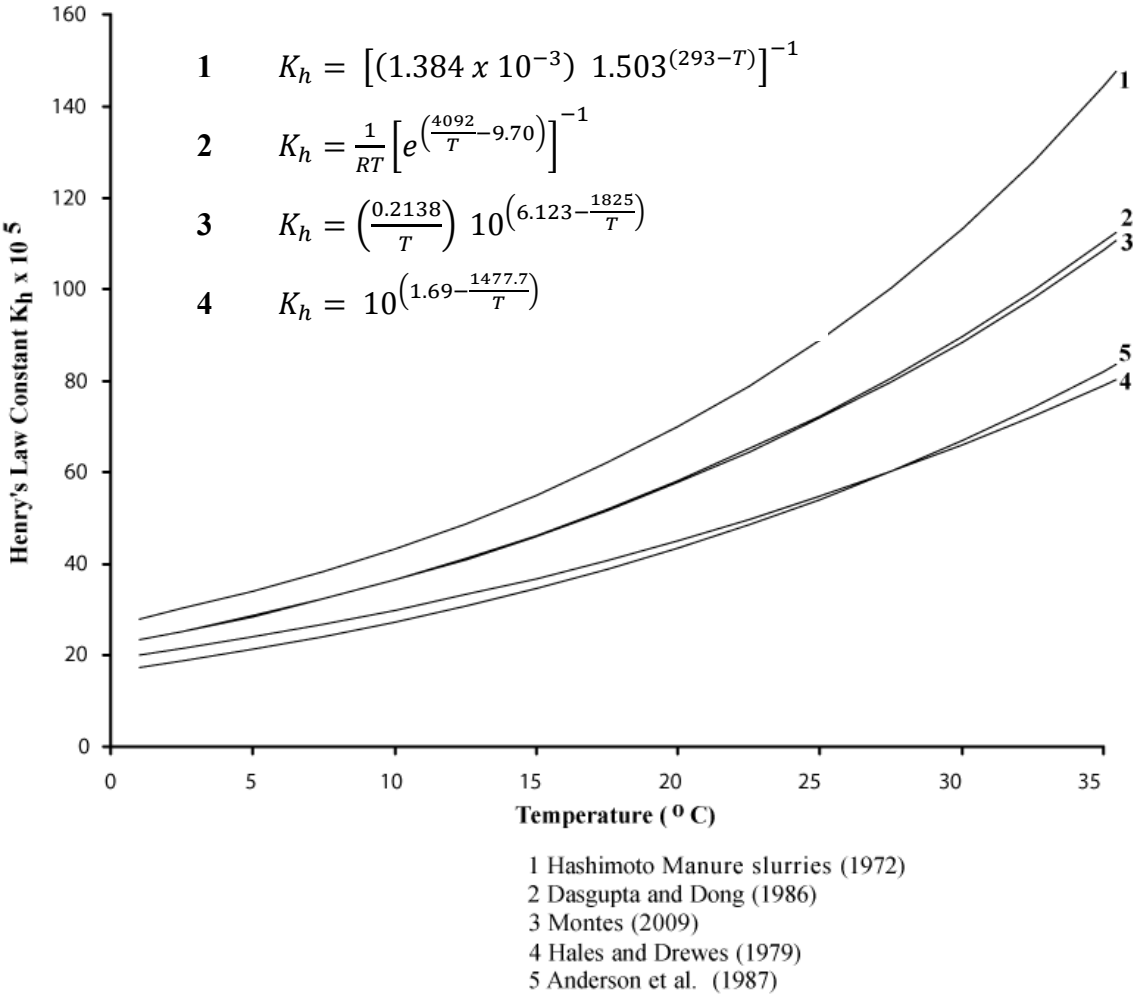

Figure 1.13. Comparison of Henry constant literature values from ammonium solutions and animal waste. Modified and shown with permission from reference (*17*).

Objectives:

1) The first objective is to assess if N isotopes can be used to identify sources of ammonia contributing to N deposition in RMNP. Chapter two will focus on isotope characterization of emission sources and receptor sites.

2) The second objective of this research is to develop and adapt a laboratory system capable of studying ammonia emissions from soil surfaces, such as, CAFOs and RMNP. Chapter three focuses on analysis of ammonia emissions from soils in sub-alpine ecosystems and effects of ammonium wet deposition on short term enhancement of ammonia emission.

3) The third objective is to measure the Henry and acid dissociation constants in animal waste. Chapter four focuses on measurements of Henry constants and acid dissociation constants in CAFO matrices. Chapter five focuses on determining reaction rates and activation energy of urea hydrolysis within the CAFO matrices.

CHAPTER TWO

Assessing the Efficacy of Nitrogen Isotopes to Distinguish Colorado Front Range Ammonia Sources Affecting Rocky Mountain National Park [1]

2.1 Introduction

Reactive nitrogen (Nr) is produced in increasing amounts as a result of to the demands on energy consumption (combustion of fossil fuels, etc.) and food production (fertilizer production, etc.) (*110*). Moreover, Nr originates from many different sources including transportation, agriculture, power plants and industry (*41*). Nr plays a pivotal role in numerous ecosystem properties by restraining productivity (*42*). Inputs of Nr into elevated ecosystem often lead to increased productivity resulting in eutrophication; continuous introduction of Nr can cause high levels of nitrate in surface water and soil acidification (*43, 44*). Nr is deposited into ecosystems by wet deposition and dry deposition. Deposition of Nr has been demonstrated in the western United States due to increases in human activity including agricultural, industrial and suburban development (*26, 41, 111*).

Ammonia is one form of nitrogen (N) and is the most abundant basic gaseous species in the atmosphere (*112*). Primary sources of ammonia are livestock production, fertilizer use, and fossil fuel consumption (*41*). Ammonia plays an important role in neutralizing acidic gases (nitric acid and sulfuric acid) through the formation of aerosols (*113*). Different atmospheric residence times have been reported for ammonia gas and ammonium aerosols (*114, 115*)

[1] The work presented in Chapter 2 was modified from prepared documents for submission to the Journal of Atmospheric Environment. Special thanks to Dr. Jay Ham, Dr. Doris Chen, Christina Williams, Dr. Katie Benedict, Damaris Roosendaal, Dr. Jeffrey L. Collett, Jr., and Dr. Gina McKee. Work presented herein includes denuder preparation, extraction, and concentration measurements by Dr. Doris Chen, and mapping by Dr. Gina McKee

Aerosol particles have low deposition velocities and long transport compared to gases with reported travel distances as high as 2500 km which may result in negative effects in pristine areas (*36, 37*). Moreover, ammonia and ammonium are water soluble and can be scavenged within cloud droplets or scavenged in falling precipitation below the cloud.

In particular, sub-alpine ecosystems are vulnerable to small increases in N deposition, which can lead to negative effects at rates as low as 3-5 kg N ha^{-1} yr^{-1} compared to background rates at 0.2 kg N ha^{-1} yr^{-1} (*46, 52, 116*). RMNP is one such ecosystem adversely affected by increases in Nr. East of RMNP is home to one of the most rapidly expanding human populations in the country (*48*) and northeastern Colorado is one of the most productive agricultural regions in the United States (*50*). Recent studies have investigated the sources of Nr in RMNP and it was reported that wet deposition of ammonia, nitrate, dry deposition of ammonia, and wet deposition of organic N were the most important N inputs (*3, 4, 56, 57*).

These studies found that upslope conditions caused by mountain-valley cycles, or synoptic forcing, or both, resulted in large deposition events that primarily affected areas east of the continental divide. Thus, the east side of RMNP was exposed to higher rates of N deposition compared to the west side (*44, 117*). Both measurements and modeling are unable to completely identify sources of Nr (*3, 118, 119*). There is still uncertainty as to how much each source type (native, agricultural, industrial, mobile sources, etc.) contributes to Nr deposition in RMNP.

The use of N isotopes has shown promise in its ability to distinguish N sources (*8, 68*). Moreover, isotopic tracers of N measured in precipitation, surface water, and gas samples have shown promise in identifying emission source contributions, transport, deposition, and/or ecosystem shifts (*14, 59, 62, 80-83, 85*). However, the use of these N isotopes in the past has

been limited due to analytical techniques requiring large sample volumes, with low throughput, and high labor cost.

The major goal of this study is to determine whether the isotopic signature of N can be used as a tracer for ammonia deposited in RMNP by various sources within Colorado. Furthermore, gaseous and aerosol concentrations, and wet deposition were monitored in RMNP to assess if temporal trends in N wet deposition were correlated to the observed isotopic values.

2.2. Materials and Methods

2.2.1 Study Sites and Sample Preparation

The study was conducted from May 2011 to October 2011. Sites were chosen based on the following criteria: all sites 1) must be near a weather station to access local environmental conditions, and 2) must represent a known or suspected source of ammonia or a possible transport pathway. Figure 2.1 shows the eight field locations and Table 2.1 includes site descriptions. All gaseous ammonia samples were collected using phosphorous acid impregnated polyethylene cartridges (Sigma Aldrich, RAD168, Saint Louis, MO) within porous diffusive bodies called radiellos (Sigma Aldrich, RAD1201) mounted inside inverted high density polyethylene (HDPE) buckets. The radiello is a cylindrical passive sampler composed of an inner phosphorous acid impregnated polyethylene adsorbing cartridge surrounded by a highly resistant, porous polypropylene diffusive body (http://www.radiello.com/english/index_en.html) and has been adopted by the National Atmospheric Deposition Program (NADP) to monitor gaseous ammonia concentrations across the US. This design allows the samplers to be exposed for long integration periods, as well as, be able to tolerate high concentration environments.

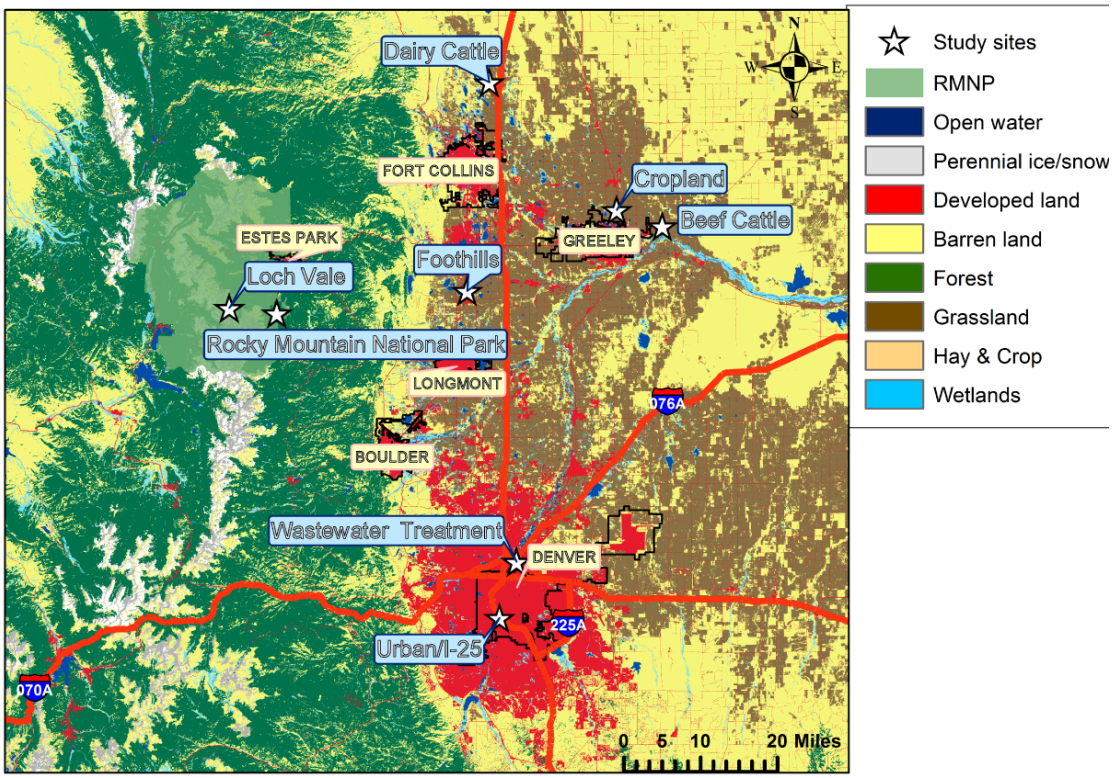

Figure 2.1. Topographical map of radiello locations in the Colorado front range. Sites are shown in white stars. Land usage is shown in the legend on the right. Shown with permission from Dr. Gina McKee.

Table 2.1. Site descriptions for all ammonia sampling radiello locations denoting site type, latitude, longitude, and elevation. Precipitation samples were collected at RMNP and Loch Vale Watershed *denotes Loch Vale Watershed operated by the National Trends Network (CO98).

Site Name	Site Type	Latitude	Longitude	Elevation *(m)*	Site Description
RMNP	Receptor	40.2783°	-105.5457°	2784	Pristine ecosystem 11 km SSE of Estes Park
Beef Cattle	Animal Production	40.4434°	-104.5953°	1420	Perimeter of feed yard within 10 m of holding pen
Dairy Cattle	Animal Production	40.7160°	-105. 0226°	1585	Center of operation between milking parlor and housing
Urban	Urban/Mobile Sources	39.7040°	-104.9976°	1580	Commercialized area near busy interstate
Wastewater	Wastewater Treatment	39.8098°	-104.9558°	1580	Center of WWTP treating both industrial and residential
Cropland	Agricultural	40.4746°	-104. 7080°	1449	Rural location between two small towns, surrounded by cropland
Foothills	Transport	40.3219°	-105. 0770°	1533	Rural near no known ammonia source
Loch Vale Watershed*	Receptor	40.2878°	-105.6628°	3159	Pristine ecosystem east of continental divide

Radiellos were deployed for two week, and monthly integrations, or both. Samples were collected from both beef and dairy CAFOs, cropland, a major wastewater treatment plant (WWTP), treating both industrial and residential waste, near a busy interstate/commercialized area (urban), at a rural location (foothills) with no known ammonia sources, and within RMNP. All radiello sites are within approximately ninety km of RMNP. Upon collection, samples were transported to the lab and extracted using 18.2 MΩ water, and kept frozen until analysis. Additionally, at the RMNP site, weekly integrations of NH_3, HNO_3, and SO_2 gas concentrations and NH_4^+, NO_3^-, SO_4^{2-} aerosols were collected using URG (Chapel Hill, NC) annular denuders/filter packs (*120*). Air was drawn (10 L min^{-1}) through a Teflon-coated cyclone (D_{50} =2.5μm) and passed through two annular denuders followed by a filter pack, and a backup NH_3 denuder. The first denuder was coated with sodium carbonate for collection of nitric acid and sulfur dioxide (*56*). The second denuder and backup denuder were coated with phosphorous acid for collection of ammonia gas. The filter pack collects particles using a Nylon (PALL nylasorb, 1 μm) filter. The backup denuder collects any volatilized ammonia off the nylon filter (*63*). Weekly integrations of wet deposition were collected using an automated precipitation collector (N-CON Systems Company, 00-120-2, Crawford, GA).

2.2.2 Chemical Extraction and Analysis

Radiello cartridges were soniciated in 18.2 MΩ water and analyzed following the Ammonium Monitoring Network (AMoN) protocol (http://nadp.sws.uiuc.edu/nh3Net/). Ammonium was measured using an ion chromatograph (Dionex, ICS 2100, Sunnyvale, CA,) utilizing a CS-12a analytical and guard column for separation, a CSRS 300 4-mm suppressor, and a DS6 heated conductivity detector. Radiellos have been shown to underestimate ammoniaconcentrations by 37% at low (<8 ppbv) concentrations (*121*) and 15% at 20 ppbv

(*122*). Thus, all ambient ammonia concentrations (ppbv) were determined using equation 2.1 with a corrected flow rate (Q) using ambient temperature and pressure (*122*).

$$C_{ppbv} = 0.944 \frac{m_{\mu g\ NH4}}{Q(t)} 1{,}000{,}000 \frac{24.465}{17.031} \quad \text{(Eq 2.1)}$$

2.2.3 Isotope Preparation and Analysis

The radiello extracts should contain primarily ammonium; however, all wet deposition samples contain other forms of N, such as, nitrate and organic N. To ensure accurate measurements of only ammoniacal-N, the aqueous samples were diffused onto acid impregnated filters (*5*). A filter pack was created using two Teflon membranes (Millipore, LCWP02500, Darmstadt, Germany) and a phosphorous acid (Acros-Organics, AC20115-5000, Geel, Belgium) impregnated Whatman 42 filter. Ammonium samples were placed in HDPE bottles, made brackish by adding ACS grade sodium chloride, a filter pack was added, and the samples were adjusted to a pH of 9.4 by adding ashed ACS grade magnesium oxide. Bottles were shaken for two weeks at 40 °C in an incubated shaker. Isotopic standards USGS-25 and IAEA-2 were diffused to correct for isotopic fractionation during the diffusion process. The N isotopes of ammonium impregnated filters were determined at Colorado State University by a Carlo Erba NA 1500 (Milano, IT) elemental analyzer coupled to a VG Isochrom continuous flow Isotope Ratio Mass Spectrometer (IRMS) (Isoprime Inc., Manchester, UK). δ^{15}N‰ is calculated according to equation 1.3. Due to the constraints caused by low masses in some radiello samples, ammonium samples were oxidized to nitrite using a hypobromite solution (*62, 123*). Nitrite samples were denitrified to N_2O using *Pseudomonas aureofaciens* (*124*) and analyzed on a Delta V isotope ratio mass spectrometer interfaced to a GasBench online gas preparation and introduction system at University of California-Riverside.

2.2.4 HYSPLIT Modeling

HYSPLIT (http://ready.arl.noaa.gov/HYSPLIT.php) modeling was used to assess source area influences during each wet deposition integration period (*125-129*). Twenty-four hour back trajectories were modeled using North American Mesoscale at a 12-km resolution (NAM12) starting at 500 m above the earth surface modeling vertical velocity. This resulted in eight trajectories for every 24 hours period originating near Berthoud, CO, USA (40.31°, -105.08°) location. Back trajectories were modeled for all weeks wet deposition was collected in RMNP.

2.3. Results

2.3.1 Ammonia Concentration

The average ammonia concentrations fall into two groups 1) CAFO sources and 2) other sources (Figure 2.2). CAFO sources had the 1st and 2nd highest average ammonia concentrations, ranging from 183 ppbv to 717 ppbv; over an order of magnitude larger than non-CAFO sources. Beef cattle average ammonia concentration decreased over the sampling period with the highest concentration nearly four times larger than the lowest concentration. Wastewater treatment plant's average ammonia concentration was third highest among sampled sites (24.1 ppbv), and showed variability with the highest concentration in late July. Cropland exhibited similar trends with an average concentration of 16.0 ppbv. The ammonia concentration at the foothills site decreased over the sampling period with ambient concentrations between 6.24 and 12.2 ppbv**.** Urban sources had the second lowest average ammonia concentration (7.05 ppbv) and demonstrated no overall trend over the study. The ammonia concentration at the RMNP remained low with an average of 0.565 ppbv and a range of 0.392 to 0.933 ppbv. No significant difference was observed for average concentrations between two week and monthly integrations

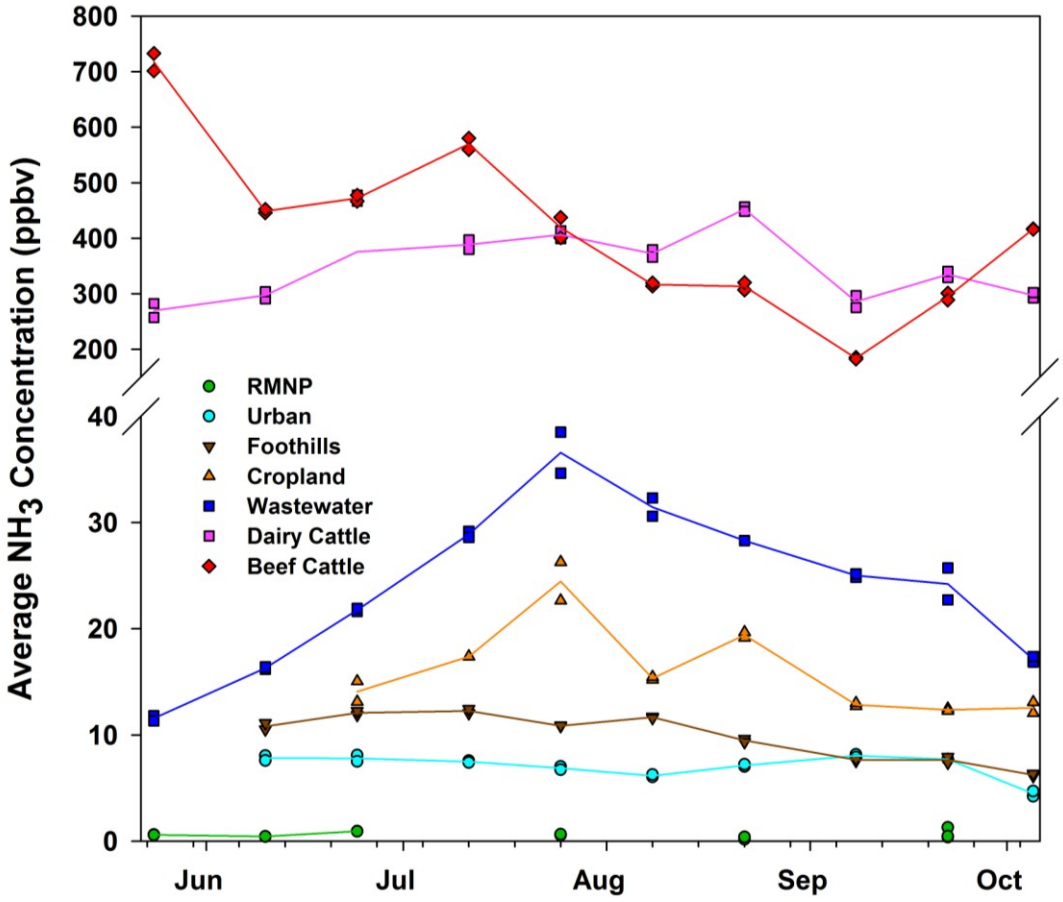

Figure 2.2. Time series of ammonia concentration (n=2,4) over the study period, (May-Oct. 2011). Points represent two week integration periods, except for RMNP−monthly integrations.

($p < 0.05$). Trace gases and aerosols were collected in RMNP to assess phase apportionment (Figure 2.3). The mean concentration of ammonia collected from annual denuders was 0.628 ppbv and ranged from 0.551 to 0.701 ppbv. Average ammonia concentrations collected from denuders and radiellos were not significantly different for monthly integrations ($p = 0.048$). Gas fractions ($NH_3/(NH_3+NH_4^+)$, $HNO_3/(HNO_3+NO_3^-)$, $SO_2/(SO_2+SO_4^{2-})$ μmol m^{-3}/ μmol m^{-3}) of total gas and aerosol concentrations ranged from 0.28 to 0.69, 0.23 to 0.66, and 0.22 to 0.93 for NH_3, SO_2, andHNO_3, respectively. The ammonia fraction varied over the sampling period and was correlated to average temperature ($r^2 = 0.65$; $p < 0.001$). Total concentrations (gas and particle phases) ranged from 0.017 to 0.041, 0.005 to 0.023, and 0.003 to 0.010 μmol m^{-3} for reduced N, sulfur species, and oxidized N, respectively. The average total concentrations for NH_3/NH_4^+, SO_2/SO_4^{2-}, and HNO_3/NO_3^- were 0.686, 0.435, and 0.163 ppbv, respectively. Investigating particle correlations, the $NH_4/(SO_4+NO_3)$ (μeq m^{-3}/ μeq m^{-3}) ratios were close to 1, varying from 0.70 to 1.1 (Figure 2.4). In contrast, the NH_4/NO_3 ratios varied widely (2.9 to 20) over the study period; however, ammonium is strongly correlated with sulfate ($r^2 = 0.65$; $p <0.001$). NH_4/SO_4 (μeq m^{-3}/ μeq m^{-3}) ratios vary from 0.80 to 1.6 with the larger ratios occurring early in the study (May).

2.3.2 Ammonia Isotope Ratios

Ammonia isotopes were measured to assess if differences existed among sources to allow for tracking of ammonia pollution (Figure 2.5). Table 2.2 summaries all the sources characteristic observed over the study. This study showed a spread of $\delta^{15}N$‰ values from various different sources, however, all sources, on average, are depleted in ^{15}N. Beef cattle, dairy cattle, and cropland mean isotopic values were -20.9‰, -28.2‰, and -26.4‰, respectively. Moreover, the WWTP was the most depleted at -35.7‰. The urban site was near a busy

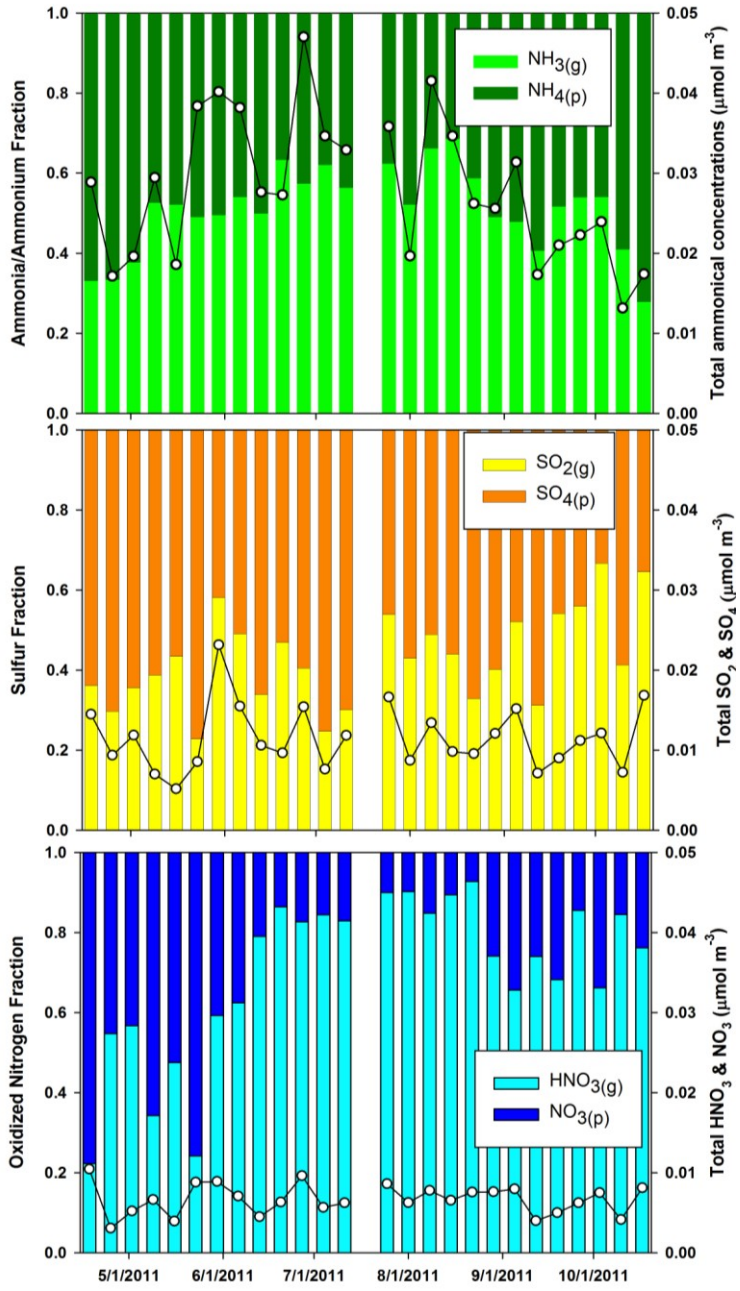

Figure 2.3. Average weekly speciation of ammonia/ammonium, sulfur dioxide/sulfate, and nitric acid/nitrate (µmol m^{-3}/µmol m^{-3}) from URG samplers at the RMNP site. Total gas and particle concentration (µmol m^{-3}) is shown on the right axis. July 18th is unavailable because of an electric outage during sampling.

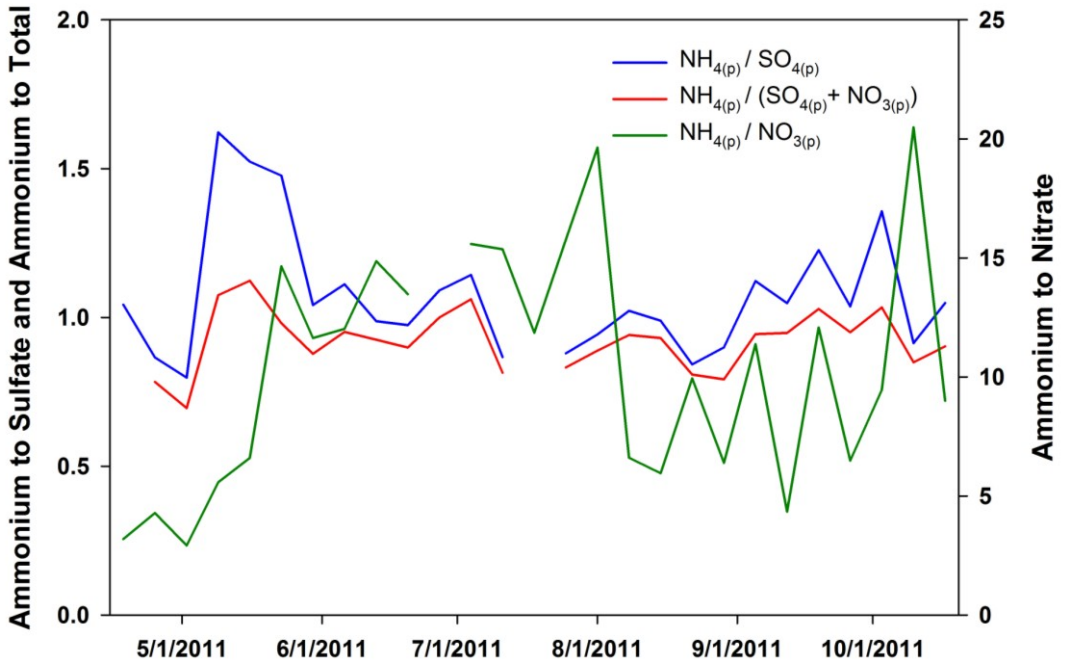

Figure 2.4. Average weekly particle ratios demonstrating ammonium association with sulfate, nitrate, and total sulfate and nitrate. Ammonium to sulfate (blue) and ammonium to total sulfate and nitrate (red) are shown on the left axis. Ammonium to nitrate (green) is shown on the right axis.

Table 2.2. Average values of two week and monthly integrations of $\delta^{15}N\text{-}NH_3$ (‰) values for gas sampled from radiellos. Standard deviation is the pooled value from $\delta^{15}N$ (‰) analysis and radiello samples.

Site Name	Two Week Sample			Month Sample		
	Average (‰)	Standard Deviation (‰)	Sample Value (n)	Average (‰)	Standard Deviation (‰)	Sample Value (n)
Urban	-16.9	8.5	15	-17.4	9.2	5
Foothills	-22.4	7.3	13	-22.0	8.8	5
Cropland	-26.4	2.9	9	-22.9	3.0	5
Wastewater Treatment	-35.7	3.4	10	-33.8	3.8	7
Dairy Cattle	-28.2	3.7	15	-26.0	4.0	7
Beef Cattle	-20.9	3.6	16	-21.0	3.2	6
RMNP	-	-	-	-29.9	3.7	8

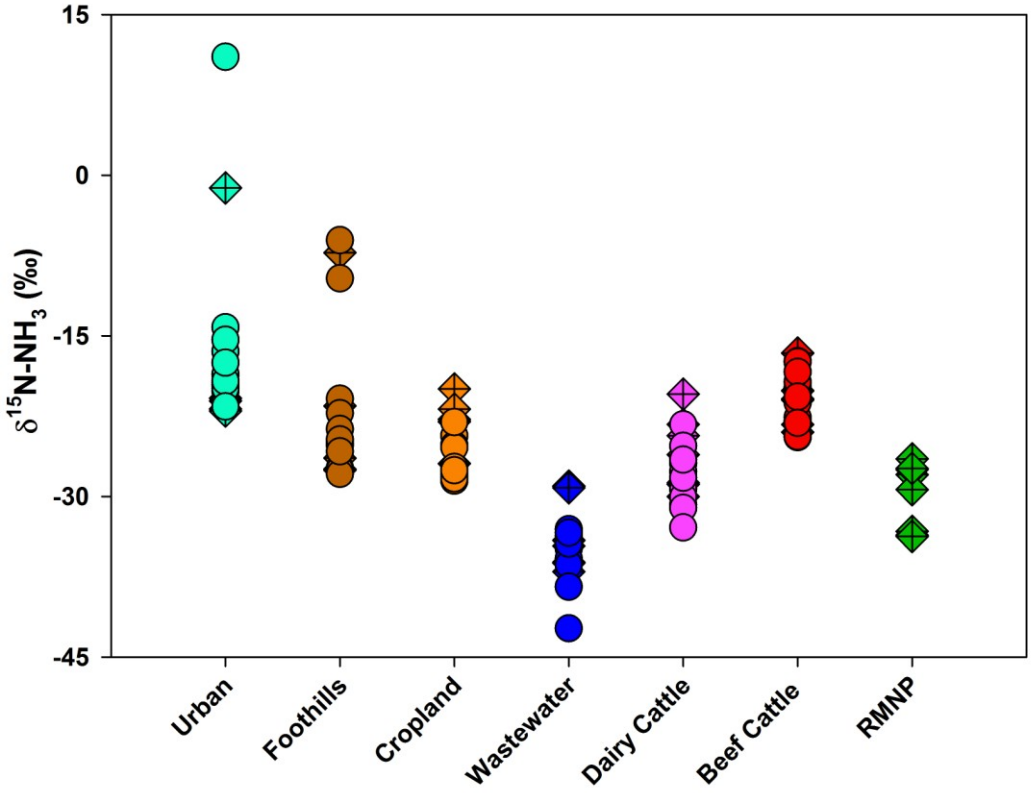

Figure 2.5. Comparison ammonia nitrogen isotopes for radiello sites sampled from two-week (circle) and monthly (crossed-diamonds) integrations in the Colorado Front Range.

interstate/urbanized area and attempted to capture mobile sources. The urban site had the highest values at -16.9‰, while the foothills site was -22.4‰. RMNP was the second most depleted site at -29.9‰. Many δ^{15}N‰ samples were significantly different and are summarized in Table 2.3 ($p < 0.05$). In general, agricultural related sources have limited variation throughout the study period. However, the foothills site exhibited a bi-modal distribution early in the study period ranging from -6.1‰ to -28.0‰ (Figure 2.6). Urban showed one large outlier at 11.0‰ at the end of June. The monthly integration during this period (-1.18‰) showed the same behavior. Comparisons between monthly to two-week isotopic values were not significantly different ($p < 0.05$).

Table 2.3. Significant $\delta^{15}N‰$ source difference over the study. All sources except RMNP were compared by two-week samples. RMNP was compared to monthly $\delta^{15}N‰$ values. x indicates redundancy, * indicates significantly different, and no symbols indicates not significantly different.

	Urban	Foothills	Cropland	Wastewater Treatment	Dairy Cattle	Beef Cattle	RMNP
Urban	x	x	x	x	x	x	*
Foothills		x	x	x	x	x	*
Cropland	*		x	x	x	x	*
Wastewater Treatment	*	*	*	x	x	x	
Dairy Cattle	*	*		*	x	x	
Beef Cattle			*	*	*	x	*

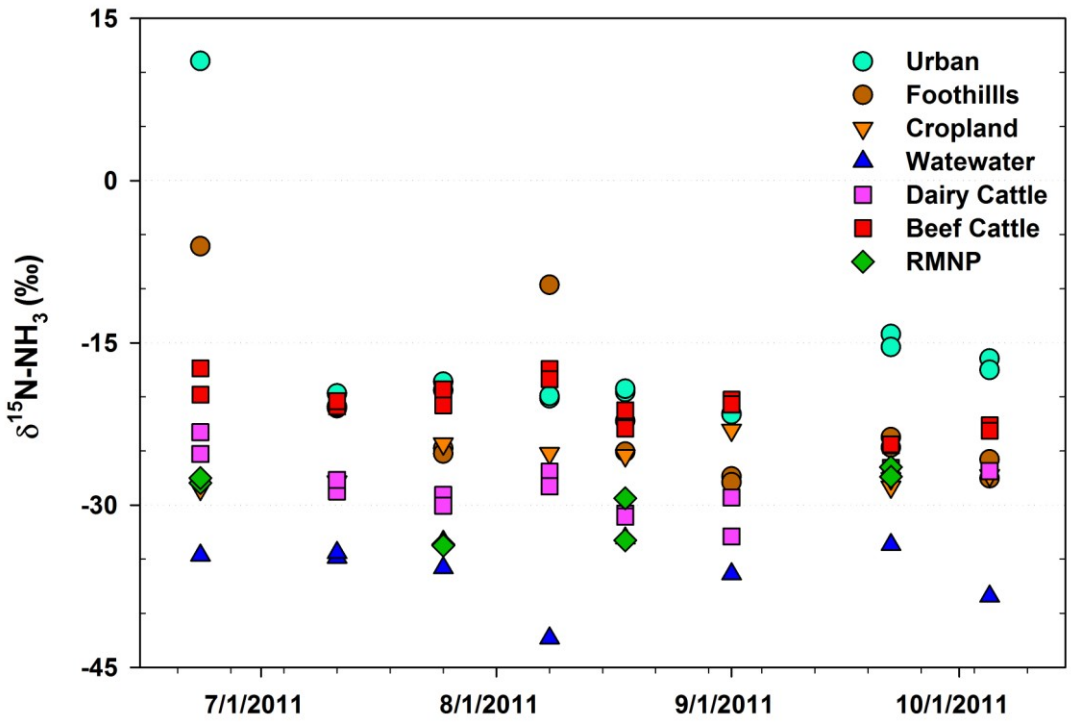

Figure 2.6. δ^{15}N-NH_3 (‰) isotopic values for two week integrations at each sampling site from June to October 2011. RMNP (green) represents monthly integrations.

2.2.3 Ammonium Isotope Ratios in RMNP Wet Deposition

In addition to gaseous δ^{15}N-NH_3 measurements, collected wet deposition was measured at the RMNP receptor site for thirteen of the twenty-six monitored weeks (Figure 2.7) to assess changes in source contributions. In general, δ^{15}N-NH_4^+ values at the RMNP site remained between -3.2‰ and -8.9‰, however, the weeks of May 9th (-15.2‰) and 16th (-12.7‰) illustrated much lower values compared to the study period. Moreover, samples from Loch Vale Watershed (National Trends Network, CO89) were obtained for comparison to the RMNP site (Figure 2.7). Loch Vale Watershed lies 374 m higher than the RMNP site. The number of samples (n=4) analyzed was smaller due to lower ammonium deposition at Loch Vale Watershed; however similar trends in weekly deposition were observed (Figure 2.8). With this

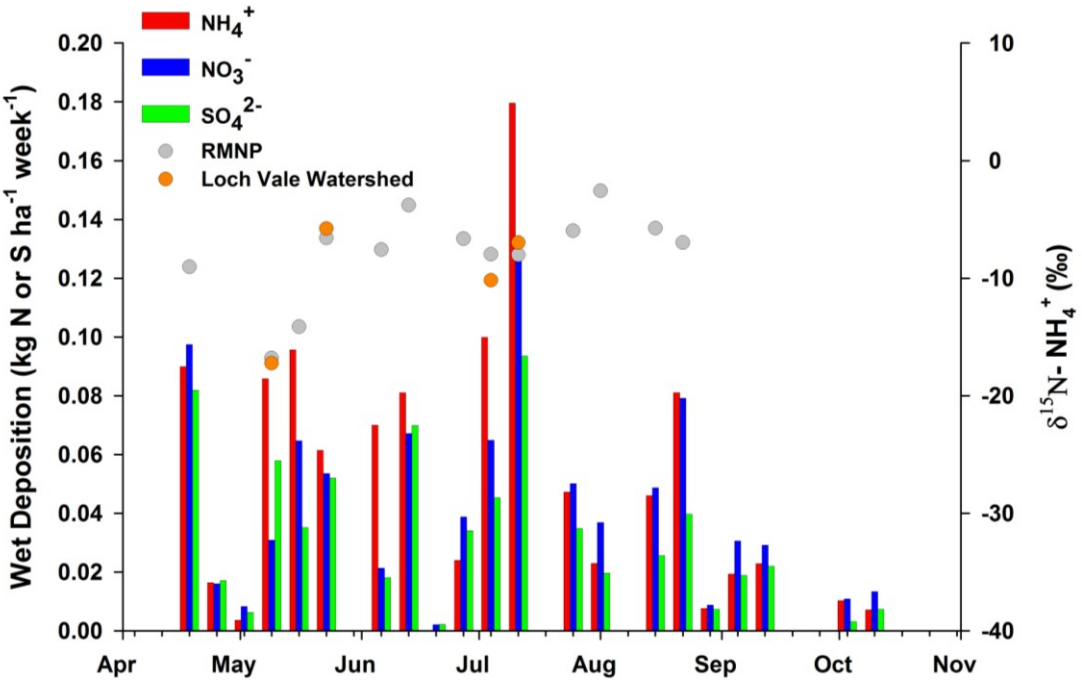

Figure 2.7. Comparison of nitrogen wet deposition measured in RMNP during the field study of 2011. Ammonium isotopes from Loch Vale Watershed (orange circle) and RMNP (gray circle) wet deposition are shown on the right axis. Ammonium (red), nitrate (blue), and sulfate (green) collected in wet deposition.

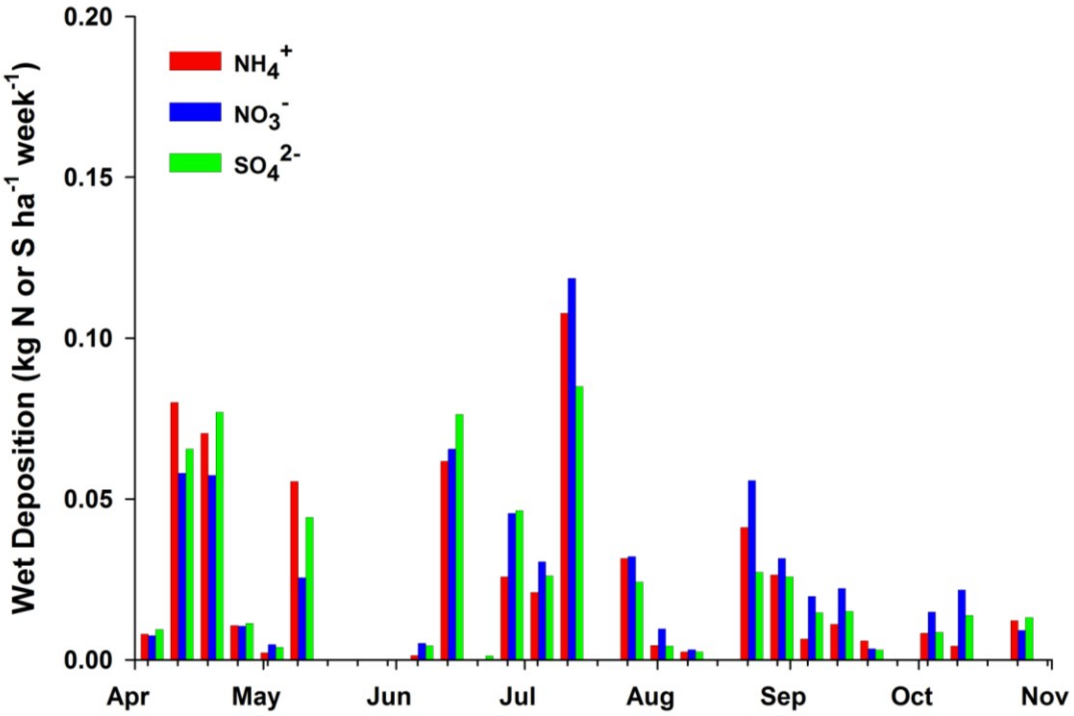

Figure 2.8. Weekly wet deposition of ammonium (red), nitrate (blue), and sulfate (green) at Loch Vale Watershed during the study period in 2011. Data was compiled from National Trends Network (Site CO98).

limited information, the δ^{15}N‰ values exhibited similar values when comparing week to week including the week of May 9th. Only the July 4th δ^{15}N‰ values differed more than analytical error (0.73‰) (*5*) between RMNP and Loch Vale Watershed.

2.4 Discussion

2.4.1 Gaseous and Aerosol Concentrations

Average ammonia concentrations measured at feedlots were similar compared to other measurements (93.3 – 2011 ppbv) at similar sites (*13, 130-134*). Factors affecting ammonia concentration beyond meteorology include sampling height, changes in site management practices, and number of animals (*133*). This sampler was placed on the perimeter of the site within 10 meters of the pens. The beef feedlot pen nearest to the sampler was emptied early in

the study which most likely had an effect on the average ammonia concentration over the study period.

Wastewater treatment and cropland ammonia concentrations varied over the sampling period. Wastewater ammonia concentrations were correlated with average temperature at the site ($r^2 = 0.41$; $p = 0.045$). Wastewater and cropland ammonia concentrations were higher than other sources of ammonia, excluding animal production. To our knowledge, no gaseous ammonia concentrations have been reported previously in the literature from a WWTP. The average cropland ammonia concentration (16.0 ppbv) in this study was slightly higher to previous measurements over various cropland (3.2 -11 ppbv), however, it is unknown if these areas in this study were fertilized during the study period (*135*). Moreover, this study closely matched rural agricultural concentrations (10 ppbv) measured at similar sites in the Front Range (*122*).

Urban, foothills, and RMNP ammonia concentrations varied little over the sampling period. Urban ammonia concentrations were similar to background urban concentrations (average = 5.2 ppbv) measured within a park in Rome, Italy (*136*), but were larger than street level concentrations (2.4-3.8 ppbv) measured in Manchester, UK (*137*). Furthermore real-time measurements of ammonia measured in Georgia, USA from car exhaust were lower on average (1.35-3.32 ppbv) (*138*). The foothills site is probably more analogous to measurements in rural areas not associated with agriculture in the Front Range. Measurements were found to be less than 8.6 ppbv (6 μg m^{-3}) (*122*) while measurements in a suburban area were 5-7 ppbv (0.2-0.3 μmol m^{-3}) (*57*).

RMNP average ammonia and ammonium concentrations were low in comparison to all other regions; although, they were similar to measurements made previously at this site (*3, 56, 57, 139*). Moreover, concentrations of sulfur dioxide, sulfate, nitric acid, and nitrate were similar

to measurements made at the site by CASTNET (ROM 406). The strong correlation between ammonium and sulfate compared to ammonium and nitrate can be explained by the phase equilibria of these particles. Ammonium nitrate equilibrium is to be dependent on humidity and temperature affecting partitioning with the gas phase (*39*). Ammonium sulfate is not sensitive to changes in humidity and temperature (*40*) under atmospheric conditions. Humidity and temperature have opposing diel trends. This behavior will enhance ammonium nitrate partitioning to the gaseous nitric acid and ammonia of during daytime hours. Ammonium nitrate partitioning to gaseous forms resulting from increases in temperature and deceases in humidity will decrease the NO_3^-/NH_4^+ ratio and reinforce the observed correlation between ammonium and sulfate aerosol.

Variation in wind direction and wind speed can drastically affect the concentration and consequently $\delta^{15}N‰$ results in mixed source areas. Meteorological effects on average ammonia concentration can be large especially near strong emitters. Because of variable wind directions, samplers were placed near the center of operations when possible. Nevertheless, it can be difficult to speculate as to the cause of increasing or decreasing trends in ammonia concentration.

2.4.2 Gaseous Ammonia Isotopes

Confined animal feeding operations, wastewater treatment, and cropland had similar isotopic values which were expected since the mechanisms for ammonia production and loss are similar (Figure 2.5). Most likely, these source's emissions were dominated by transformation of urea to ammonium by urease activity and/or breakdown of organic matter followed by ammonia volatilization. Both of these processes support depletion of the heavier isotope (^{15}N) in the gaseous product (*13*).

Urban isotopic values were significantly different than some agricultural sources. The isotopic values exhibited a large range (-21.5 to 11.0 ‰) possibly indicating a variety of sources contributing at different periods. Ammonia isotope measurements conducted within urbanized areas are limited, however tunnel studies found vehicle exhaust to measure -4.6 to -2.2‰ (*62*). Ammonia emitted from coal combustion was found to range from -4.3‰ to -7.2‰ (*7*). Additionally, ammonia gas emitted from steel factory coking stacks was -20.1‰ (*11*). Although the average values measured here were similar to steel factories, no known steel factories were near the site. Furthermore, the observed urban isotopic values could be a result from movement of eastern agricultural air into the Denver area. It remains uncertain as to what specific sources would be contributing most to the collected ammonia, but aerosol formation is common in urbanized areas. Aerosol formation generally results in gaseous ammonia becoming depleted (shifts of -5 to -15 ‰) in ^{15}N while the aerosol becomes enriched (shifts of +5 to +15 ‰) in ^{15}N compared to the initial gas (*64*). The presence and extent of aerosol formation may be contributing to depleted isotopic values and the large range observed in this study.

RMNP ammonia isotopes were the 2nd lowest among studied sites. Limited isotopic measurements of ammonia gas have been made at pristine mountain locations. However, the depleted ^{15}N ammonia values gases do indicate impact of depleted local gases (natural and anthropogenic), or aerosol formation, or both. In the literature, agriculture and ammonia volatilization are among the most depleted sources (Figure 1.9); therefore local sources are probably not significant contributors to the observed isotopic value. Upslope flow regimes can transport high concentrations of ammonia and ammonium into RMNP most likely contributing ammonia/ammonium to the airshed (*57*). As stated above, aerosol formation generally results in enrichment in aerosol phases and depletion in gaseous phase of ammonia (*64*). Moreover, annual

denuder integrations NH_3 fractions were shown to be between 40%-60%, indicating the importance of both aerosol and gases in RMNP airshed. These non-local sources of ammonia and ammonium along with aerosol processing most likely result in depletion of ^{15}N ammonia in the gas phase observed in RMNP.

The foothills site was chosen due to its location as a rural location, as well as, the site was north of the city center of Denver, and in between the agricultural northeastern part of Colorado and RMNP. To my knowledge, no ammonia N-isotopic values were available in the literature for rural locations. The foothill $\delta^{15}N‰$ values have the second largest range compared to other sources. The foothills value could be a mixture of urban and agricultural sources; however, only one month (late June to early July) experienced higher isotope values compared to the rest of the study. The higher value observed at the foothills site did occur concurrently with the higher value observed at the urban site indicating a possible correlation between the two sites during this period.

When applying simple mixing models, the difference in $\delta^{15}N$ ratios and source variability strongly dictate the application of isotopic information (*140*). For example, when applying a two source model (average Ag [beef cattle, dairy cattle and cropland] versus mobile sources (*62*) to a suggested resultant mixture (foothills); fractions of 87% (Ag) and 13% (mobile) can be attributed using the data in Table 2.2. However, the 95% confidence intervals around the aforementioned fractions would be ±21%. This is in large part due to the variability within the sources and mixture. Differences in $\delta^{15}N$ between two sources can strongly affect the confidence interval (*140*). This demonstration benefits from the large difference between the differences between the two sources (21.8‰), however the large variance with the source, mixture, or both, produce a large confidence interval (*140*). This demonstrates the limited use of isotopes in an

underdetermined system given the inherent difference between the ammonia sources and their variability. Moreover, a three source system using only one isotopic value is not capable of a unique solution. Ammonia is known to be released from a large variety of sources, and ammonia can be altered during transport (deposition, aerosol formation, etc.). These factors all contribute to an inherently undetermined system further complicating the use of $\delta^{15}N$ as tracers.

2.4.3 Ammonium Isotopes in Wet Deposition

Previous work has shown that wet deposition is the primary pathway for N deposited in RMNP (*3, 56*). Wet deposition represents a combination of gas and aerosol (*64*). Thus, ammonium isotopes were measured in wet deposition to assess if different sources were contributing reduced N during the study period. The ammonium isotope values in wet deposition were similar for most of the 2011 study. The range of observed isotopic values agrees with previous studies in Pretoria South Africa, North Carolina, USA, and Chesapeake Bay, USA (*14, 64, 91*), although, the lower values were most comparable to studies in areas of China and Germany (*7, 15, 90, 92*). Moreover, Loch Vale Watershed and the RMNP site exhibited similar $\delta^{15}N\text{-}NH_4^+$, including the lower $\delta^{15}N\text{-}NH_4^+$, indicating that similar sources contributed ammonium at various elevations.

Beyond the role of emission source differences, many post emission processes can affect the isotopic distribution of N in ammonium. These processes include scavenging rate and aerosol formation. The rate and frequency of precipitation can affect the washout rate of ammonia and ammonium in the atmosphere (*11, 15*). Furthermore, other studies have found correlations between $\delta^{15}N‰$ with precipitation volume, SO_2 concentration (precursor for $(NH_4)_2SO_4$ formation), and temperature (*15*). No trend was observed between the ammonium isotopic value

and SO_2 concentration; although a correlation was observed between ammonium isotopic value with temperature ($r^2 = 0.462$; $p = 0.01$) and precipitation volume ($r^2 = 0.308$; $p = 0.049$).

To investigate aerosol correlations, NH_4/SO_4, NH_4/NO_3, and $NH_4/(SO_4+NO_3)$ ratios were plotted in Figure 2.4. Ammonium and sulfate were strongly correlated over the study period with the exception of May 9th and May 16th. An increase (51% and 42%) was observed in the ammonium/sulfate ratios during these sampling weeks, respectively. The weeks of May 9th and May 16th exhibited lower isotopic values in wet deposition. Denuder measurements of ammonia and ammonium show a relatively equal contribution to the total reduced N concentration (Figure 2.3). Average ammonium and nitrate concentration remained relatively constant while average sulfate concentration dropped 34% and 51% (relative to the average), respectively during this interval. This shift in NH_4^+/SO_4^{2-} ratio might be responsible for this change in isotopic composition. Ammonium sulfate aerosol can become enriched as much as 33‰ compared to its parent gas (*64*). The lack of sulfate associated ammonium aerosol may explain this effect; however, to our knowledge little is known about the aerosol isotopic equilibrium fractionation between NH_4^+ and NO_3^- on ammonium-N isotopes. Another known mechanism for ammonium depletion in wet deposition is frequent rain events over a short interval (<3 days) due to preferential incorporation of the heavy isotope by exchange reactions (*11*). Weekly differences among $\delta^{15}N\text{-}NH_4^+$ sampled from wet deposition showed a relatively constant range of values outside of two sampling dates (May 9th and May 16th). Post emission reactions, mixing, or lack thereof most likely played a role in altering the N isotope values relative to their sources thus limiting the use of the N isotopic composition as a standalone source tracking tool.

2.4.4 HYSPLIT Modeling

To provide additional information to concentration and isotopic information, back trajectory models were used to identify source areas likely contributing to wet deposition in RMNP. HYSPLIT modeling was used to assess spatial influences during each weekly wet deposition integration period. Nearly all of the weeks studied had both easterly (Front Range, CO) and westerly influences. Figure 2.9 shows back trajectories for the week of May 16th, 2011where a low ammonium-N isotope value (-12.7‰) was observed in the wet deposition. Figure 2.10 shows back trajectories for the week of July 11th representing the largest observed deposition of N in this study. Both of these weeks (May 16th and July 11th) experienced similar amount of precipitation (51.7, 44.9 mm), however, the amounts (0.13, 0.52 kg N ha^{-1} week^{-1}) and apportionments of N were largely different with ammonium and organic N dominating on May 16th and July 11th, respectively.

Furthermore, both of these periods showed large contributions from east of RMNP. One observed difference was the residence time of easterly air within the Front Range or near RMNP before wet deposition was observed in RMNP. This delay between sources of ambient ammonia/ammonium moving into more urbanized areas near RMNP and precipitation in RMNP should allow for aerosol formation. This will result in depleted gaseous ammonia and enriched ammonium in aerosol given adequate time. Moreover, ammonia gas has a higher deposition velocity than ammonium aerosols resulting in an increased fraction of aerosol; correlation between elevation and percent aerosol was observed in previous work (*57*). These chemical and physical processes would most likely cause enrichment in ^{15}N in the airshed compared to source emissions.

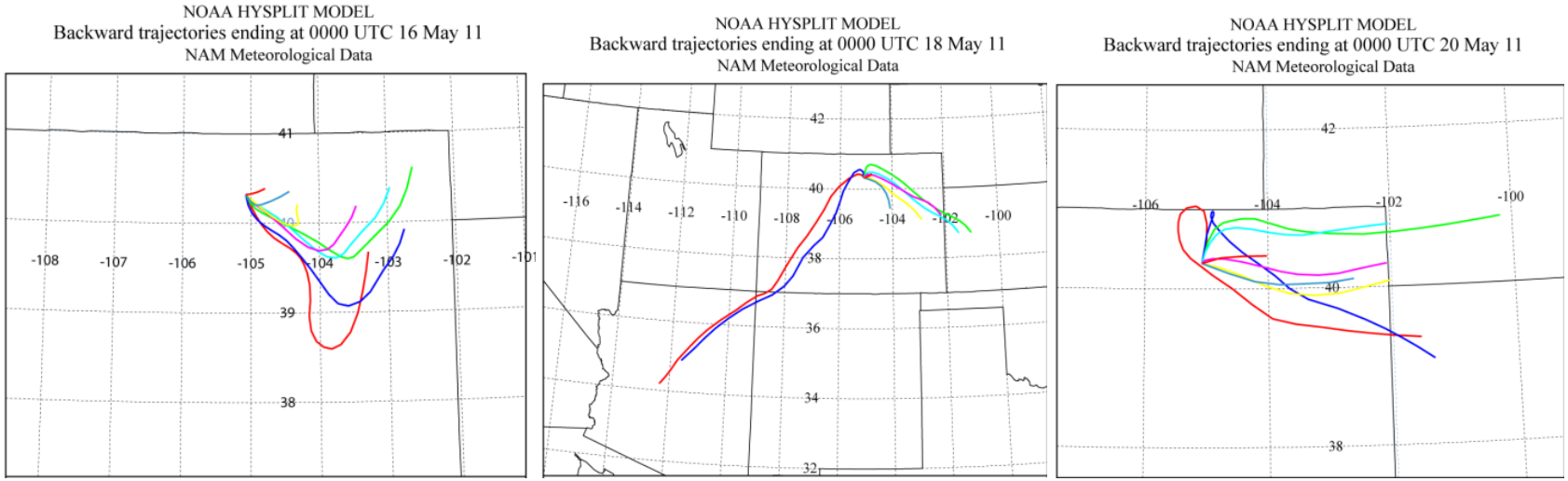

Figure 2.9. HYSPLIT 24 hour back trajectories from Berthoud, CO (40.32° N, 105.08° W) for May 16th , 18th, and 20th, 2011. Each trajectory begins every 3 hours resulting in 8 trajectories in total. Rainfall occurred in RMNP on May 18th, 19th, and 20th.

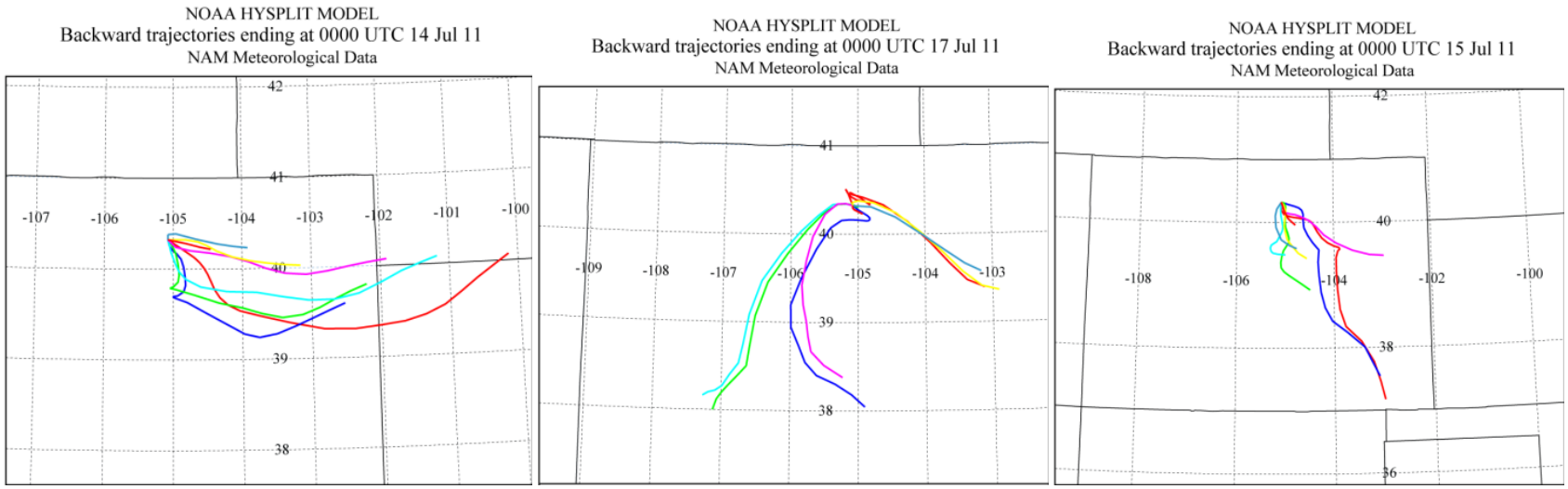

Figure 2.10. HYSPLIT 24 hour back trajectories near Berthoud, CO (40.32° N, -105.08° W for July 14th, 15th, and 17th. Each trajectory begins every 3 hours resulting in 8 trajectories in total. Rainfall occurred in RMNP on July 15th, 16th, and 17th.

During the week of May 16th, 2011, the ammonium/sulfate ratio increases from the overall trend indicating ammonium aerosol association with other species (nitrate or organics). However, organic N was low during this period compared to other deposition weeks. It is likely that the short residence (<24 hours) time does not allow for ammonia gas to deposit via dry deposition, ultimately resulting in the observed low ammonium isotope value. During nearly all weeks easterly flow patterns were observed. However, the long residence time of ammonia/ammonium in the Front Range area (>24 hours) may allow for a shift towards ammonium sulfate associated aerosol and dry deposition of ammonia gas. The NH_4^+/SO_4^{2-} ratios during the week of July 11th, 2011was very close to 0.87, near the average (1.07) observed over the study, indicating possible aging of the aerosol. Furthermore, the ON fraction was the largest amongst the three forms of N (NH_4^+, NO_3^-, ON) indicating influences of different sources and aging of air since water soluble organic N is primarily made through secondary processing in the atmosphere (*141, 142*). HYPSLIT modeling, ammonium sulfate association, and the large amount of organic N likely explain the observed isotopic enrichment.

2.5. Conclusions

Evidence of ecosystem shift is evident in Rocky Mountain National Park (RMNP) due to, in part, deposition of reactive nitrogen (Nr). Identifying the most likely sources of Nr is a priority, but inherently challenging. Thus, the major goal of this study was to determine if $\delta^{15}N‰$ measurements of ammonia and ammonium at various emission sources as well as in RMNP could be used to elucidate the most probable source contribution in order to help guide future N management strategies. $\delta^{15}N\text{-}NH_3$ ratios at agricultural sites were similar to each other, WWTP $\delta^{15}N\text{-}NH_3$ ratios were the most depleted, foothills $\delta^{15}N\text{-}NH_3$ ratios were similar to Ag

suggesting a transported agricultural influence, and urban $\delta^{15}N\text{-}NH_3$ ratios were the highest, but lower than previous work suggesting Ag source influence. RMNP $\delta^{15}N\text{-}NH_3$ ratios overlapped Ag sources but were more depleted, consistent with depletion from aerosol formation known to be important at this elevated site.

Moreover, $\delta^{15}N\text{-}NH_4^+$ measured in wet deposition at RMNP did demonstrate variability during the study period. However, the complexity of interacting sources, phase partitioning, and scavenging made interpreting these ratios challenging. $\delta^{15}N\text{-}NH_3$ ratios had limited use as a standalone tracer for ammonia released from different sources and wet deposition in RMNP; most likely due to post emission reactions and mixing prior to deposition in RMNP. The challenges associated with an inherently underdetermined system (many source types and only one isotope parameter) in combination with the process influence (e.g., from aerosol formation) make standalone use of the isotope information challenging. With some assumptions, however, (e.g., averaging similar Ag values together; ignoring isotopic depletion from aerosol formation) you can gain some insight into the likely importance of different source types (e.g., Ag vs. mobile source emissions) and check source apportionment findings from other approaches. Recommended future studies should include investigating isotope fractionation ammonium nitrate versus ammonium sulfate aerosol formation, higher temporal resolution in $\delta^{15}N\text{-}NH_4^+$ deposited in wet deposition, and parallel measurements of $\delta^{15}N‰$ in gaseous ammonia and ammonium aerosols.

CHAPTER THREE

Ammonia Emissions from Sub-Alpine Forest and Mountain Grassland Soils[2]

3.1 Introduction

The amount of reactive nitrogen (Nr) has continued to increased due to human activity (*110*). Nitrogen (N) emissions come from many sources including transportation, agriculture, power plants and industry (*41*). Among the forms of reactive N, ammonia is an important basic gaseous species in the atmosphere affecting air quality (*112*). Ammonia, emitted from both biogenic and anthropogenic sources, often reacts with sulfuric acid and nitric acid to form aerosols (*113*). The formation of aerosols increase the lifetime and thus results in transport and deposition of Nr over long distances (*2*). These reactive forms of N can be deposited into sensitive ecosystem away from their emission sources (*42, 43*). In particular, rapid expansion of urbanization has increased N deposition in the western United States (*143*). Predicted N deposition rates in the Colorado Front Range vary from 1 to 7 kg N ha^{-1} yr^{-1} (*51*). Recently, reported N deposition values were 3.65 kg N ha^{-1} yr^{-1} (*4*). Current deposition exceeds the critical load for diatom populations, 1.5 kg N ha^{-1} yr^{-1} (*46*) and vegetation, 3.0 kg N ha^{-1} yr^{-1} (*144*), which could adversely affect sensitive ecosystems within RMNP.

The Colorado Front Range (Cheyenne, WY to Colorado Springs, CO) has a rapidly expanding human population that adjoins an agricultural region (*49, 50*) and lies east of the Rocky Mountains. Sub-alpine mountain ecosystems bordering the Front Range are vulnerable to

[2] The work presented in Chapter 3 was modified from documents submitted to the Journal of Atmospheric Environment. Special thanks to Damaris Roosendaal, Dr. Jay Ham, Christina Williams, Dr. Jeffrey L. Collett, Jr., and Kira Schonkwiler-Arnold.

small increases in N deposition (e.g., 3 to 5 kg N ha^{-1} yr^{-1}) (*44*). Observed negative impacts include eutrophication and acidification that can affect surface water, soil chemistry, lake diatom communities, and decreased biodiversity (*52*). These observations led to the RMNP Initiative, whose goal is to study and recommend action on air quality issues facing the park. As part of this goal, the RMNP Initiative has developed a plan to reduce N deposition to 1.5 kg N ha^{-1} yr^{-1} by 2032 (*145*).

The Rocky Mountain airborne nitrogen and sulfur study (RoMANS) study was conducted in 2006 to improve the understanding of N and sulfur deposition, their forms, and their sources (*3*). The RoMANS study, used both measurement and modeling to suggest that local sources contributed 32% of the reduced N wet deposition (18% of total N deposited) during the summer study period (*3*). Local sources encompass the area of RMNP and are designated as naturally occurring ammonia emission from terrestrial and aquatic ecosystems within the park (*3*), with soils being a likely contributor. Source apportionment was conducted using a "weight of evidence" approach by comparing results from varying analyses. RoMANS investigators observed a repeating diurnal pattern in gaseous ammonia concentration within the park suggesting a local temperature-dependent source may be present. (*3*). However, several processes can contribute to the diurnal concentration cycle, including: mountain-valley flow regimes, bi-directional behavior from vegetation, and diel temperature-dependent emissions from soils, etc. (*118, 146, 147*).

Ammonia is produced in soils by mineralization of organic matter and N fixation. Ammonia can sorb to various soil constituents, undergo nitrification, or volatilize into the air. Previous studies have investigated ammonia deposition/emission from managed grasslands and native forests using micrometeorological techniques. (*148-151*). These tower-based techniques

measure the inputs into and out of a forest or grassland ecosystems by measuring above the forest canopy or grassland vegetation. Ammonia deposition and emission varied from –14.1 to 4.7 mg NH_3-N m^{-2} day^{-1} (–0.163 to 0.055 μg NH_3-N m^{-2} s^{-1}) over coniferous forest canopies, and –17.3 to 8.64 mg NH_3-N m^{-2} day^{-1} (-0.200 to 0.100 μg NH_3-N m^{-2} s^{-1}) for grasslands (*148, 149, 151, 152*). Previous studies have also reported net emissions based on bi-directional measurements for both non-agricultural grassland (0.3 kg N ha^{-1} yr^{-1}) and fir forest (0.05-0.14 kg N ha^{-1} yr^{-1}) ecosystems (*32, 153, 154*). Limited research has been conducted to determine ammonia emissions directly from the forest floor. Chamber-based studies reported a large range from 0.002 mg NH_3-N m^{-2} day^{-1} (0.09 kg NH_3 km^{-2} $month^{-1}$) to 9.0 mg NH_3-N m^{-2} day^{-1} (≈3.3 kg NH_3 ha^{-1} $month^{-1}$) for ammonia emissions from pine forest soils (*155, 156*).

Due to the uncertainty in ammonia fluxes from native soils, the goal of this study was to determine the magnitude of ammonia loss in a emission oriented laboratory chamber apparatus from intact soils collected from native sub-alpine grasslands and forests in the RMNP. A sub objective was to investigate the effects of N wet deposition on short term enhancements of soil ammonia emissions. Ammonia emissions from native grassland and forest soils will be put into perspective of measured wet deposition.

3.2 Materials and Methods

3.2.1 Sample Site, Sample Collection, and Preparation

The sampling location was adjacent to Longs Peak Trailhead, Colorado, USA, located roughly 11 km SE of Estes Park, Colorado at 2,743 m above mean sea level. Previous studies have been conducted at this location (CASTNET ROM 406) allowing for comparison and access to meteorological information (*3, 56, 57, 118, 119, 139*). Annual average precipitation at the site

is 405 mm while seasonal average air temperatures range from 14 °C in summer to -4.3 °C in winter. This location has forested and mountain grasslands areas in close proximity. The forest soil samples consisted of alfisols (mixed, superactive, Ustic Haplocryalfs) dominated by Lodgepole pine (*Pinus latifolia*) and Aspen (*Populus tremuloides*) trees. The sampled forest soils included the Oi, A1, and partially the A2 horizons composed of decomposed plant material, gravelly loam, and a gravelly sandy loam, respectively. The grassland soil samples consisted of inceptisol soils having a mica rich sub-surface (paramicaceous, shallow Ustic dystrocryepts). Montane grasslands are usually dominated by *Leucopoa kingii* and *Muhlenbergia montana* in the Colorado Front Range (*157*). The sampled grassland cores included the Oe, A1, and partially the Bw horizons composed of moderately decomposed plant material and organic matter, coarse gravelly sandy loam, and a very gravelly sandy loam, respectively.

Soil samples were taken every two weeks starting on June 20th, 2011, and ended on September 12th, 2011; for a total of seven sampling dates over the summer. Six intact soils from each soil type were taken along a 25 m transect. The forest and mountain grassland transects were 100 m apart. Intact forest and grassland cores were taken from the soil surface using a 12.7-cm deep and 12.7-cm diameter sharpened steel ring. The soils (referred to as cores) were carefully removed from the soil with litter/vegetation as to not disturb the soil surface. The sampled cores were wrapped in foil and placed into low density polyethylene (LDPE) bags. Bagged cores were placed in a cooler for transport and promptly prepared for the experiment at the laboratory.

3.2.2 Chamber Measurements

The multi-chamber system was modeled based on the system used (*158*) to study soil ammonia emissions from livestock systems (Figure 3.1) (more information in Appendix 1). The

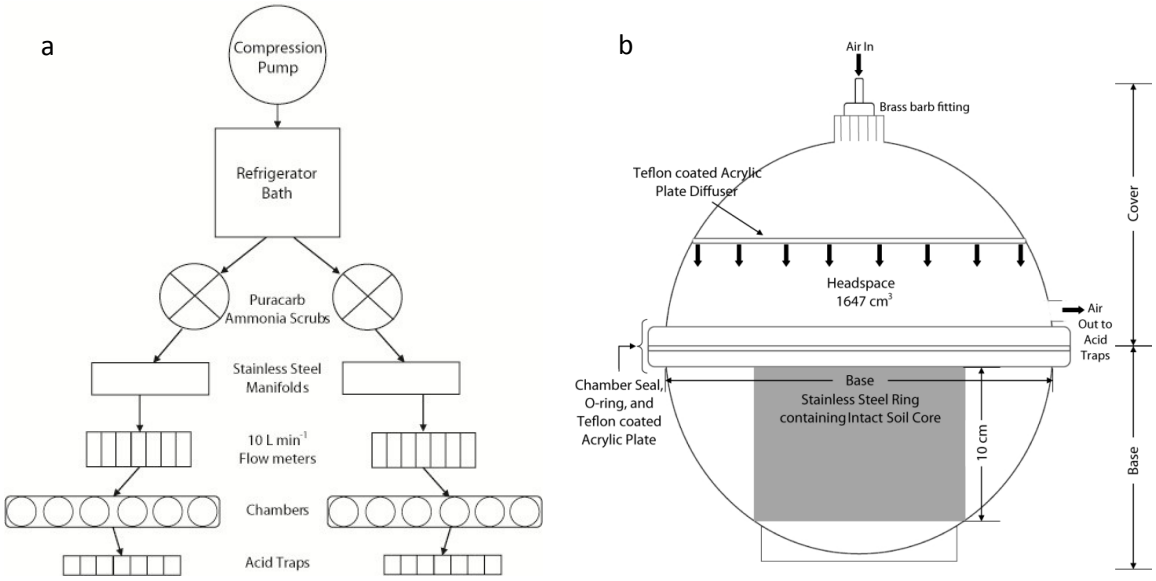

Figure 3.1. Schematic of the dynamic flow-through chamber apparatus (a), and schematic of a modified dessicator showing fitting modification and position of steel ring containing intact soil core (b). Bottom of steel ring was sealed to prevent interaction with airflow.

air supply for the chambers consisted of a compressor pump(Marathon Electric, M550NGX, Wausau, WI) that routed air through a water bubbler assembly that was submerged in a chilled water bath for dew point control. The supply air bubbled through two, half-full 1.5-L water bottles chilled to 11.5 °C (i.e., the desired dew point temperature) which equated to a relative humidity (RH) between 44 and 54 %. The temperature and humidity entering the chambers were verified and logged using a temperature and humidity data logger (Onset Corporation U23-001, Bourne, MA) placed in the blank chamber. The source air was routed to an ammonia scrubber (Purafil: Puracarb AM Media, Doraville, GA) and directed to flow meters (Dwyer, GFM2110AIR, Michigan City, IN) connected to the soil chambers.

Twelve modified vacuum desiccators (Scienceware, *420200000*, Wayne, NJ) served as chambers (Fig.1b) in which the walls were coated with fluorinated ethylene propylene (FEP) tape (CS Hyde, 23-FEP-1.5-36, Lake Villa, IL) to limit ammonia sorption. The intact soil cores

were centered in the desiccators inside the steel ring that was set flush with top of the core (i.e., creating a flat horizontal surface across the entire chamber). Prior to installing the soil core, the bottom of the core was sealed with 2 L LDPE plastic bags taped to the side of the steel rings to prevent ammonia volatilization. The soil experiments were performed at flow rates of 5 L min^{-1} or 3.04 chamber exchanges min^{-1}, which corresponded to an aerodynamic conductance of 10.6 mm s^{-2} as measured using a heat-transfer sensor (*159, 160*) (Figure 3.2).

This conductance is typical for a soil surface within a plant canopy (*161*). Fluorinated ethylene propylene tubing (Ozone Solution, FEP-125x250, Hull, IA) was used for all post chamber tubing connections. Exhaust air from the chambers was routed through FEP tubing to bubbler-style acid traps made from 240 mL glass bottles (Qorpak, GLA-00832, Bridgeville, PA)

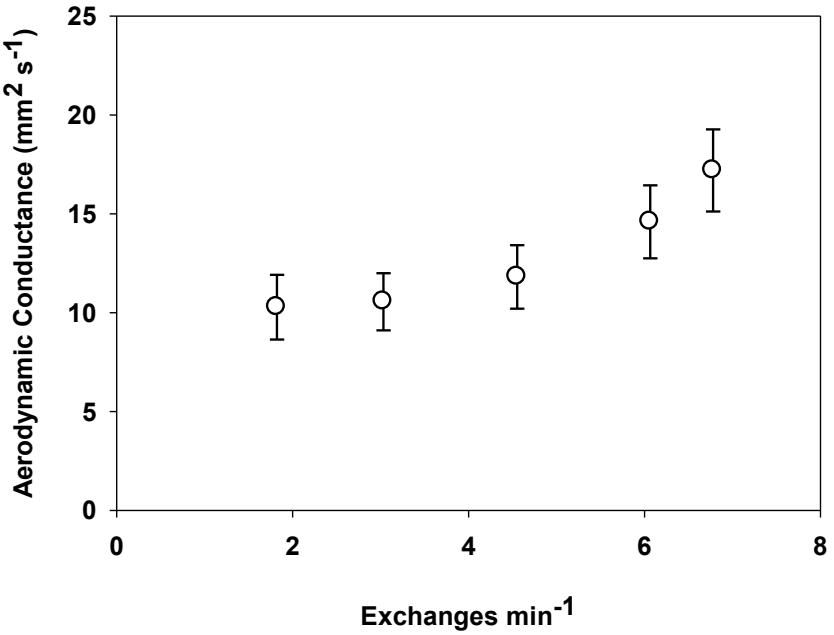

Figure 3.2. Aerodynamic conductance as a function of headspace exchanges per minute. Each measurement is the average of a ten minute exposure. Measurements were made spatially throughout the chamber (n=5).

containing 100 mL 0.05 M phosphorous acid (Acros-Organics, AC20115-5000, Geel, Belgium) to trap and convert ammonia to ammonium. When cores where brought in from the field, chamber measurements were made over a 96 hour time period in which each acid trap was changed every 48 hours. The chambers were cycled with scrubbed air overnight prior to the start of each soil emission experiment to ensure an equilibrated system. The scrubbed air resulted in an average ammonia concentration of 0.008 μmol NH_3 m^{-3} based on integrated mass measurements. Acid traps were weighed before and after each experiment for volumetric calculations. The experimental conditions were within the range of 22.4 (±0.3) to 24.2 (±0.3)°C, relative humidity of 44.0 to 54.1% and dew points of 9.6 to 13.2°C. Intact soil cores were weighed at the start and end of the experiment to assess water loss from evaporation.

3.2.3 Wet Deposition

Weekly wet deposition was monitored at the field site to establish if a relationship existed between large deposition events and ammonia emission. Weekly integrations of wet deposition were collected using an automated precipitation collector (N-CON Systems Company, 00-120-2, Crawford, GA). Bucket blanks were conducted every month. Collected samples were weighed and stored in 1 L HDPE bottles and an aliquot of the collected precipitation was used for pH and speciation measurements. Samples were frozen for future analysis.

3.2.4 Laboratory Simulation of Wet Deposition using Isotopically-labeled Nitrogen

In addition to measuring ammonia emissions from the cores, the chamber system was used to study volatilization following a simulated wet deposition event. The goal was to determine if wet N deposition would enhance ammonia emission from soils in RMNP. Paired soil coring occurred at three sampling locations along each transect from the 2011 study period.

Soil cores were gathered on July 11th, 2012 and prepared in the same manner as stated above. The paired samples were either treated with pure water (denoted zero NH_4^+ deposition henceforth) or an isotopically labeled ammonium solution (denoted high NH_4^+ deposition henceforth). The ammonium in the high deposition (315 μM) was labeled with 10% ^{15}N-ammonium chloride (Sigma Aldrich, 348465, Saint Louis, MO) and diluted with ACS grade ammonium chloride (Fisher Scientific, A661-500, Waltham, MA) to result in a 1-2% ^{15}N tracer. The isotopically-labeled deposition experiment was conducted in order to simulate a large deposition sub-event.

3.2.5 Analysis

Ammonium collected in the multi-chamber bubblers was measured using an ion chromatograph (Dionex, ICS-2100, Sunnyvale, CA) utilizing a CS-12a analytical and guard column for separation, a CSRS 300 4-mm suppressor, and a DS6 heated conductivity detector. All other cations (Na^+, K^+, Mg^{2+}, Ca^{2+},), anions (Cl^-, NO_2^-, NO_3^-, SO_4^{2-}), and ON were determined according previously described methods (*56*).

Soil analysis was performed by combining soil core samples from each location within each transect. Soils were ground, sieved (2mm), composited for all twelve sampling sites, and analyzed at Colorado State University's soil testing lab for total N, organic matter content, ON, exchangeable ammonium and nitrate, and C:N ratio analysis. pH was measured using a microelectrode (Microelectrodes Inc., MI-410, Bedford, New Hampshire).

Isotopes of volatilized ammonia were measured by oxidation to nitrate (*62, 123*) followed by a bacterial denitrification (*124*) at University of California-Riverside's facility for isotope ratio mass spectrometer. Samples were oxidized and denitrified with USGS-25 and IAEA-N-2 standards for correction. Isotope analysis was conducted on a Delta V isotope ratio mass

spectrometer interfaced to a GasBench online gas preparation and introduction system. Isotopic values were given delta notation according to Equation 1.3.

3.3. Theory and Calculation

3.3.1 Predicting Diurnal Temperature Fluctuations on Ammonia Flux

In nature, ammonia emissions are often temperature dependent and tend to follow the diurnal patterns of air or surface temperature. However, all chamber measurements were conducted at room temperature (approximately 22.8 C). However, laboratory results can be scaled to different temperatures using an ammonia volatilization model (Equation 3.1) (*162*). Where J_{vola} (kg m^{-1} s^{-1}) is the flux of ammonia, h_m (m s^{-1}) is the mass transfer coefficient, K_a

$$J_{vola} = h_m \left(\frac{K_a K_H}{10^{-pH}} C_{NH_4^+} - C_{NH_3} \right) \quad \text{(Eq. 3.1)}$$

is the acid dissociation constant, K_H is the Henry constant, $C_{NH_4^+}$ (kg m^{-3}) is the aqueous ammonium concentration and C_{NH_3} (kg m^{-3}) is the gaseous ammonia concentration above the surface. Temperature strongly affects K_a and K_h as predicted using the models of (*17, 105*), respectively.

$$K_a = 10^{\left(0.05 - \frac{2788}{T}\right)} \quad \text{(Eq. 3.2)}$$

$$K_h = 10^{\left(1.69 - \frac{1477.7}{T}\right)} \quad \text{(Eq. 3.3)}$$

The ratio between the fluxes at two different temperatures can then be derived from Equation 3.1 as Equation 3.4; where J_T is the unknown flux at some temperature T, J_{22} is the

$$\frac{J_T}{J_{22.8}} \approx \frac{K_{a,T}\, K_{H,T}}{K_{a,22.8}\, K_{H,22.8}} \quad \text{(Eq. 3.4)}$$

known observed flux at the reference temperature, (i.e., the lab chamber temperature), while the values of K_a and K_h are modeled at T or 22.8 °C using equations 3.3 and 3.4 Equation 3.5 assumes that h_m and pH are independent of T, and that C_{NH_3} is minimally affected by temperature, a reasonable assumption considering that air was scrubbed of ammonia (0.008 μmol m^{-3}) prior to entering the chamber. Thus, equations 3.2, 3.3, and 3.4 allow estimation of a theoretical within-chamber flux, J_T, between 5 and 35 °C using only the emission data collected at room temperature, $J_{22.8}$. The average hourly temperature from June 2011 to September 2011 was used to define a diurnal temperature pattern at the RMNP sampling location. These calculated emissions are not intended to predict absolute emissions from soils in the park, but to demonstrate the relative temperature sensitivity to emissions.

3.4 Results

3.4.1 Soil Analysis

The nitrate concentration (28 mg/kg, 10 mg/kg) and pH (6.0, 5.3) of the grassland soils were significantly different than forest soils ($p < 0.05$) (Table 3.1). Moreover, C:N ratios (3.04, 11.6) and average gravimetric moisture contents (0.072, 0.051) were significantly different in grassland and forest soils ($p < 0.10$). The grasslands did have a large range of average moisture content (0.04-0.11) within the sampling transect. The amount of precipitation measured (349 mm) in the summer was 20% lower than the historical average. Ammonium concentration, organic matter, total N, and ON were not significantly different between the two soils.

Table 3.1. Moisture, C, N, and pH analysis of grasslands and forest soils. Averages of all collected grassland and forest cores (n=7). One standard deviation shown in parentheses. * significantly different $p < 0.05$ ǂ significantly different $p < 0.10$

	Mountain Grassland	***Forest***
Moisture Content (g/g)ǂ	0.072 (0.028)	0.051 (0.0087)
OM (%)	10.25 (5.2)	11.05 (4.1)
Organic N (%)	1.41 (0.72)	0.88 (0.99)
NH_4^+-N (mg/kg)	13.77 (6.23)	10.57 (4.7)
NO_3^-–N (mg/kg)*	27.80 (10)	9.52 (4.8)
Total N (%)	1.41 (0.72)	0.88 (0.99)
***C:N*ǂ**	3.04 (0.77)	11.6 (9.6)
pH*	6.0 (0.27)	5.3 (0.33)

3.4.2 RMNP Soil Ammonia Emissions

For each of the four-day chamber experiments, it was assumed that no significant difference in emissions existed between the first and second 48-hour measurement periods (Figure 3.3). In other words, there was no temporal trend in emissions once the cores were placed in the chambers. Thus, all data will be reported as the average of the two measurement periods (i.e., the 96-h average). The average quantifiable ammonia emission, with confidence intervals, from June 20th to September 12th for grassland (0.45±0.12 mg NH_3-N m^{-2} day^{-1}) was significantly different ($p < 0.001$) than forest (0.21±0.02 mg NH_3-N m^{-2} day^{-1}) soils (Figure 3.4). All NH_3-N samples were detectable (>0.04 mg NH_3-N m^{-2} day^{-1}), but not all were quantifiable (>0.14 mg NH_3-N m^{-2} day^{-1}). The maximum observed emission was in June for sub-alpine forests (0.30 mg NH_3-N m^{-2} day^{-1}) and in August for sub-alpine grasslands (1.8 mg NH_3-N m^{-2} day^{-1}) (the laboratory temperature was 22.8 ^{0} C; Table 3.2).

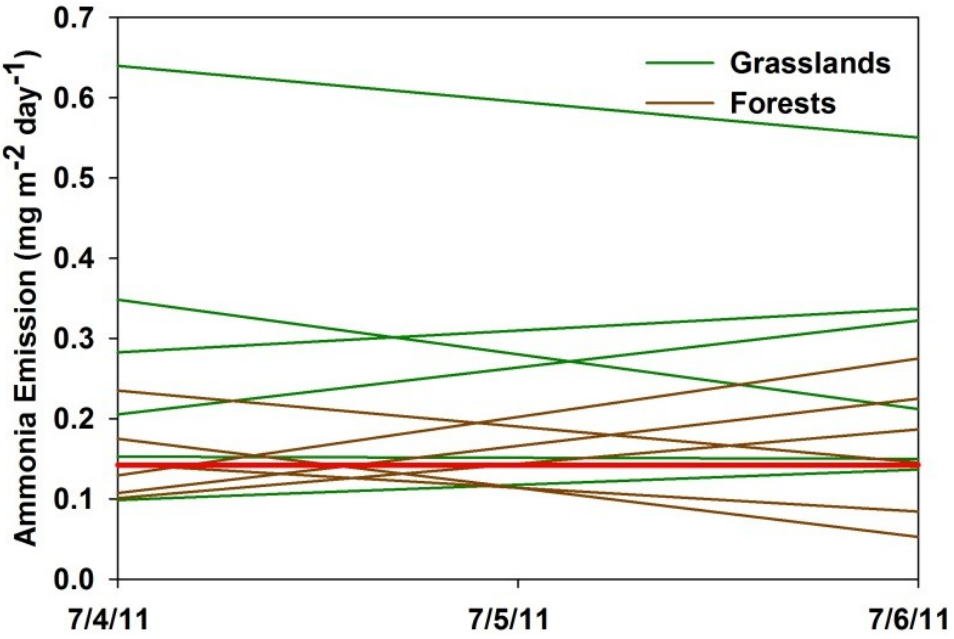

Figure 3.3. Ammonia emissions from grassland and forest soils over the July 4th 2011 emission experiment. The green and brown lines represent ammonia emissions from grassland and forest soils over the study, respectively. Little variation is observed from single cores over the study. This trend is consistent throughout these experiments. The red line indicates the limit of quantification (0.14 mg NH_3-N m^{-2} day^{-1}).

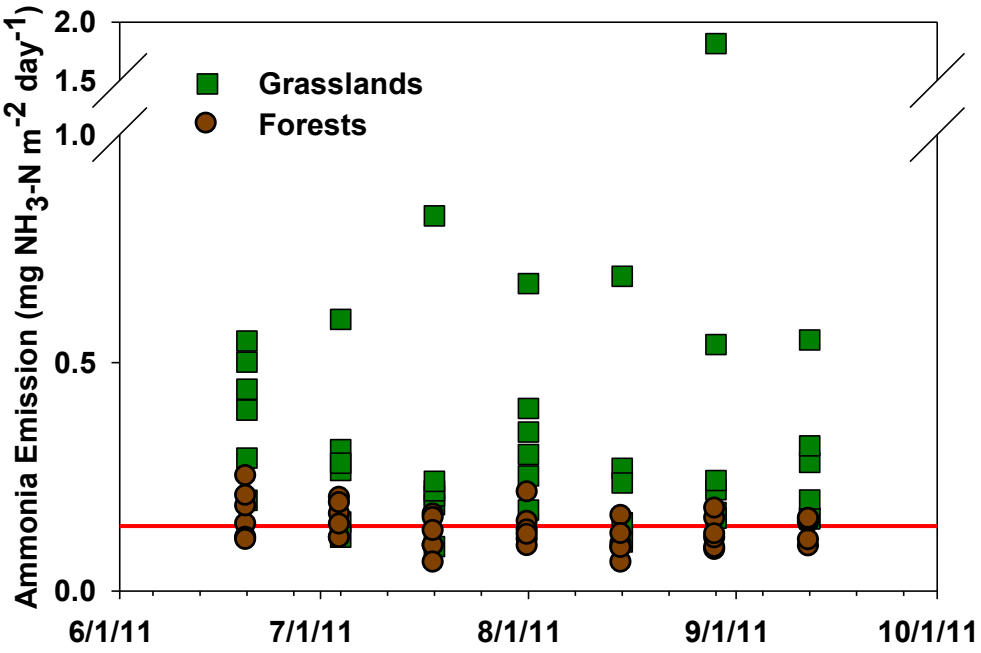

Figure 3.4. Ammonia emission from grassland and forest cores over the study period. The green squares and brown circles represent ammonia loss from grassland and forest soils, respectively. The y-axis is broken to demonstrate a large emission observed on August 29th. The red line indicates the limit of quantification (0.14 mg NH_3-N m^{-2} day^{-1}).

Table 3.2. Comparison of minimum, maximum, and mean ammonia emissions from grassland and forest soils over the study period. The global minimum, maximum, and mean are shown in the bottom row; parenthesis show confidence interval. "<LOQ" indicates the minimum ammonia emission was below the limit of quantification (<0.14 mg NH_3-N m^{-2} day^{-1}). The mean air temperature during the experiment is shown on the far right column.

Sample Date	Forest (mg NH_3-N m^{-2} day^{-1})			Grassland (mg NH_3-N m^{-2} day^{-1})			T_{air}
	Mean	**Min**	**Max**	**Mean**	**Min**	**Max**	**Mean**
6/20/2011	0.25	<LOQ	0.30	0.47	0.24	0.54	22.7
7/4/2011	0.23	<LOQ	0.24	0.38	<LOQ	0.60	22.9
7/18/2011	0.20	<LOQ	0.20	0.40	<LOQ	0.82	22.7
8/1/2011	0.20	<LOQ	0.26	0.44	0.22	0.67	22.2
8/15/2011	0.20	<LOQ	0.20	0.47	<LOQ	0.69	22.8
8/29/2011	0.20	<LOQ	0.22	0.61	<LOQ	1.8	22.9
9/12/2011	0.18	<LOQ	0.18	0.38	0.19	0.55	23.2
Global	0.21 (0.04)	<LOQ	0.30	0.45 (0.4)	<LOQ	1.8	22.8 (0.3)

3.4.3 Wet Deposition

Twenty-one weekly deposition samples were collected over 26 weeks (182 days) (Figure 3.5). Large inputs of ammonium, nitrate, ON, and sulfate were found in precipitation. Total N deposited by wet deposition during the spring (April 18th- May 31st) and summer (June 1st – August 31st) was 0.76 and 1.27 kg N ha^{-1}, respectively. The inorganic fraction of N corresponded to 0.62 and 0.87 kg N ha^{-1} during the spring and the summer. Ammonium contributed the most N at 46% and 40% during the spring and summer period; while the nitrate contribution to deposition was relatively constant with 36% and 29% during the spring and summer,

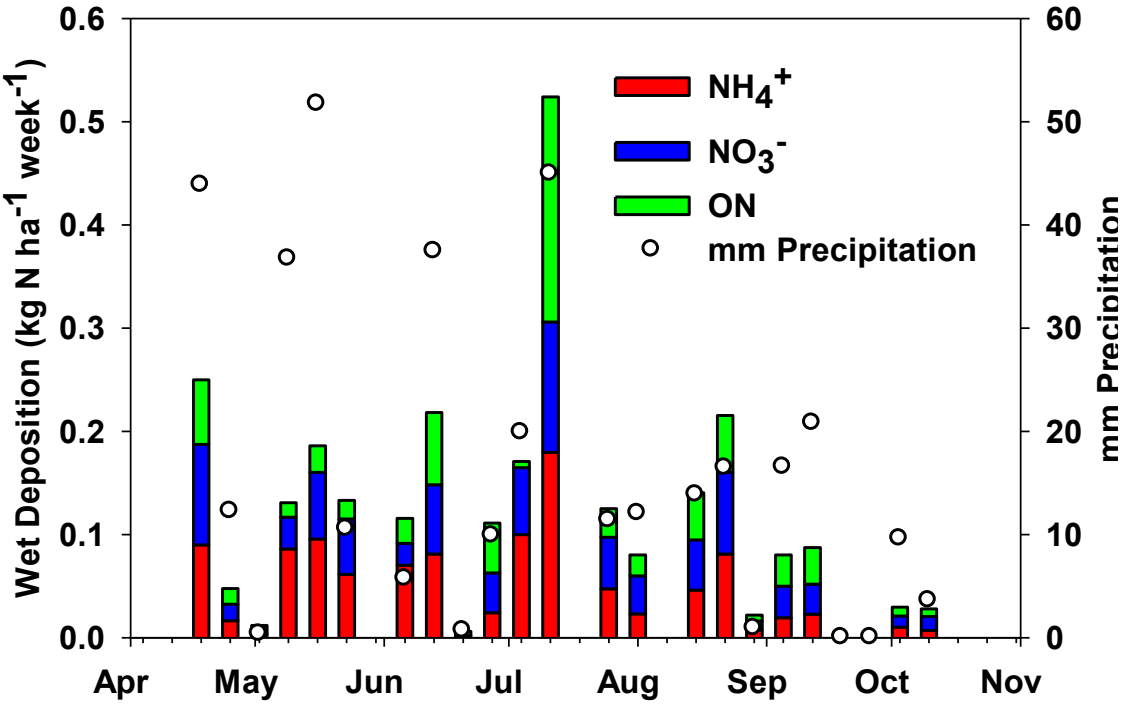

Figure 3.5. Weekly N wet deposition (ammonium, nitrate, and organic nitrogen) measured during the study period. Amount of precipitation (circle) can be seen on the secondary y-axis.

respectively. Organic nitrogen was a significant portion of total deposition, contributing 18% in the spring and 31% in the summer. The amount of precipitation was similar in the spring (143 mm) and the summer (159 mm). No correlations were observed over the study period between the prior week ammonium deposition and average ammonia emission from grassland (r^2= 0.047; p=0.681) and forest (r^2=0.039; p=0.91) soil cores. The pH ranged from 4.57 to 6.00 in the deposition samples and the total amount of N deposition over the study period (April 18th, 2011 to October 18th, 2011) was 1.072, 0.899, and 0.742 kg N ha^{-1} for ammonium, nitrate, and ON, respectively.

3.4.4 Impact of Ammonium Deposition on Ammonia Emission: ^{15}N analysis

To further explore the potential impact of N (ammonium) deposition on the short term enhancement of ammonia emission from soil, a wet deposition event was simulated in the laboratory. The average emission from grassland and forest soils with a zero NH_3-N deposition treatment (i.e., water) was 1.52 mg NH_3-N m^{-2} day^{-1} and 0.32 mg NH_3-N m^{-2} day^{-1}; while, the high deposition treatment (i.e., isotopically labeled ammonium, 315 μM) resulted in 1.08 mg NH_3-N m^{-2} day^{-1} and 0.44 mg NH_3-N m^{-2} day^{-1} for grasslands and forests, respectively (Figure 3.6). Moreover, there was no significant difference in ammonia emission between the zero and high deposition treatments (n=3) for either grasslands (p = 0.641) or forest soils (p = 0.429). This shows that an atmospheric deposition event likely has no impact on short term NH_3 losses due to the presence of ammonium in precipitation.

Collected volatilized ammonia N-isotopic values were measured to confirm the effects of N deposition on ammonia emissions. There was no significant difference (p = 0.463) between N isotopic values in the forest soils for zero deposition (-16.5‰ ± 13.6‰, n=3) and high deposition (-10.2‰ ± 4.0‰, n=3) treatments (Figure3.6). A significant difference (p < 0.001) between zero

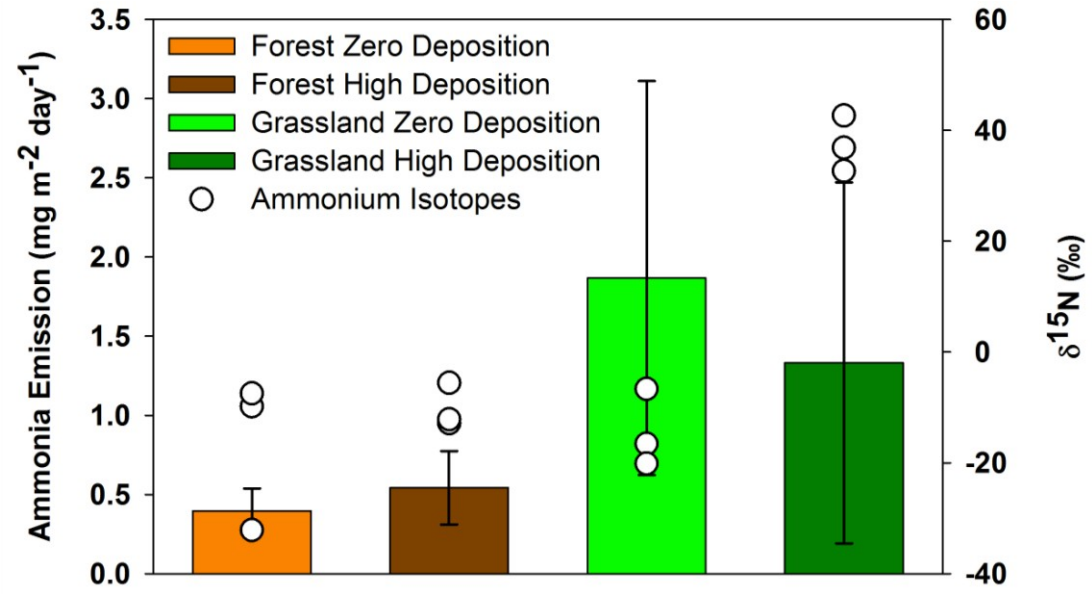

Figure 3.6. Comparison of ammonia emission and volatilized ammonia N isotope values from low and high deposition treatments (n=3) from laboratory simulated deposition events. Error bars represent one standard deviation. $\delta^{15}N$ values are shown on the secondary y-axis. The isotopically labeled ammonium synthetic precipitation solution's $\delta^{15}N$ was 3,682‰.

deposition (-14.5‰ ± 7.0‰, n=3) and high deposition (37.4‰ ± 5.0‰, n=3) treatments was observed in the grassland soils, indicating that some of the labeled ammonium did re-volatilize, but not enough to cause a significant increase in total volatilization compared to the control. The labeled ammonium in the precipitation had an isotopic value of 3,682‰. The observed difference in isotopic values indicated that the NH_4^+ deposition had no impact on short term (<4 days) emissions (re-emission) of ammonia in forest soils, and only a minor (<2% of added ammonium-N) impact on short term emissions (re-emission) of ammonia from grassland soils.

3.4.5 Influence of Temperature on Ammonia Emissions

A diurnal pattern for ammonia emission was predicted by equation 3.4, in order to estimate the ammonia emissions under field conditions at constant humidity and aerodynamic conductance. Using Equations 3.2, 3.3, and 3.4, a normalized K_aK_h product was constructed for

all temperatures measured in RMNP from June to September 2011 relative to the experimental temperature (22.8 °C). The composite diurnal temperature cycle and predicted average forest and grassland soil emissions are shown in Figure 3.7. The maximum temperature was 17.9 °C, corresponding to 2.2 x 10^{-6} mg NH_3-N m^{-2} s^{-1} and 1.0 x 10^{-6} mg NH_3-N m^{-2} s^{-1} for grassland and forest soils, respectively. The minimum average temperature was 10.1 °C, corresponding to 0.92 x 10^{-6} and 0.42 x 10^{-6} mg NH_3-N m^{-2} s^{-1} for grassland and forest soil emissions. Over a day, the integrated emissions would equal 0.12 mg NH_3-N m^{-2} day^{-1} and 0.058 mg NH_3-N m^{-2} day^{-1} fort grassland and forest soils.

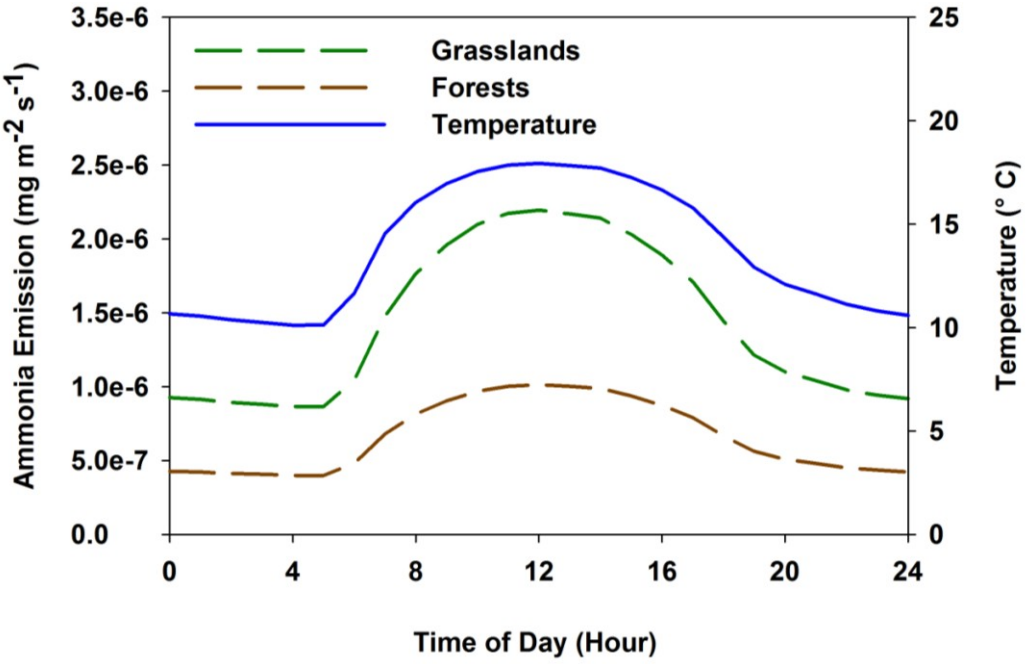

Figure 3.7. Predicted diurnal ammonia emissions over the average diurnal cycle in RMNP from June to September 2011 for grassland and forest soils. Values are calculated using Equation 3.4 from average ammonia emission observed at 22.8 ° C, and temperature dependent models of ammonia acid dissociation (Equation 3.2) and Henry constants (Equation 3.3). Grassland and forest emissions are shown in green and brown (dashed lines). Observed temperature is shown in blue (solid line).

3.5 Discussion

3.5.1 Ammonia Emission Data

The average ammonia emission observed in the laboratory-based system for the sub-alpine grassland and forest soils was 0.45 mg NH_3-N m^{-2} day^{-1} and 0.21 mg NH_3-N m^{-2} day^{-1}, respectively. No temporal change in ammonia flux was observed, likely indicating an equilibrated ammonia concentration between the headspace and the chamber walls. The incoming ammonia scrubbed air (0.008 μmol NH_3 m^{-3}) is within previous 24 hour denuder integrations at the same site (*57*). Because temperatures in the park are much lower than those within the chambers, the temperature dependent ammonia flux model (Equation 3.4) was used to demonstrate the sensitivity of ammonia emissions to actual temperatures measured in RMNP. The temperature-corrected predictions of ammonia emissions for the field site were roughly 3.5 times lower for grasslands (0.12 mg NH_3-N m^{-2} day^{-1}) and forests (0.058 mg NH_3-N m^{-2} day^{-1}) compared to the laboratory measurements at 22.8 °C (Figure 3.7). Adjusted grassland emissions were lower than reported for other non-fertilized agriculture grassland studies, with mean emissions varying from 0.3 mg NH_3-N m^{-2} day^{-1} (*148*) to 3.4 mg NH_3-N m^{-2} day^{-1} (*163*). However, these studies were conducted in low elevation, non-fertilized, managed grasslands using relaxed eddy accumulation and meteorological models. Temperature adjusted forest emissions were in agreement with emissions previously reported from the forest floor (0.002 to 9.0 mg NH_3-N m^{-2} day^{-1}) (*155, 156*) and above forest canopies (-0.829 to 8.64 mg NH_3-N m^{-2} day^{-1}) (*148, 149, 151, 152*)

The observed difference between NH_3 emissions from forests and grasslands can likely be attributed to differences in soil properties (Table 3.1). The difference in pH between grasslands (6.0) and forest (5.3) likely plays a large role in available ammonia within the soil.

Previous studies have stated that soils below pH 6.5 were excluded from large ammonia emission (*151*), however, emission models have indicated an increase in ammonia emission up to 20% when changing the pH from 5 to 6 (*156*). Ammonium concentrations were not significantly different between forests and grasslands; however, the difference in pH will result in differences in available ammonia in the soil solution. Additionally, the higher C:N ratio, nitrate concentrations, and moisture content support higher microbial activity in grasslands (*156*). These conditions could enhance mineralization, resulting in more aqueous NH_4^+ at the soil-air interface in the grassland, and leading to increased NH_3 volatilization. Ultimately, our findings suggest that mountain grasslands may play a larger role than forests in the ammonia dynamics of high elevation ecosystems.

3.5.2 Wet Deposition

Total inorganic N deposition (i.e., 1.97 kg N ha^{-1} yr^{-1}) was similar to previously reported values (i.e., 2-4 kg N ha^{-1} yr^{-1}) near this site and surrounding sites (*164*), although our study does not cover a complete year (Table 3.3). Precipitation weighted averages in the spring are lower for all N species and sulfate than averages in the summer (Table 3.4). The determined N and S concentrations and speciation of inorganic Nwere similar to previous work at the same site; specifically, ON contributed a similar fraction to the N wet deposition in this study (*56*). Deposition of ON could have an impact on near-surface N-cycling and NH_3 volatilization.

Interestingly, previous studies have shown that fewer precipitation events occur in the spring than the summer and can contribute larger amounts of N within single precipitation events (*56*). This study found that the number of weeks containing deposition in the spring was similar to the number of events in the summer, and that the summer contained the largest deposition period — July 11th to the 18th (Figure 3.5). The largest deposition values of ON and sulfate were

Table 3.3. Comparison of seasonal and total wet deposition observed during the 2011 campaign. Results are shown for the spring, summer, and total sampling periods with apportionment percentage for N species in the second row.

	kg N, S, or K ha^{-1}						
	N-NH$_4^+$	***N-NO$_3^-$***	***ON***	***IN***	***TN***	***S-SO$_4^{2-}$***	***K$^+$***
Spring	0.35	0.27	0.14	0.62	0.76	0.25	0.01
	46%	36%	18%				
Summer	0.50	0.37	0.40	0.87	1.27	0.30	0.072
	40%	29%	31%				
Total	1.07	0.90	0.74	1.97	2.71	0.69	0.10
	40%	33%	27%				

Table 3.4. Comparison of precipitation weighted averages for species ($NH+^+$, NO_3^-, SO_4^{2-}, ON, K^+) observed during the 2011 campaign. Results are shown for the spring, summer, and total sampling periods.

Precipitation-Weighted Average (mg/L)				
		Spring	**Summer**	**Total**
N-NH$_4^+$	Mean	0.29	0.49	0.36
	Min	0.13	<LOQ	<LOQ
	Max	1.14	1.23	1.23
N-NO$_3^-$	Mean	0.77	1.27	1.05
	Min	0.08	0.18	0.08
	Max	2.60	2.43	2.60
S-SO$_4^{2-}$	Mean	0.48	0.69	0.55
	Min	0.07	0.19	0.07
	Max	1.97	0.35	1.97
ON	Mean	0.09	0.31	0.20
	Min	0.04	0.03	0.03
	Max	0.17	0.62	0.62
K$^+$	Mean	0.01	0.06	0.03
	Min	<LOD	0.03	<LOD
	Max	0.14	0.21	0.21

also observed during this week (0.52 kg ha^{-1} of total N). Additionally, the three largest potassium deposition values were observed from June 27th to July 18th (Figure 3.8). Previous studies have shown the presence of organic aerosol, potassium, and sulfate in aged biomass burning (*165-168*). This suggests that biomass burning might have played a role in wet deposition during this period.

Hybrid Single Particle Lagrangian Integrated Trajectory (http://ready.arl.noaa.gov/HYSPLIT.php) modeling showed that this week (July 11th-18th) exhibited strong synoptic forcing from the east, as well as flow from the south, south-east. The Las Conchas fire in New Mexico, began on June 26th, 2011, and ended on August 3rd, 2011, after burning more than 633 square km (*169*). Thus, emissions from biomass burning may have contributed to this deposition period.

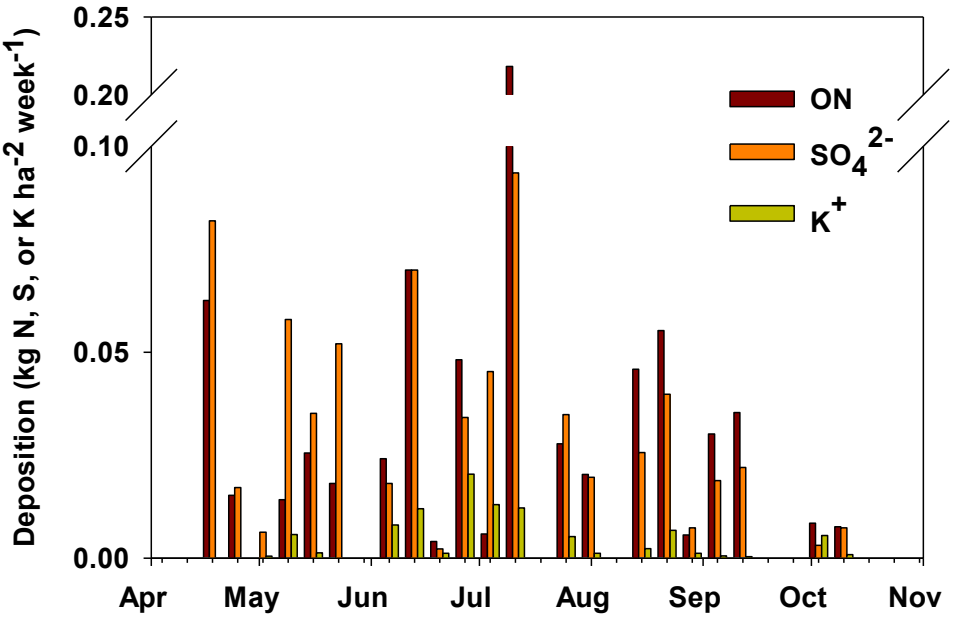

Figure 3.8 Weekly wet deposition of ON (red), sulfate (orange), and potassium (yellow) measured during the study period.

No correlation was observed between the prior week's ammonium wet deposition and the average ammonia emissions from forests and grasslands; however, the possible delay (<7 days) between N deposition and soil sampling may not have provided adequate resolution to assess short term enhancement of ammonia emission. In the laboratory study of deposition effects, the lack of differences between treatments (zero and high deposition) on ammonia emission suggests that inorganic N deposition has a relatively small impact on short term ammonia release. Thus, ammonia emission is likely controlled by other soils processes such as mineralization.

Grasslands demonstrated higher ammonia emissions than forests; however, grasslands (shrub land, herbaceous) only encompass roughly 6.8 % of the area in RMNP (*170*). Assuming the temperature adjusted ammonia emissions for forests were upper bounds during daylight hours and daylight hours represented emission while nighttime hours represented deposition (50% emission, 50% deposition) (*150*), the total ammonia emitted would result in 0.0264 kg NH_3-N ha^{-1} $summer^{-1}$ lost from forest soils. The ammonia lost to the air from RMNP soils would equate to only 5.3% of the observed ammonium deposited via wet deposition during this same interval. Thus, even if all the soil emissions from the park were hypothetically recycled back to the surface via wet deposition, soils could only account for a very small portion of the total N deposition. This apportionment should be viewed with caution and was only calculated to show the minimal impact that forest soils have on N deposition. Many factors can affect ammonia emissions, including temperature, humidity, and soil roughness. Furthermore, vegetative surfaces and canopy effects can drive ammonia flux from emission to deposition and vice versa (*171*).

3.6 Conclusions

Ammonia emissions from sub-alpine grassland and forest soils are very low in comparison to studies in lowland and agricultural soils. Chamber-based measurements of ammonia emissions from grassland and forest soils were significantly different (i.e., 0.45 ± 0.12 mg NH_3-N m^{-2} day^{-1} for grasslands versus 0.21 ± 0.02 mg NH_3-N m^{-2} day^{-1} for forests). An emission model was used to simulate the diurnal temperature cycle measured in RMNP, and showed that the temperature corrected ammonia emission were approximately 0.12 mg NH_3-N m^{-2} day^{-1} for grasslands and 0.058 mg NH_3-N m^{-2} day^{-1} for forests. The total amount of N deposition over the study period (182 days) was 1.07, 0.90, and 0.74 kg N ha^{-1} for ammonium, nitrate, and ON, respectively. Ammonium in wet deposition does not appear to be directly correlated to short term re-emission of ammonia from the soil surface.

CHAPTER FOUR

Ammonia Henry Constants Determined in Feedlot Systems Using a Two-Phase Partitioning Approach

4.1 Introduction

Across the United States, livestock and manure management account for 50% of the ammonia emission inventory (*13, 34*). Nitrogen (N) use efficiency in livestock can be very low resulting in large amounts of excreted N. For example, in beef cattle in feedlots, only about 20% of the N consumed in the feed is retained, the remaining 80% is excreted (*172*), mainly as urea in the animal's urine. Often, up to 50 % of the excreted N is lost to the air through ammonia volatilization (*13*). Volatilization is likely the most important loss mechanism at confined animal feeding operations (CAFOs). Ammonium in CAFOs is readily formed from urea in urine by urea hydrolysis; this process is aided by urease enzymes (discussed in Chapter 5) (*104, 108, 173, 174*). Aqueous ammonium (NH_4^+) is in equilibrium with aqueous ammonia (NH_3); furthermore, the NH_3 (aq) is in equilibrium with the NH_3 (g) above the soil surface (Figure 4.1).

Previous studies have attempted to predict ammonia volatilization from various agricultural sources using an ammonia volatilization model (Eq. 4.1) (*17, 21, 162*). This equation

$$J_{vola} = h_m \left(\frac{K_a K_H}{10^{-pH}} C_{NH_4^+} \right) \qquad \text{(Eq. 4.1)}$$

is very similar to Equation 3.1; however, the ammonia concentration above the surface is ignored because the concentration of ammonium at the interface $C_{NH_4^+}$ is much larger. At first look, it is apparent that ammonia flux is strongly dependent on the pH, the Henry constant, K_h, (Eq. 1.2), the acid dissociation constant, K_a, (Eq. 1.1), and the total aqueous ammonium

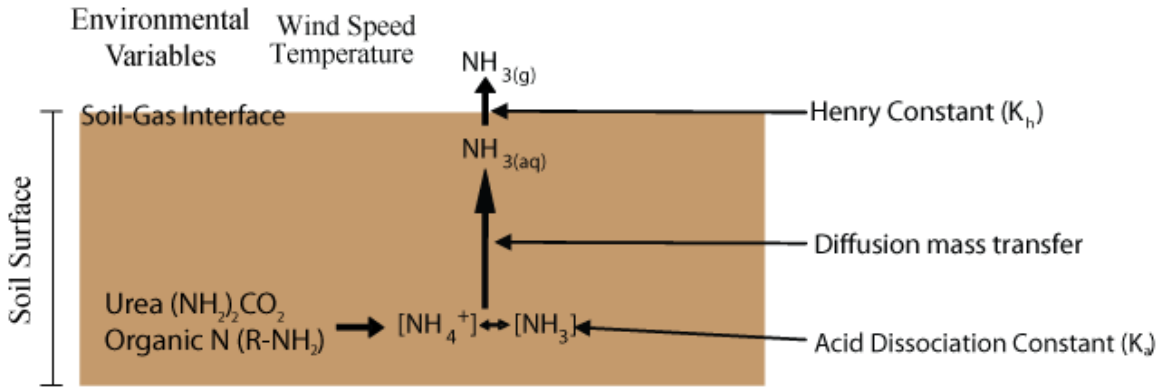

Figure 4.1. Ammonia and ammonium cycling from production, pH equilibrium, diffusion, and exchange at the soil surface. Both wind speed and temperature impact these processes at the soil-gas interface. Modified from (*13*).

concentration. The distribution of NH_4^+ and NH_3 is sensitive to changes in soil pH (*17*). Small changes in pH can lead to drastic changes in the fraction of ammonia available for volatilization (Figure 4.2). Understanding the variables controlling the emission of NH_3 is important in order to develop best management strategies for manure handling and developing accurate models for ammonia losses from CAFOs .

Acid dissociation and Henry constants have a strong dependency on temperature. According to equation 4.1, ammonia flux is sensitive to the product of the K_a and K_h, thus any inaccuracy in these measurements is compounded. For example, aqueous solutions products of K_a and K_h (*18, 19*) are 770% higher than K_a and K_h values measured in poultry animal waste (*22*). Thus predictions of ammonia volatilization can change by a factor of 7.7x depending on literature sources used. Numerous formula for K_h have been defined in the literature with various expressions and units (*21*), in this work we used K_H reported in M atm^{-1} (Eq. 4.2). $NH_{3(g)}$ is the partial pressure (atm) of gaseous ammonia, γ is the activity coefficient and $NH_{3(aq)}$ is the concentration (M) of ammonia in solution.

$$K_h = \frac{NH_{3(g)}}{\gamma_{NH_3} NH_{3(aq)}} = \frac{1}{K_H} \left(\frac{atm}{M}\right) \qquad \text{(Eq. 4.2)}$$

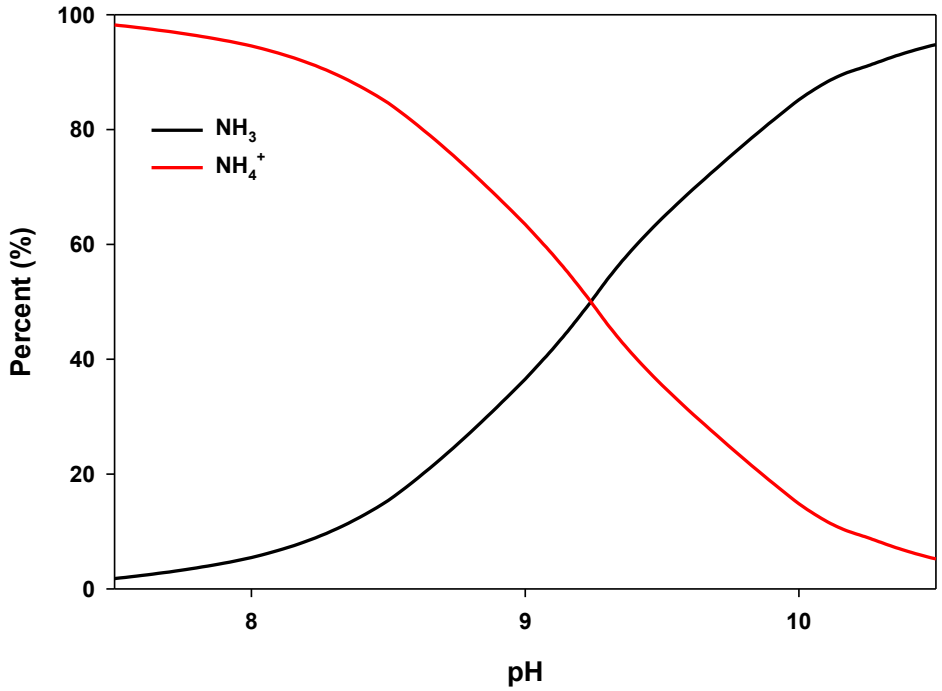

Figure 4.2. Calculated percent of ammonium and ammonia from aqueous values (*18*) for pH commonly observed in animal waste.

Acid dissociation and Henry constants have been determined previously in simple ammonium solutions (*19, 105, 107*) and in more complex matrices including poultry slurries, swine slurries, and anaerobic digesters (*22, 106-108*). These studies have used various approaches to calculate ammonia fractions, K_a, or K_H by determining differences in emission rates above a solution at various pH (*106*), use of gas porous membranes to speciate ammonia from ammonium within anaerobic digesters (*107*), and manure thin films within closed containers (*108*). More recent studies have demonstrated the difficulty in measuring the Henry constant in waste related matrices due to CO_2 emissions, as a result of microbial activity, resulting in increased surface pH (Eq. 4.3-4.4) (*108, 175, 176*). While these pH effects are more

$$HCO_3^- + H^+ \leftrightarrow H_2CO_3(aq) \leftrightarrow CO_2(aq) + H_2O \quad \text{(Eq. 4.3)}$$

$$CO_2(aq) \leftrightarrow CO_2(g) \quad \text{(Eq. 4.4)}$$

exacerbated in anaerobic digesters or lagoons due to large microbial production of CO_2 (*175, 176*), they may still be present at feedlot surfaces and dairies.

Thus, the major goal of this study is to determine the ammonia Henry constant and ammonium acid dissociation constant in feedlot slurries in order to improve our current understanding of ammonia loss from feedlots. Both measurements within the bulk aqueous phase and the air above a slurry were conducted.

4.2 Materials and Methods

4.2.1 Sample Collection and Preparation

Animal waste was collected from the surface of free stall dairy barn floors, a beef cattle calf pen, and a beef cattle mature steer pen. Dairy samples were collected in plastic containers using a shovel. These samples contained mostly feces, urine, and water. Beef cattle manure samples were collected from the top five cm of the pen surface using a shovel and placed into plastic containers. All samples were transported to the laboratory and stored in the freezer for future experiments. Animal wastes were thawed and slurries were prepared for the experiments. Animal waste was mixed using a blender to ensure a homogenous sample. Animal waste was added to create slurries at 1:5 and 1:10 waste to water by mass. Slurries totaled roughly 1.8 L in volume. Slurries were split in three subsamples. One sample (0.8 L) was prepared unaltered while another sample (0.8 L) was adjusted to pH = 12 using 6 M NaOH. The remaining subsample (0.2 L) was frozen for later analysis.

4.2.2 Apparatus and Experimental Approach

The apparatus developed for this study consisted of 10.2 cm poly vinyl chloride (PVC) pipe cut to allow placement of a blade valve (Praher Valves, 21084, Ontario, Canada) (Figure 4.3). The PVC pipe is capped and sealed using PVC adhesive on the top and bottom. The blade valve slid over the PVC pipe and is sealed with silicone adhesive at the start of each experiment. Luer lock fittings were mounted on the outside of the headspace and aqueous components of the apparatus. One meter of high density and porous PTFE tubing (International Polymer Engineering, 032-03-F1, Tempe, AZ) was placed in the aqueous phase and connected to the walls by plastic compression fittings. Slurry was poured into the bottom half of the apparatus, sealed, and placed in an incubated shaker at the desired temperature and shaken at 120 revolutions per minute (rpm) for 90 minutes. A nitrogen tank was connected to both the headspace and aqueous components of the apparatus. A ten L min^{-1} ball-float flow meters (Dwyer, GFM2110AIR, Michigan City, IN), or a peristaltic pump, or both were used to control the flow rate and the total volume. Flow rates corresponding to 1.000 L min^{-1} and 0.170 L min^{-1} were used for headspace and aqueous components of the system, respectively (*107*). Flow rates were verified using a Bios Defender 510 volumetric flow meter (Lakewood, CO). Fluorinated ethylene propylene (FEP) tubing (Ozone Solution, FEP-125x250, Hull, IA) was used for all post apparatus connections. Total volume used for headspace integrations was 10 L and aqueous integrations ranged from 1.0 L to 0.25 L depending on temperature (10 to 25 °C).

Ammonia from headspace and aqueous integrations was trapped with 0.1 M phosphorous acid. Volume of phosphorous acid was determined by mass measured via ion chromatography (Dionex, ICS 2100, Sunnyvale, CA,) utilizing a CS-12a analytical and guard column for separation, a CSRS 300 4-mm suppressor, and a DS6 heated conductivity detector. Moles of

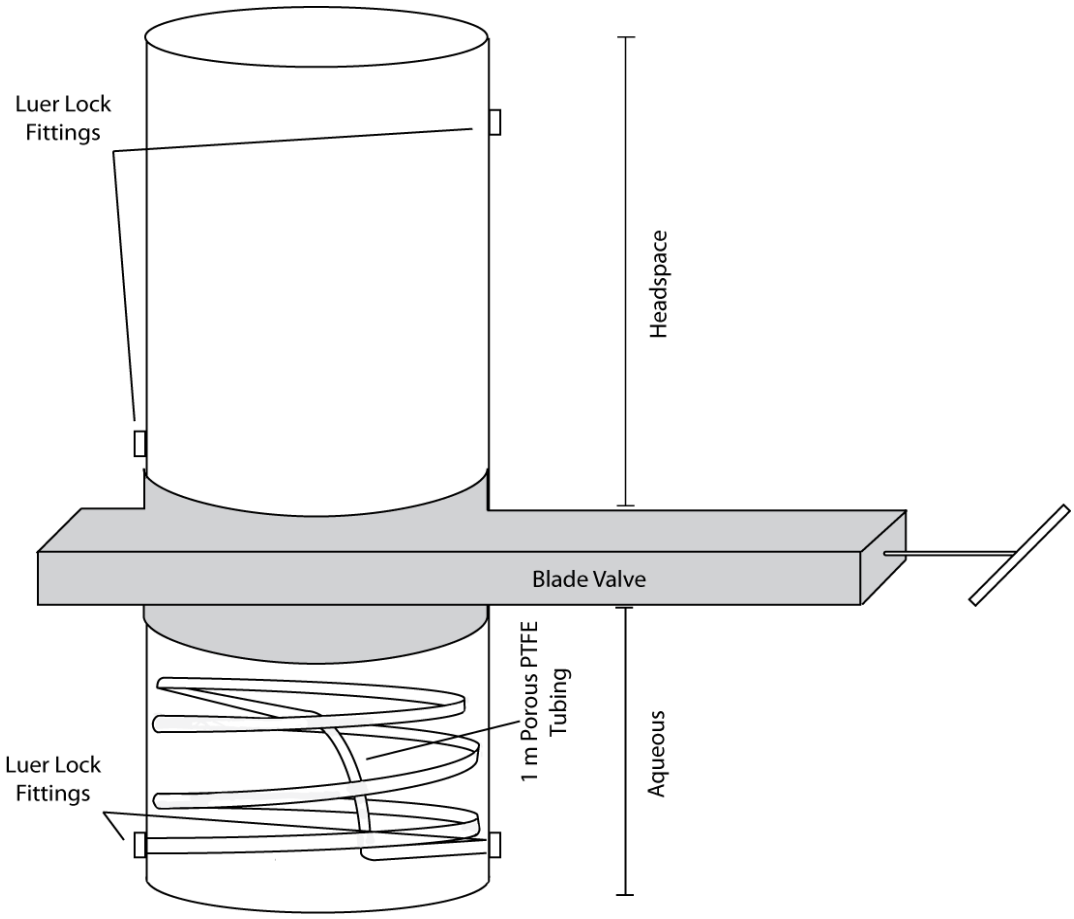

Figure 4.3. Schematic of the apparatus used for Henry and acid dissociation constant determination. The headspace is 1.95 L; the aqueous phase is 0.800 L separated by a blade valve. 1 m PTFE porous tubing is submerged in the aqueous phase.

ammonia (n_{NH_3}) were converted to partial pressure (P_{NH_3}) using the ideal gas law (Equation 4.5). R is the ideal gas constant, T is the temperature in Kelvin, and V is the volume of the

$$P_{NH_3} = \frac{n_{NH_3} RT}{V} \quad \text{(Eq. 4.5)}$$

headspace or the volume flushed through the porous PTFE tubing. Volume of headspace was determined by mass using deionized water. Ionic strength was calculated from the solution's electrical conductivity (EC) according to equation 4.6 (*177*). The K_H was calculated according to

$$I = 1.6 \times 10^{-2} \text{ (EC)} \quad \text{(Eq. 4.6)}$$

equation 4.2and the activity of neutral species is assumed to be equal to $10^{(0.1 \times \text{Ionic Strength})}$ (*178*). Ammonium activities were calculated using the Davies equation (Eq. 4.7) (*18*). Where c represents charge, I is ionic strength and $\gamma_{NH_4^+}$ is activity coefficient. In determination of K_a, the ionic strength was assumed to be the same at all pH values (i.e., pH 8-9 and 12). It is reasonable

$$\log \gamma_{NH_4^+} = -0.5\,(c^2)\left(\frac{\sqrt{I}}{1+\sqrt{I}} - 0.3I\right) \quad \text{(Eq. 4.7)}$$

to assume that the activities are nearly constant at high ionic strength based on previous work (*106*). At a feedlot surface, EC of soils (0.34 S m^{-1}) was over three times lower when than compared to animal waste (1.06 S m^{-1}) (*179*). The moles of ammonium present in solution at natural (8-9) pH were calculated by the difference in ammonia partial pressures between the natural and adjusted (pH = 12) solution. The K_a was calculated according to equation 4.8 (*22, 106*) where $[H^+]$ is the hydronium concentration, $\rho_{NH3.\ pH=9}$ is the ammonia partial pressure at natural pH, and $\rho_{NH3.\ pH=12}$ is the ammonia partial pressure at pH 12.

$$K_a' = \frac{\left[\rho_{NH3,\,pH=9}\right][H^+]}{\left[\frac{\rho_{NH3,\,pH=12} - \rho_{NH3,\,pH=9}}{\rho_{NH3,\,pH=12}}\right]} = \frac{\left[\rho_{NH3,\,pH=9}\right]\left[10^{-pH}\right]}{\left[1 - \frac{\rho_{NH3,\,pH=9}}{\rho_{NH3,\,pH=12}}\right]} \quad \text{(Eq. 4.8)}$$

4.2.3 Aqueous Ammonia Experiments

The apparatus was first tested with known ammonium solutions. NH_4Cl and NH_4OH were used to generate 0.001, 0.010, 0.100, 1.000 M ammonia solutions which were pH adjusted to 9.3 and 12 using 6M NaOH. Activity coefficients were assumed to be near or at unity. Both pH and ammonium concentrations were measured at the start and the end of the experiment. All standardization experiments were conducted at 25 ° C within an incubated shaker.

4.2.4 Feedlot Soil Experiments

Animal waste was added to 18.2 MΩ deionized (DI) water in order to generate slurries suitable for the experiments. Two different total solids (TS) contents (i.e., 2.7% and 6.7%) were used for the dairy waste slurries and two animal types (calves, mature steers; TS: 14.1, 12.7%) were used for the beef waste slurries. Experiments were conducted at 10 °C, 15 °C, and 25 °C. Each experiment consisted of four replicates,

4.3. Results

4.3.1 Validation of Two-Phase Partitioning Approach for K_H and K_a Determination

Aqueous NH_4Cl and NH_4OH solutions were used to validate the approach of headspace integrations and porous tubing‘s capabilities to speciate ammonia in the aqueous phase. All K_H were calculated based on solutions at pH 12 with the assumption that the aqueous fraction of ammonia was 1. These calculations preformed in the lab will be referred to as measured equilibrium constants, as to not be confused with previous modeling studies. The system was found to be accurate (average relative error = 1.1%) and precise (average relative standard

deviation (RSD) = 3.3%) when compared to all K_H measured for all concentrations in the aqueous phase, however, headspace based measurements were not as accurate (average relative error = 1.5%) or precise (average RSD=5.2%) for all concentrations, excluding the measurements at 0.001 M total ammoniacal nitrogen (TAN) (Figure 4.4).

The average K_H and 95% confidence intervals measured for TAN concentrations in the range 0.001-1.000 M were not significantly different ($p > 0.05$) between aqueous, 55.1 (±0.2) M atm^{-1}, and headspace, 55.4 (±0.9) M atm^{-1}, based measurements; however, aqueous based measurements were more precise than headspace derived K_H values. K_a values were determined using equation 4.6; using the difference in the calculated partial pressures of ammonia from slurries at pH 9 and 12 to determine the fraction of ammonia and ammonium in solution. The system was found to be sufficiently accurate (average relative error = 12%) and precise (RSD) = 8.8%) for all K_a measured for TAN concentrations from 0.010 to 1.000 M (excluding 0.001 M) in the aqueous phase, and headspace based measurements were as sufficiently accurate (average relative error = 12%) and precise (average RSD=8.4%) for all concentrations excluding the measurements at 0.001 M TAN (Figure 4.5).

Measured K_a values at 0.001 M TAN in the aqueous and headspace were 44 and 48% lower than accepted values, however, the 95% confidence interval did contain the accepted value for the headspace measurements (*18*). It is believed that these TAN concentrations were too low and were excluded in future determinations. Based on validation experiments conducted at 0.010 to 1.000 M TAN, average aqueous derived K_a values (4.87×10^{-10}) were not significantly different ($p > 0.05$) from the headspace derived K_a value (4.98×10^{-10}). These K_a values were measured based on activities in solution. It was assumed that NH_4Cl or NH_4OH were the only contributors to ionic strength. Using activity corrections, K_a values and 95% confidence intervals

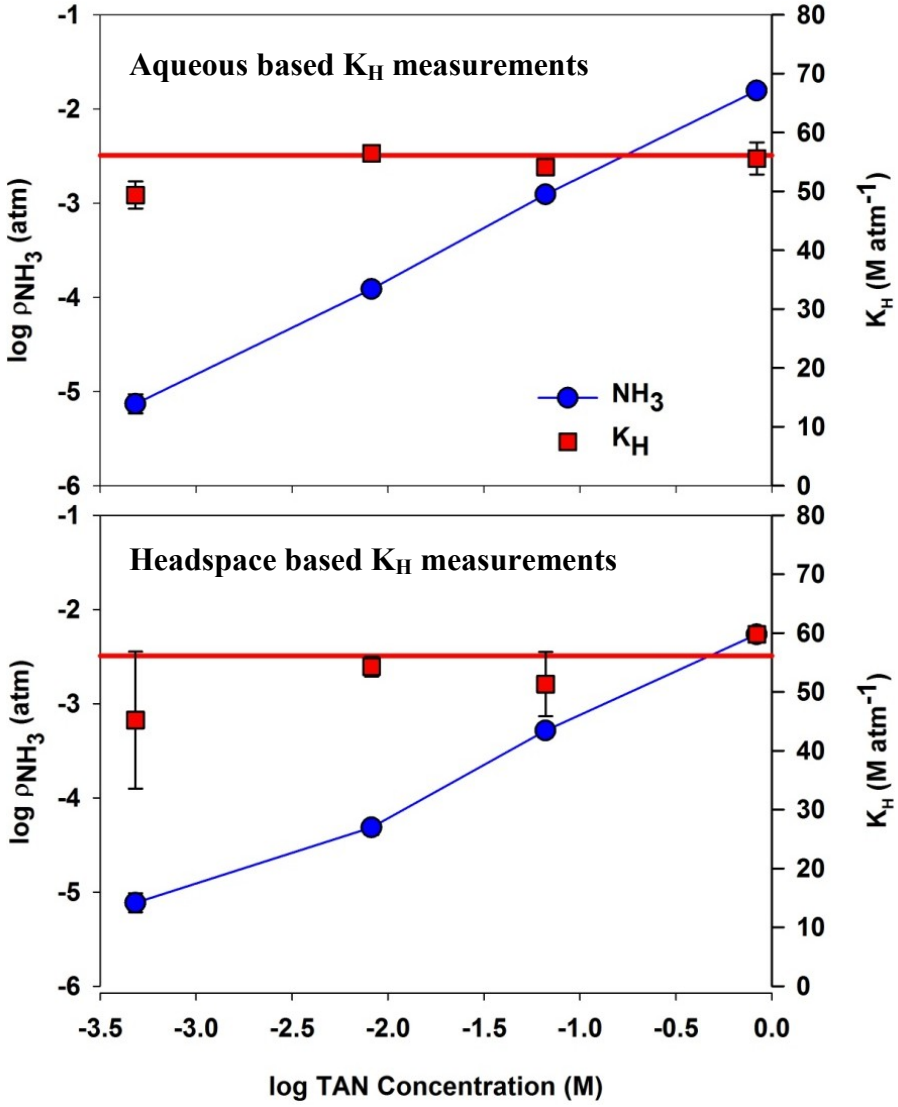

Figure 4.4. Measurements of Henry constants (K_H) as a function of the TAN concentration. Comparisons of partial pressures calculated for the aqueous phase (top) and headspace (bottom) are shown in blue, while measurements of K_H are shown in red squares. Error bars represent one standard deviation (n=4). The redline represent the most commonly reported K_H value for an aqueous ammonium solution (56.1 M atm^{-1}) (*19*).

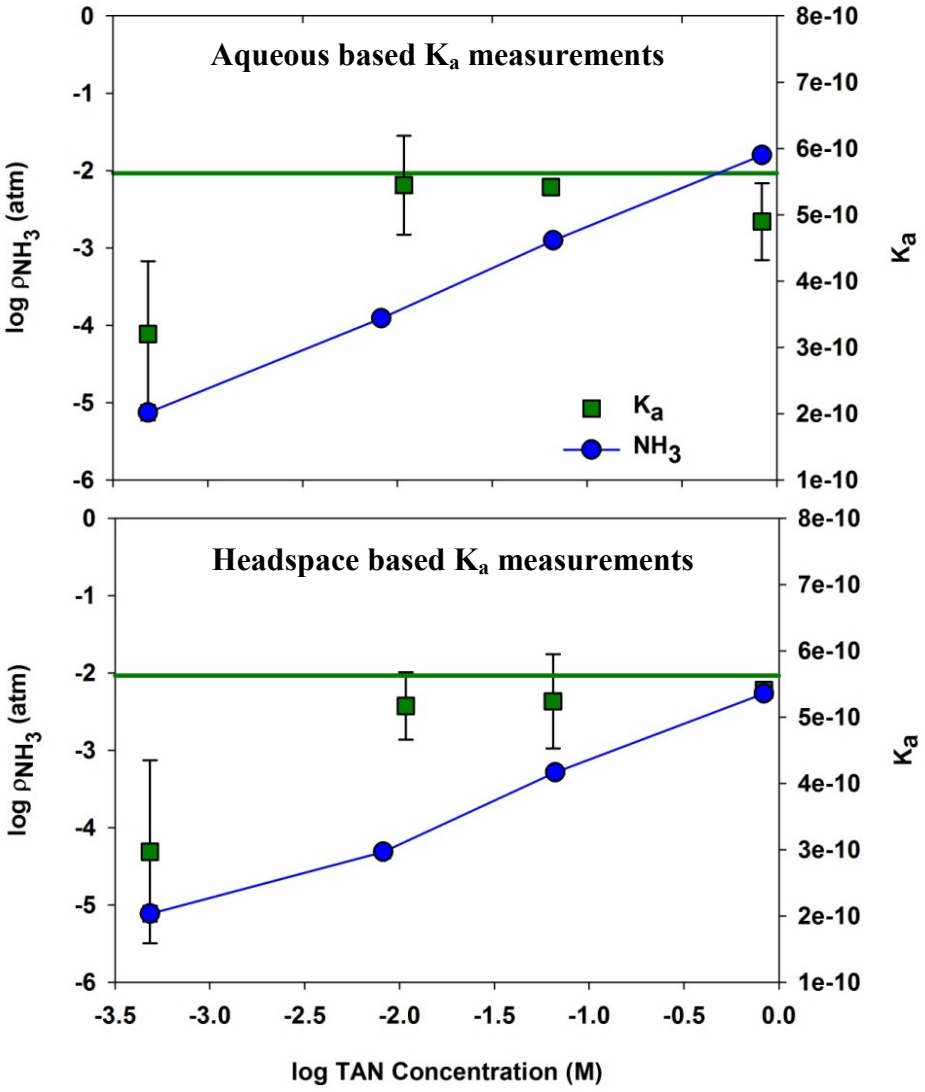

Figure 4.5. Measurements of acid dissociation constant (K_a) in various TAN solutions. Comparisons of partial pressures calculated in aqueous phase (top) and headspace (bottom) are shown in blue, while measurements of K_a are shown in green. Error bars represent one standard deviation (n=4). Commonly accepted K_a value (5.69×10^{-10}) for aqueous ammonium solutions is shown as a green line (*18*).

were 5.25×10^{-10} ($\pm 0.5 \times 10^{-10}$) and 5.27×10^{-10} ($\pm 0.4 \times 10^{-10}$). The accepted K_a values (5.69×10^{-10} M) for simple solutions did fall within the 95% confidence interval of the results from this study (*18*).

4.3.2 Slurry Properties of Animal Waste

Animal waste and slurry properties are shown in Table 4.1. Beef cattle waste contained significantly higher ($p < 0.05$) organic matter, organic N, TAN, and total N than dairy waste. No significant differences ($p < 0.05$) existed within beef treatments (mature versus calves) or dairy treatments (2.7% versus 6.7%) except for total solids between dairy slurries. Pooled values for beef slurries (mature and calves) and dairy slurries (2.7% and 6.7%) were significantly different only in percent total solids. Thus no significant difference existed in TAN concentrations or EC measurements.

One underlying assumption in this experiment was that pH adjustment to 12 would not affect the ionic strength. Although it has been suggested that changes in pH can affect other slurry properties such as sorption (*17*), ionic strength was of primary concern in ammonium activity coefficients. Calculations of the ionic strengths were not significantly different between the two pH values for all treatments except for beef calves (Figure 4.6). Moreover, the range of ammonium activities was similar across treatments within beef and dairy slurries used for this study. Beef cattle slurries had lower activities however were not significantly different from dairy slurries.

Table 4.1. Animal waste and slurry properties for materials used for K_H and K_a determinations. Top table shows raw waste measurements and the bottom table shows measurements of each slurry treatment used in the experiment. Average values are shown with standard deviations shown in parenthesis (n= 3). <LOQ indicates lower than the limit of quantification *indicates significantly different at 95% confidence interval.

		Dairy Fecal Mixture	Beef Cattle Mature	Beef Cattle Calves
Initial Waste	**Dry Matter (%)***	13.4 (0.1)	70.4 (0.7)	63.5 (3.4)
	Organic Matter (%)*	5.0 (0.4)	27.2 (0.4)	33.8 (2.6)
	Total C (%)	1.7 (0.2)	15.8 (0.7)	19.6 (1.1)
	Total N (%)*	0.38 (0.1)	1.17 (0.06)	1.51 (0.06)
	Organic N (g/kg)*	2.5 (0.8)	9.4 (0.4)	12.5 (0.1)
	TAN (g/kg)*	1.3 (0.1)	3.6 (0.1)	2.6 (0.1)
	NO_3^- (g/kg)	<LOQ	<LOQ	<LOQ

		Dairy 2.7%	Dairy 6.7%	Beef Mature	Beef Calves
Slurries	**Total Solids (%)**	2.7 (0.1)‡	6.7 (0.2)‡	14.1 (0.8)	12.7 (0.7)
	pH	8.34 (0.2)	8.6 (0.4)	8.2 (0.4)	8.1 (0.6)
	TAN (mol/L)	0.012 (0.002)	0.02 (0.01)	0.02 (0.01)	0.019 (0.008)
	EC (S m^{-1})	0.41 (0.8)	0.70 (0.9)	1.02 (0.7)	1.16 (0.01)
	Ionic Strength	0.07 (0.1)	0.11 (0.02)	0.13 (0.01)	0.14 (0.02)

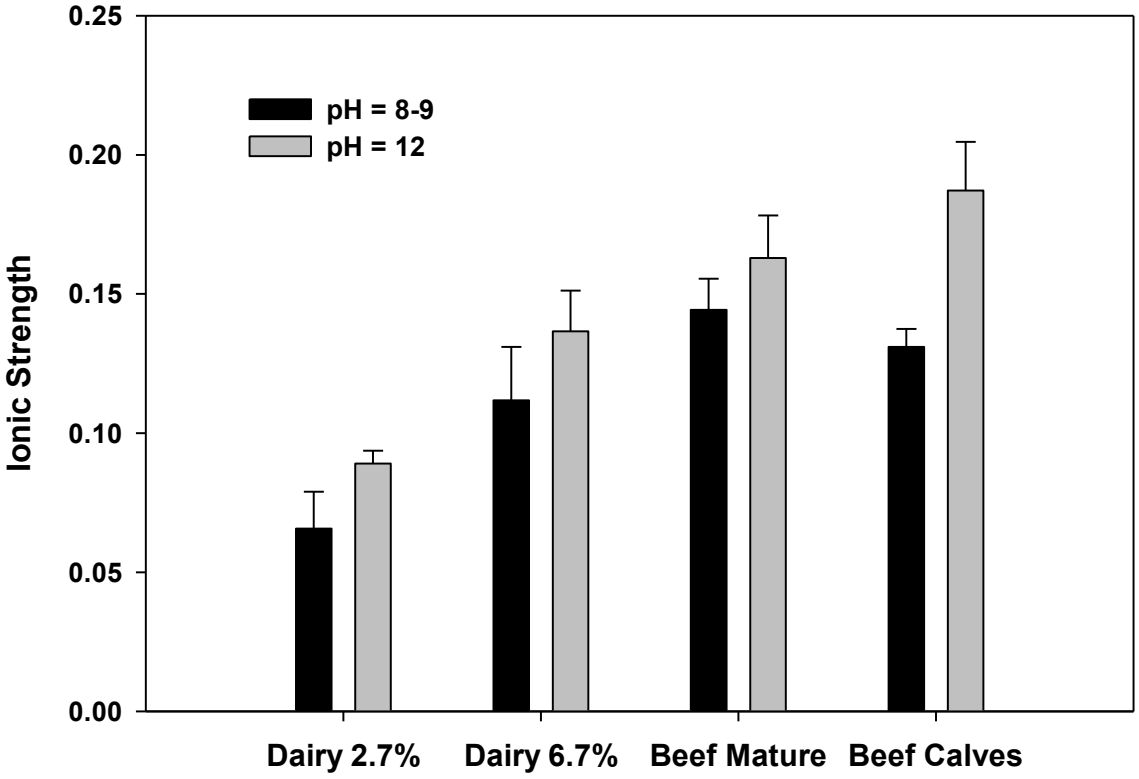

Figure 4.6. Comparison of calculated ionic strengths based on electrical conductivity measurements between dairy (TS = 2.7% and 6.7%) and beef mature (TS = 14.1 %) and calves (TS = 12.7 %) waste slurries at natural pH (8-9) and pH 12.

4.3.3 Henry Constants for Animal Waste Derived Ammonia

Previous determinations of K_H and K_a constants for poultry, dairy and swine waste slurries were questioned as to their applicability to beef waste systems due to large variation in literature values (Figures 1.12 and 1.13) (*17, 22, 106, 107*). Differences in literature values could be attributed to differences in soil properties due to salt content affecting sorption to soil (*17*). Moreover experiments presented herein were conducted in order to evaluate the impact of determining the K_H based on headspace versus solution phase measurements (*22, 106-108*). Measurements of the K_H for dairy slurries (Figure 4.7) and beef slurries (Figure 4.8) at 10, 15, and 25 °C were conducted at pH 12.

When comparing average K_H values for dairy treatments (2.7% versus 6.7%), no significant difference ($p < 0.05$) was observed within aqueous or within headspace at 10, 15, 25°C. Significant differences, however, were observed for measured K_H values between the aqueous and headspace at temperatures at 10 and 15°C for both dairy (33, 22%) and beef (39, 43%) waste slurries. Headspace measurements of K_H were lower than values derived from aqueous measurements, indicating higher headspace ammonia partial pressures in comparison to the ammonia partial pressures measured within the porous tubing.

4.3.4 Determination of Acid Dissociation Constant for Ammonia in Animal Waste

For dairy slurries, all aqueous measurements of K_a were significantly different ($p<0.05$) from headspace measurements at 10, 15 at 25 °C, except for dairy slurry (TS 6.70%) at 10 °C (Figure 4.9). Dairy slurry K_a values measured at 25 °C demonstrated the largest deviation from the reported literature values of 9.53×10^{-11} to 5.00×10^{-10} (*17, 21, 22*) and the most variability. Beef manure slurries did not demonstrate large deviations as dairy slurries in measured K_a values

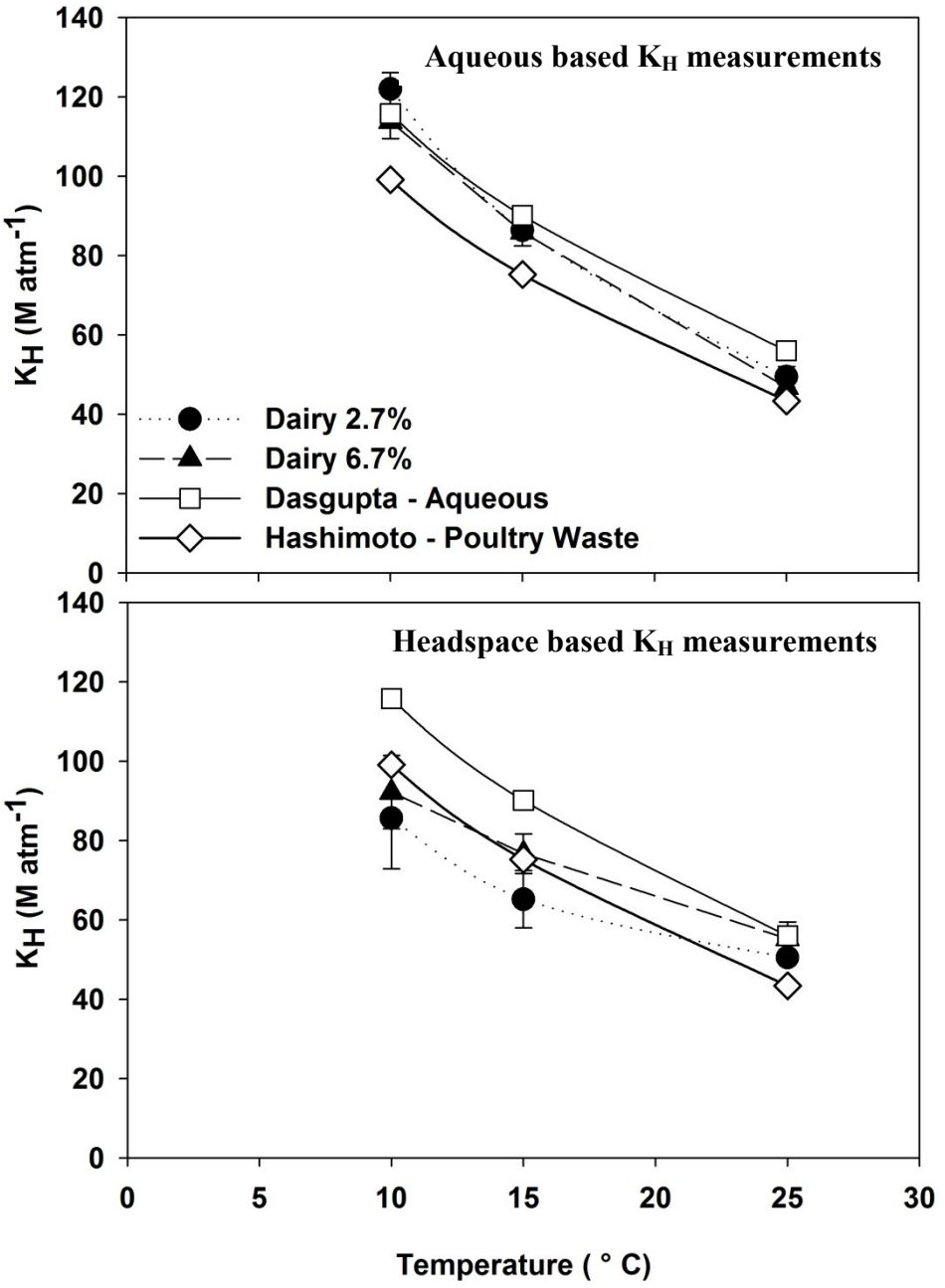

Figure 4.7. Comparisons of K_H dependency on temperature for dairy manure slurries at two solid contents (2.7% & 6.7%). Error bars represent one standard deviation (n=3). Aqueous phase (top) and headspace (bottom) derived calculations are compared to previously reported aqueous (open squares) (*19*) and dairy waste (open diamonds) (*20*) K_H values.

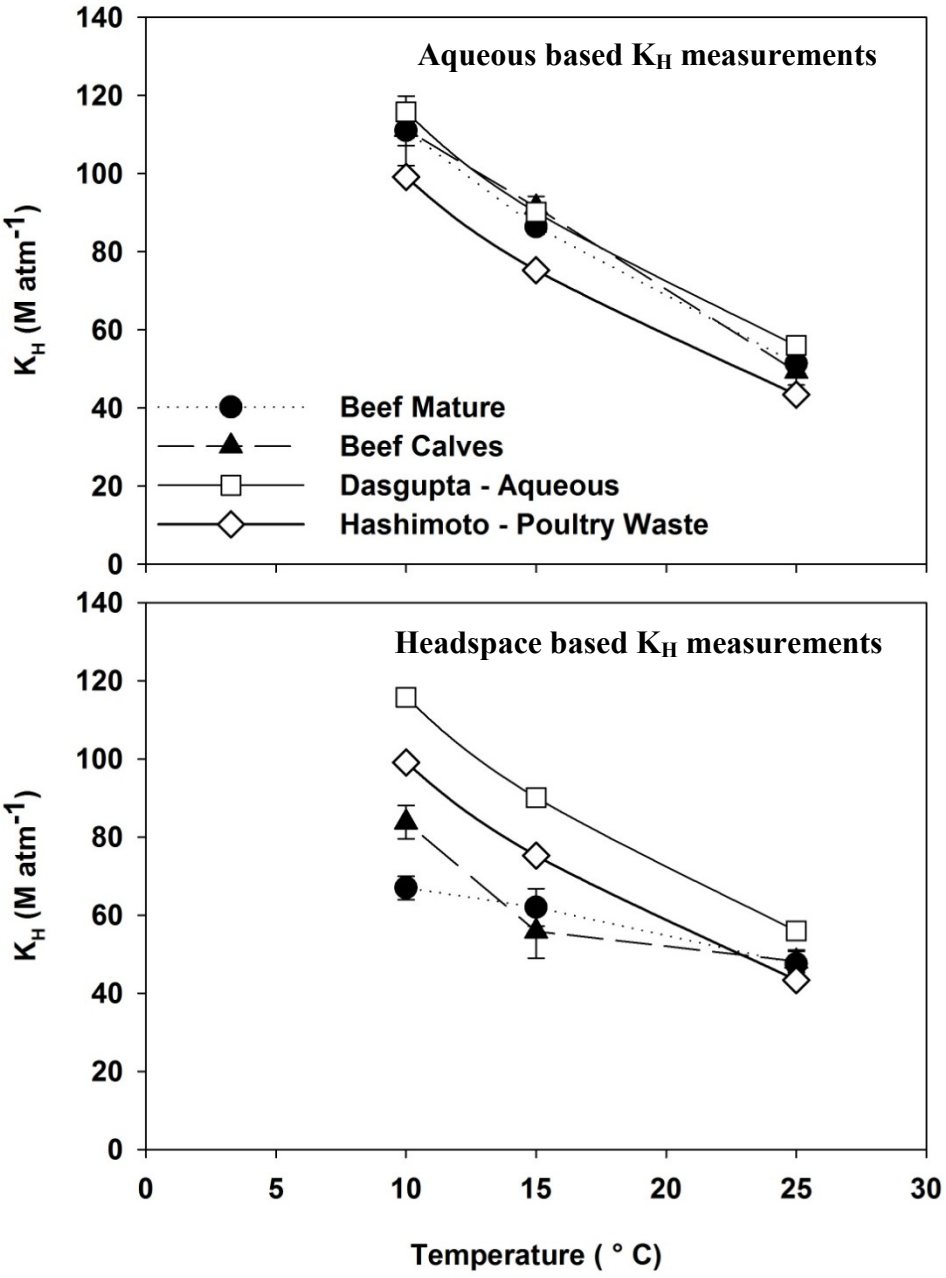

Figure 4.8. Comparisons of K_H dependence on temperature measured in beef waste slurries within two different animal types (mature & calves). Error bars represent one standard deviation (n=3). Aqueous phase (top) and headspace (bottom) measurements are compared to aqueous (open squares) (*19*) and dairy waste (open diamonds) (*20*) K_H literature values.

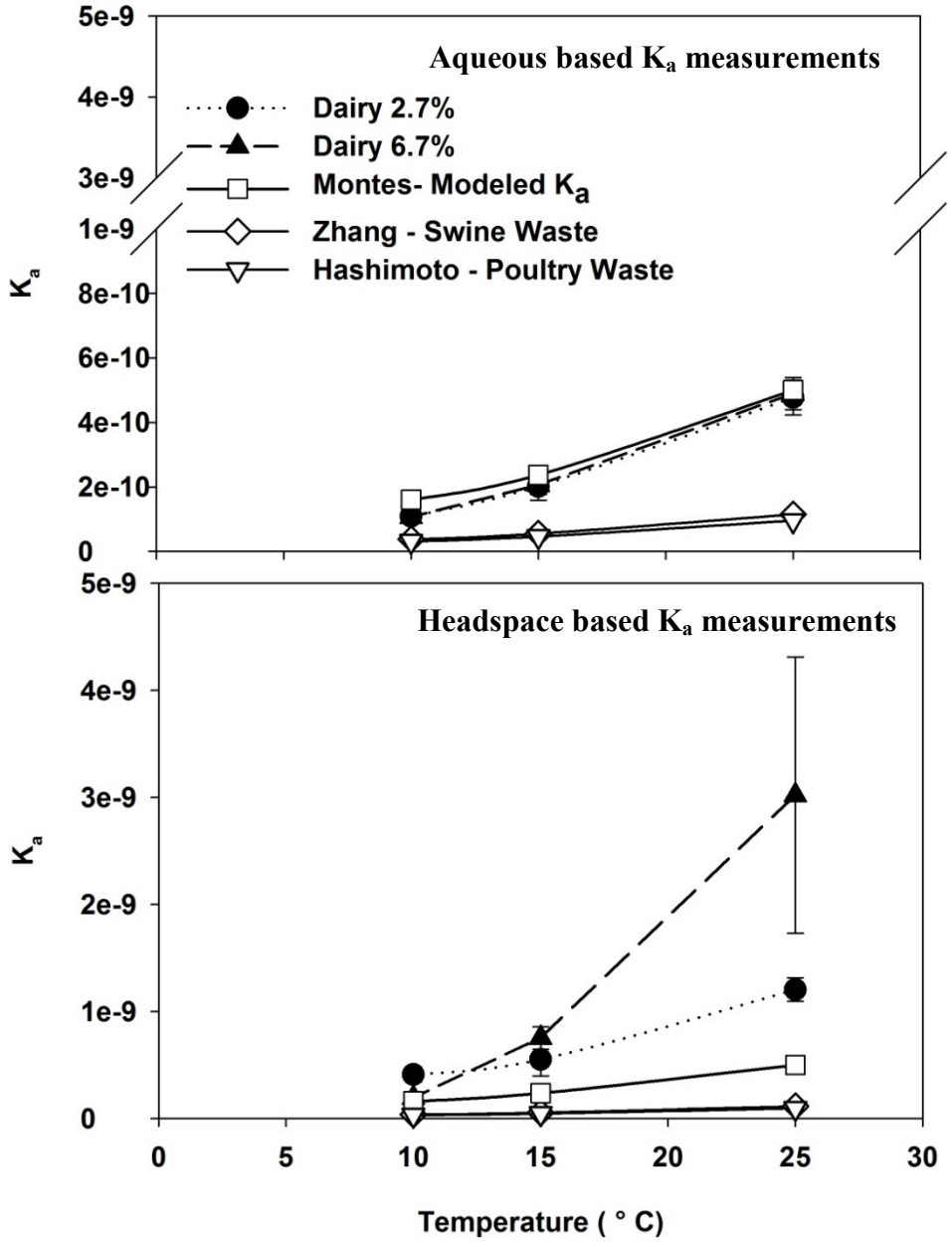

Figure 4.9. Comparisons of K_a dependence on temperature measured in dairy cattle waste slurries at two solid contents (2.7% & 6.7%). Error bars represent one standard deviation (n=3). Aqueous phase (top) and headspace (bottom) measurements are compared to a K_a literature values (open squares, diamonds, triangles) (*17, 21-23*).

at 25 °C (6 x 10^{-10}) (Figure 4.10). Aqueous measurements of K_a in beef feedlot slurries were not significantly different from headspace measurements at 10, 15, and 25 °C

4.4. Discussion

4.4.1 Henry Constants

Average Henry constant values measured from NH_4OH solutions above 0.001 M TAN at pH 12 were not significantly different ($p<0.05$) from previous measurements in pure aqueous (i.e., no manure) TAN solutions (*19, 107*). Difference in K_H between aqueous ammonia molar concentrations and activities were less than 5%, supporting the insensitivity of K_H to ionic strength at concentrations of less than 0.100 M (*17, 19, 107*). K_H measured at 0.001 M TAN were lower than reported values, and is believed to be near the limitations of the appartus. Adsorption of ammonia to the apparatus walls, or the PFE tubing, or both, may have lead to higher ammonia partial presures especially at low TAN concentrations. This underestimation was not observed above 0.001 M TAN.

In animal waste slurries, aqueous measured equilibrium constants (i.e., lower half of chamber) provided a more accurate option compared to headspace measruements. Aqueous derived K_H values for animal waste showed a temperature dependence similar to simple aqueous solutions (*19, 105*), while headspace measured K_H values demonstrated lower values supporting deviations observed in previous studies (*17, 22, 106*) (Table 4.2). The difference between the aqueous (lower half) and headspace (upper half) derived K_H were significantly different at temperatures below 25 °C. For instance, headspace K_H measurements were 49% and 33% higher than aqueous meaured for beef and dairy slurries at 10 °C, respectively. This supports a larger ammonia partial presure in the headspace compared to the ammonia partial pressure in the

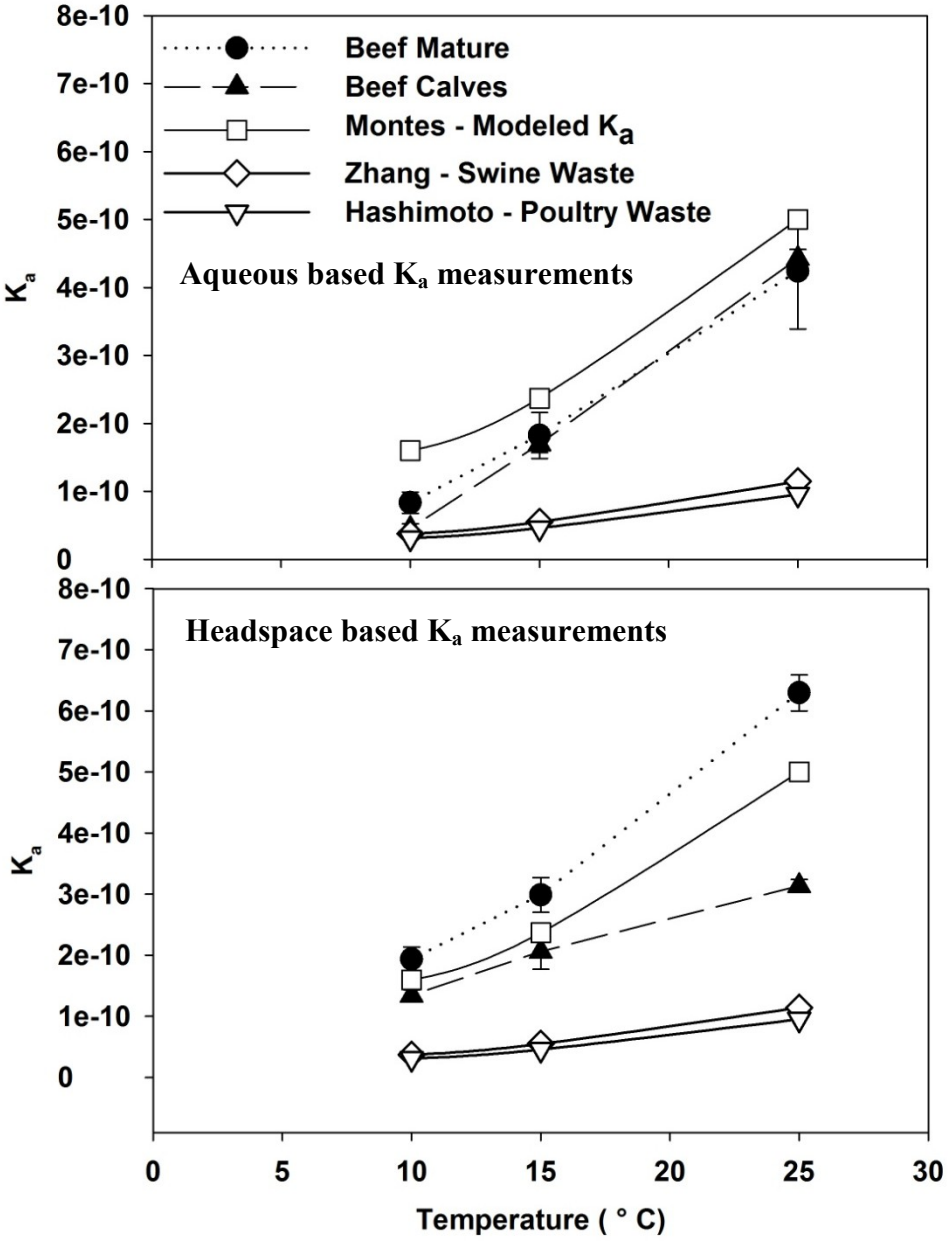

Figure 4.10. Comparisons of K_a dependence on temperature measured in beef waste slurries within two different animal types (mature & calves). Error bars represent one standard deviation (n=3). Aqueous phase (top) and headspace (bottom) measurements are compared to K_a literature values (open squares, diamonds, triangles) (*17, 21-23*).

Table 4.2. Fits of Henry constant dependence on temperature (T) from the work presented here and previous work. Numerical value shown after each equation represent the value at 25 °C. All values are reported in M atm^{-1}. R is the gas constant.

	Dairy 2.7% TS	**Dairy 6.7% TS**	**Ref**
Aqueous	$K_H = 10^{\left(\frac{2194}{T}-5.7\right)}$; 45.58	$K_H = 10^{\left(\frac{2186}{T}-5.7\right)}$; 42.84	this study
Headspace	$K_H = 10^{\left(\frac{1230}{T}-2.4\right)}$; 53.14	$K_H = 10^{\left(\frac{1247}{T}-2.4\right)}$; 60.60	this study
	Beef Cattle Mature	**Beef Cattle Calves**	
Aqueous	$K_H = 10^{\left(\frac{1784}{T}-4.2\right)}$; 60.75	$K_H = 10^{\left(\frac{2029}{T}-5.1\right)}$; 50.73	this study
Headspace	$K_H = 10^{\left(\frac{901}{T}-1.3\right)}$; 52.72	$K_H = 10^{\left(\frac{1247}{T}-2.5\right)}$; 48.13	this study
	Literature Values		
Ammonium Solution	$K_H = e^{\left(\frac{4092}{T}-9.70\right)}$; 55.96		(*19*)
Chicken Waste	$K_H = \left(\frac{1}{RT}\right)\left(\frac{1384}{1}\right)\ x\ 1.053^{(293-T)}$; 43.36		(*20, 21*)
Modeled	$K_H = \left(\frac{1}{RT}\right)\left[\left(\frac{0.2138}{T}\right)\ 10^{\left(6.123-\frac{1825}{T}\right)}\right]^{-1}$; 56.75		(*17*)

porous tubing. The role of microbially produced CO_2 has been discussed by previoius authors (*21, 108, 175, 176*) as CO_2 can increase the pH at the liquid air interface resulting in higher ammonia concentations in the gas phase. However, pH changes are unlikely since our solutions were adjusted to pH 12 to ensure all TAN was deprotonated. Moreover, the high pH in the slurry will likely trap CO_2 as carbonate thus minimizing pH sesnisitivty to microbiollay produced CO_2. It is possible that dissolution of CO_2 could lower the pH of the bulk solution, however, no change in pH was observed post experiment.

4.4.2 Acid Dissociation Constants

Aqueous measured K_a values for beef slurries were significantly different than modeled values at 10 and 15 °C, however, the headspace derived K_a values for beef slurries were in agreement with previously reported values in simple solutions (*17, 21, 22, 106*) (Table 4.3). Averaged beef K_a measurements based on aqueous phase data were 17 and 60% lower at 15 and 10 °C than modeled K_a values (*17*). At temperatures above 10 °C, K_a values did not agree with measurements conducted in animal waste (*21, 22, 106*). Averaged headspace measured K_a values for beef cattle were significantly different from modeled values at 25 °C but not significantly different at 15 or 10 °C (*17*). Aqueous measured K_a values for beef slurries at25 °C were not significantly different ($p<0.05$) to modeled K_a values (*17*). Overall, aqueous and headspace K_a values measured in beef slurries support modeled values of K_a over values determined in animal waste.

Aqueous measured K_a values for dairy slurries were not significantly different from modeled K_a values, however, headspace measured K_a values for dairy slurries demonstrated values above modeled K_a values (*17*). The relative difference between aqueous measured of K_a and modeled K_a values increased to over 14% and 33% at 15 and 10 °C. Dairy slurry (6.70%

Table 4.3. Fits of acid dissociation constant (K_a) dependence on temperature (T) from the work presented here and previous work. Numerical values shown after each equation represent the value at 25 °C.

	Dairy 2.7% TS	Dairy 6.7% TS	Ref
Aqueous	$K_a = 10^{\left(2.6-\frac{3562}{T}\right)}$; 4.50 x 10^{-10}	$K_a = 10^{\left(2.7-\frac{3579}{T}\right)}$; 4.97 x 10^{-10}	this study
Headspace	$K_a = 10^{\left(0.096-\frac{2691}{T}\right)}$; 1.18 x 10^{-9}	$K_a = 10^{\left(12-\frac{6342}{T}\right)}$; 5.36 x 10^{-10}	this study

	Beef Cattle Mature	Beef Cattle Calves	
Aqueous	$K_a = 10^{\left(4.3-\frac{4042}{T}\right)}$; 4.97 x 10^{-10}	$K_a = 10^{\left(8.5-\frac{5293}{T}\right)}$; 5.07 x 10^{-10}	this study
Headspace	$K_a = 10^{\left(0.06-\frac{2761}{T}\right)}$; 6.30 x 10^{-10}	$K_a = 10^{\left(-2.9-\frac{1977}{T}\right)}$; 3.28 x 10^{-10}	this study

	Literature Values	
Poultry Waste	$K_a = \frac{1}{6}x\ 10^{\left(-0.0897-\frac{2729}{T}\right)}$; 9.53 x 10^{-11}	(*21, 22*)
Modeled	$K_a = 10^{\left(0.05-\frac{2788}{T}\right)}$; 5.00 x 10^{-10}	(*17*)
Swine Waste	$K_a = \frac{1}{5}x\ 10^{\left(-0.0897-\frac{2729}{T}\right)}$; 1.14 x 10^{-10}	(*21, 23*)

TS) headspace K_a values were significantly higher (294%) at 25 °C and (53%) at 15 °C compared to measurements using emission rates over a swine lagoon solution (*106*). Overall, aqueous K_a values measured in dairy slurries support modeled values of K_a over values determined in animal waste.

Differences between K_a values in this work and previously modeled K_a values can be partially explained by differences in ionic strength. Increases in ionic strength will lower the activity coefficients and lower ammonia and ammonium activity. As previous work has demonstrated the overestimation of ammonia activity in waste solution (*107*). However, observed differences (up to 80%) in K_a between this study and previous studies in animal waste cannot be fully explained , in this author's opinion, by ionic strength alone. Processes such as sorption to waste could play a significant role in available ammonium (*17*). Thus, sorbed ammonium may not contribute to ammonium to ammonia equilibrium. Manure sorption studies should be explored as to the impact it plays on ammonium availability in solution. Headspace K_a measurements were higher in both beef and dairy slurries than aqueous measurements. Increases in CO_2 have been tied to increases in surface pH due to CO_2 degassing resulting in overestimations of derived K_a according to equation 4.6. Significant deviations in K_a values between headspace and aqueous measurements in dairy slurries were larger than beef slurries. Dairy waste generally has larger active populations of CO_2 producing microbes than beef waste (*104, 173, 174*). Thus, dairy slurries should be more sensitive to deviations in K_a measurements due to a higher CO_2 production potential in these systems.

Changes in pH can cause significant systematic error in the methodology applied here for K_a determination. This pH range of 8.0 – 9.5 covers the pK_a of ammonium and thus a small change in pH will result in a significant change in available ammonia (Figure 4.2). A small

change in surface pH of 0.31-0.42 and 0.10- 0.52 would account for the observed increases in measurements K_a for 2.7% and 6.7% TS dairy waste slurries, respectively. In support of the effect of pH, average changes in surface pH of 0.4 units and a maximum change of 0.6 were previously reported for thin layers of manure (*108*).

Other factors that could impact the derived K_H includes ammonia adsorption to PFE surfaces in the headspace, however, previous work showed that less than 4% and 0.4% of gasoeus ammonia was adsorbed by PFE tubing at concentrations of 1 and 10 ppmv, respectively (*102*). Moreover, ammonia adsorption to PFE was shown to be unidirectional and concentration independent (*102*). Ammonia partial pressures above waste slurries in this study were nearly 20 to 70 times higher than in the previously study (*102*). Additonally, our apparatus' surface area is 10 times higher . If the derived sorption coefficient is applied to our study, this would result in <0.1% of the ammonia gas being adsorbed to the walls in the headspace. This would not result in a systematic effect unless the ammonia partial pressure above the manure slurry is sufficiently low. Analogously, this systematic effect would be observed in an underestimation of K_H in the standardization experiments (NH_4OH). An underestimation of headspace K_H was observed at 0.001 M in the standardization experiment, however, the same effect was not observed in headspace K_H determination at 0.010 M. Thus, it is unlikely that ammonia adsorption to PFE contributed to the larger ammonia partial pressure observed in headspace determinations.

The use of porous membranes in this work was based on previous studies (*19, 107*) conducted at 25 °C to 35 °C. Ammonia diffusivity is strongly dependent on temperature with reduction in diffusivity of 35 and 24% at 10 and 15 °C lower compared to 25 °C (*23*) with all validaitons experiments being conducted in simple NH_4OH solutions at 25 °C. Accurate calculations of K_H and K_a were achieved within these validaiton studies at 25 °C. Therefore, the

flow rates used for the aqueous based measurements were sufficiently low to prevent a concentration gradient at the porous tubing interface; however, a small concentration gradient may have developed at temperatures below 25 °C due to redcutions in gas diffusivity in the solution, and at the porous tubing interface, or both. This would result in an understimation of the ammonia partial pressures and an overestimation of K_H at lower temperatures for the aqueous measured K_H.

Another possibilty for observed differences between K_H for aqueous and headspace measurements is inadequate time for the ammonia partial pressure to reach equilibrium within the slurry. This is analgous to the gas diffusivity discussed above. A large pulse of ammonia and CO_2 can be emitted from a thin surface layer at pH 9 when initially exposed to passing air (*108*). This would be similar to the initial opening of the valve between the aqueous phase and headspace phase. An initial pulse of ammonia gas into the headpsace may not have adequate time to reach equilibrium with the slurry surface thus creating an elevated ammonia partial pressure in the headspace. Moreover, the decrease in temperature would lengthen the time required to reach equilibrium due to reductions in diffusivity.

4.5. Conclusions

Henry constants (K_H) for ammonia (NH_3) calculated on the basis of aqueous phase measurements were comparable to previously reported values for other types of animal waste. However, headspace-based calculations of K_H at temperatures below 25 °C were much lower than literature values. Acid dissociation (K_a) constants determined from aqueous phase measurements of dairy and beef waste slurries support previously reported values for modeled K_a values and were higher than K_a values measured in animal waste. Headspace K_a calculations

were larger than aqueous calculation for both beef and dairy slurries; which was likely a consequence of microbially produced CO_2 resulting in changes of the surface pH. This work clearly demonstrates the impact of headspace versus and aqueous phase-based determinations of K_H and K_a constants. It remains to be determined if the reduction in gas diffusivity at lower temperatures created an artifact in the aqueous K_H and K_a determinations due to the formation of a concentration gradient. In addition, this work supports the use of porous membranes as a more robust method for measuring K_H and K_a in complex matrices. For future models, this work recommends using the modeled K_H and K_a values shown in Table 4.2 and 4.3 (*17*) but warn the reader about the role of CO_2 on surface pH. Addition of CO_2 dependence should be incorporated into ammonia emission models as a surface factor.

4.6. Future Work

The flow rates used in this work should be validated with ammonium solutions at 15 °C and 10 °C to verify if decreases in gas diffusion created concentration gradients at the porous membrane interface. This would be observed as a decreasing ammonia concentration with time as air passes through the porous tubing. Use of porous membranes provided an ideal approach compared to headspace measurement. However care should be taken to optimize the surface area of the liquid-gas interface to volume ratio. This would limit the effects of CO_2 degassing. Currently, it is believed that headspace measurements of K_H and K_a were prone to artifacts caused by rapid degassing of ammonia, and CO_2, or both without adequate time to re-establish equilibrium with the slurry. If the system described above was modified to increase the surface area to volume, equilibrium can be established more rapidly and methodological artifacts may not be as apparent. Real time measurements of CO_2 should be monitored to determine the

magnitude of CO_2 degassing. If the CO_2 partial pressure is large, biogas may be used to eliminate or minimize changes in pH. Changes in pH near the pK_a result in large changes in the ammonia fraction. Therefore, incorporation of a pH meter within the apparatus should allow for continuous monitoring of changes in pH near the surface to confirm the role of CO_2 on changes in surface pH and ultimately changes in K_H and K_a calculations.

CHAPTER FIVE

Urea Hydrolysis Kinetics Determined in Animal Waste

5.1 Introduction

As discussed in Chapter 4, ammonia emission from animal waste and fertilizer application constitute 80% of ammonia emission in the US (*34*). The importance of Henry and acid dissociation constants were discussed in chapter 4 as these constants pertain to ammonia availability in soils and ultimately ammonia emissions. The roles of ammonia and ammonium formation in these systems were not explored as a part of chapter 4, but will be discussed here. Urea nitrogen (urea-N) composes between 60 -90% of total urinary nitrogen (N) (*13*). Urea hydrolysis, mediated by urease enzymes, is the primary pathway of ammonia production in

$$(NH_2)_2CO_{(aq)} + H_2O_{(l)} \rightarrow NH_{3\,(aq)} + H_2NCOOH_{(aq)} \rightarrow 2NH_{3(aq)} + CO_{2\,(aq)} \qquad \text{(Eq. 5.1)}$$

confined animal feeding operations (CAFOs) systems (*104, 173, 174*). Urease enzymes are readily found in bacteria, fungi and higher plants (*180*). As described in Chapter 4, ammonia lost from feedlots strongly depends on the ammonium concentration gradient in the soil, temperature, the fraction of ammonia (K_a), and the ammonia partial pressure above the soil surface (K_h) (Equation 4.1) (*162*). Thus, the rate of urea hydrolysis is of great importance in understanding ammonia emission from CAFOs. Moreover, urea hydrolysis' dependency on temperature needs to be considered due to the large change in temperature throughout the year for most Colorado feedlots. If urea hydrolysis becomes the limiting rate during the winter months, urea can build up

on the pen surface. This reservoir of urea-N could then convert to ammonium during the warmer spring months resulting in large emissions of NH_3 from feedlots. Unfortunately, this is the same period of the year when upslope conditions transport N from the east into the Rocky Mountains. Previous work on urea hydrolysis has been conducted in soil matrices or soil-like matrices with few being applicable to feedlot systems at temperatures around or below 25 °C (*103, 104, 181*).

When studying kinetics in soils, extractions are a necessity and result in time delay between sampling and analysis. Thus, a quenching agent is commonly used to slow or "stop" the reaction. Other studies have used phenyl mercuric acetate (PMA), other heavy metals, and urea analogues as a quenching agent in urea hydrolysis studies (*103, 182*). In addition, development of engineered urease inhibitors have been developed in order to prevent interference from classical sterilization methods (*183*). Classical methods for sterilizing soils include irradiation, chloroform, sodium azide, etc (*184*). Urease enzymes can be present in soil and manure in an extracellular state (e.g., not a part of the bacterium, plant or fungi). Thus, inhibiting the bacteria or fungi alone will not necessarily limit urease activity. Heavy metals have shown promise in the past by non-competitive inhibition of urease enzyme; however, and a recently introduced urease inhibitor (Agrotain® containing 3-7% N-(n-butyl) thiophosphoric triamide) has shown promise as a competitive urease inhibitor (*182*). Previous studies have reported reduced urea hydrolysis rates following fertilizer application and reductions in ammonia volatilization (*94, 182, 185, 186*).

The goals of this study were to find a suitable quenching agent that did not interfere with the urea-N analysis and to measure the reaction rates and activation energy of urea hydrolysis in Colorado CAFO systems at 5, 10, 15, and 25 °C.

5.2 Materials and Methods

5.2.1. Animal Waste Sampling and Preparation

Animal waste samples were collected from a dry pen surface at a dairy and beef feedlot near Colorado State University. The samples were air dried, ground, and passed through a 2 mm sieve. The resultant sample mixture appeared to be composed of soil, manure, and feed material (plant residue). Subsamples from this parent material were used for all experiments. For all experiments, 4 g of animal waste was placed in HDPE serum bottles and incubated at 5, 10, 15, and 25 °C. The H_2O: waste ratio was 1:1 which equated to roughly 50% water capacity. The incubated shaker used was incapable of holding 5 °C, so 6 °C was used.

5.2.2 Urease Inhibitor Testing

Phenyl mercuric acetate and Agrotain were compared to assess their ability to quench or inhibit urea hydrolysis over a 48 hour period in animal waste. First, Agrotain and PMA were added to 2M KCl (soil extractant) solutions to test for inhibition of urease activity in the absence of animal waste. Previous methods used PMA within 2M KCl as an extracting solution (*103*). 4.5 quart of Agrotain is commonly added per ton of urea when used to inhibit urease activity after fertilizer application (http://www.agrotain.com/agrotaininfocenter/ratesheets/d560.aspx?type=). This translates to 1.005 nL Agrotain per mg of urea-N but to ensure complete inhibition for the duration of our experiments, it was determined that 10.6×10^3 nL per mg urea-N was necessary. A second experiment was performed where PMA/2M KCl or Agrotain/2M KCl solutions were added simultaneously with 1 mg of urea-N:gram of animal waste and urea concentration was analyzed at 2, 12, 24, and 48 hour intervals.

5.2.3 Pseudo First Order Initial Rate Experiments

Initial experiments were conducted with 1.0 mg urea-N:g waste in triplicate in order to determine the magnitude of the reaction rate. Sterile controls were made in duplicate by adding Agrotain/2M KCl with the urea addition. Urea was measured at t = 0, 0.5, 1, 2, 4, 6, 8 hours. Agrotain/2M KCl solution was added at each time point in a 10:1 solution: waste ratio, then shaken for 2 hours at 120 revolutions per minute and filtered using a Whatman 42 filter. Preliminary studies were conducted for 24 hours, but urea was normally consumed within 8 hours. Four experimental temperatures were investigated at 6, 10, 15, 25 °C. The activation energy was calculated according to the Arrhenius' equation (Equation 5.2). Where k is the reaction rate constant, A is the pre-exponential factor, E_a is the activation energy, R is the gas constant, and T is absolute temperature.

$$\ln(k) = \ln(A) + \left(\frac{-E_a}{R}\right)\frac{1}{T} \qquad \text{(Eq. 5.2)}$$

5.2.4 Michaelis-Menten Experiments

The experimental conditions for Michaelis-Menten based experiments were the same as above unless stated otherwise. Michaelis-Menten experiments, with dairy and beef animal waste, were conducted over a 30 minute time period. Substrate concentrations varied from 0.25, 0.50, 1.0, 2.0, 4.0 mg urea-N:g waste. Maximum rates (V_{max}) were calculated using Line-weaver Burk plots (Equation 5.3). Where S is the substrate concentration, k is the reaction rate constant, and K_M is the Michaelis constant (substrate concentration at which the reaction rate is half of V_{max}). Michaelis-Menten based experiments were only conducted at 25 °C, thus activation energy could not be calculated.

$$\frac{1}{k} = \left(\frac{K_M}{V_{max}}\right)\frac{1}{S} + \frac{1}{V_{max}} \quad \text{(Eq. 5.3)}$$

5.2.5 Urea Analysis

Colorimetric determination of urea was conducted following protocol from the QuantiChrom Urea Assay Kit (DIUR-500) (*187*). Measurements were performed on a plate reader (BioTek, EON, Winooski, VT) at 430, 505, 520 nm in triplicate on a 5 minute interval over 45 minutes.

5.3. Results

To test for interferences caused by Agrotain in the determination of urea, urea standards were dissolved into DI water and Agrotain/2M KCl. Calibration curves for colorimetric determination of urea in water DI water and Agrotain/2M KCl are shown in Figure 5.1. No significant differences were observed over the 45 minute analysis for all three wavelengths (430, 505, 520 nm) indicating that Agrotain did not interfere with the quantification of urea.

Since Agrotain did not interfere with colorimetric determination of urea, Agrotain's ability to quench urea hydrolysis needed to be confirmed. To ensure the reaction was stopped, quenching agents (i.e., PMA and Agrotain) were added to urea spiked waste samples 1 mg urea-N:g waste at 2, 12, 24, and 48 hour intervals. Phenyl mercuric acetate was found unable to quench the reaction at 2 hours (Figure 5.2), while Agrotain was able to inhibit urease activity over a 24 hour time period. Thus, Agrotain was selected for all experiments reported here. Urea hydrolysis reaction rates decreased with decreasing temperature and the kinetic data were best fitted using a pseudo first order decay model (Table 5.1). An example of pseudo-first order decay is shown in Figure 5.3. Half-lives ($t_{1/2}$) were very short in this study even at 6 °C (< 2 hours).

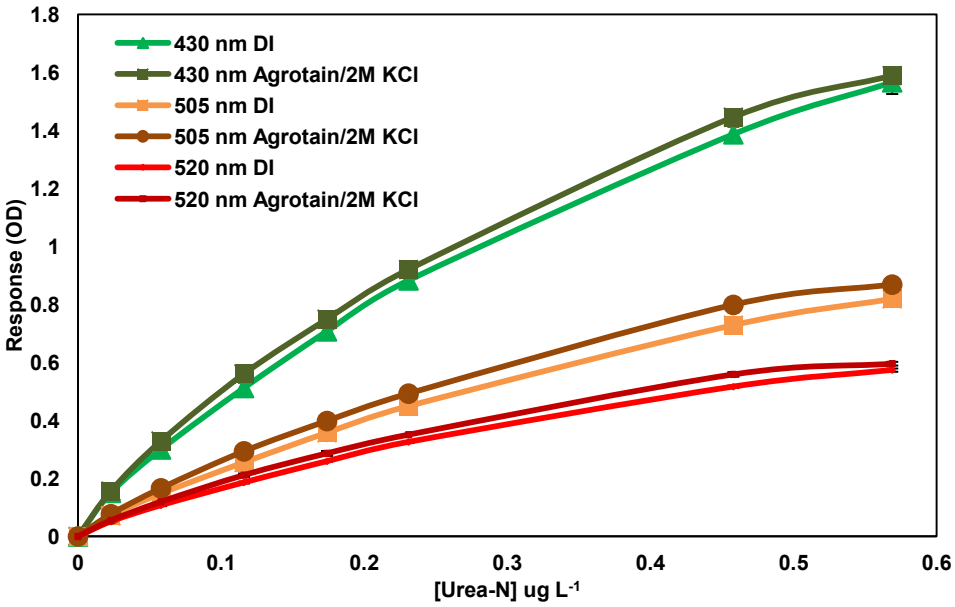

Figure 5.1. Urea-N colorimetric calibration comparison at 30 minutes of DI and extractant solution (2 M KCl/Agrotain). Error bars represent one standard deviation (n=3). Little variation was observed at 430, 505, and 520 nm used for calculation of urea-N.

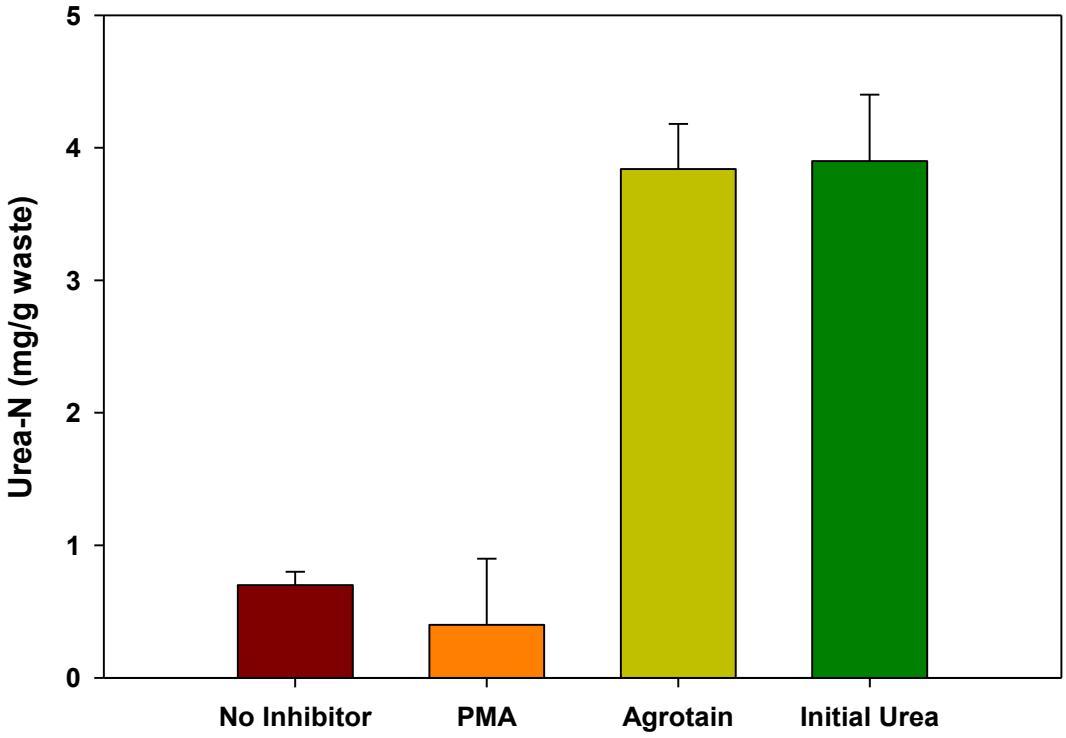

Figure 5.2. Comparison of the efficiency of quenching agents (PMA (orange) and Agrotain (yellow)) used to inhibit urea hydrolysis after 2 hours of reaction time. No inhibitor (red) was used as a control. Initial urea-N (green) content represents the urea concentration at time zero. Error bars represent one standard deviation (n=3).

Table 5.1. Summary of (initial rate) urea hydrolysis experiments. Average pseudo-first order reaction rates are shown in column 2 (n=3). Half-lives are shown on the right side of the table.

Temp (ºC)	Reaction Rate		*Half-life*	
	Mean	*Stdev*	$t_{1/2\ (hrs)}$	$t_{1/2\ (min)}$
25	1.5	0.1	*0.47*	*28*
15	0.65	0.04	*1.1*	*64*
10	0.42	0.06	*1.7*	*100*
6	0.35	0.08	*2.0*	*120*

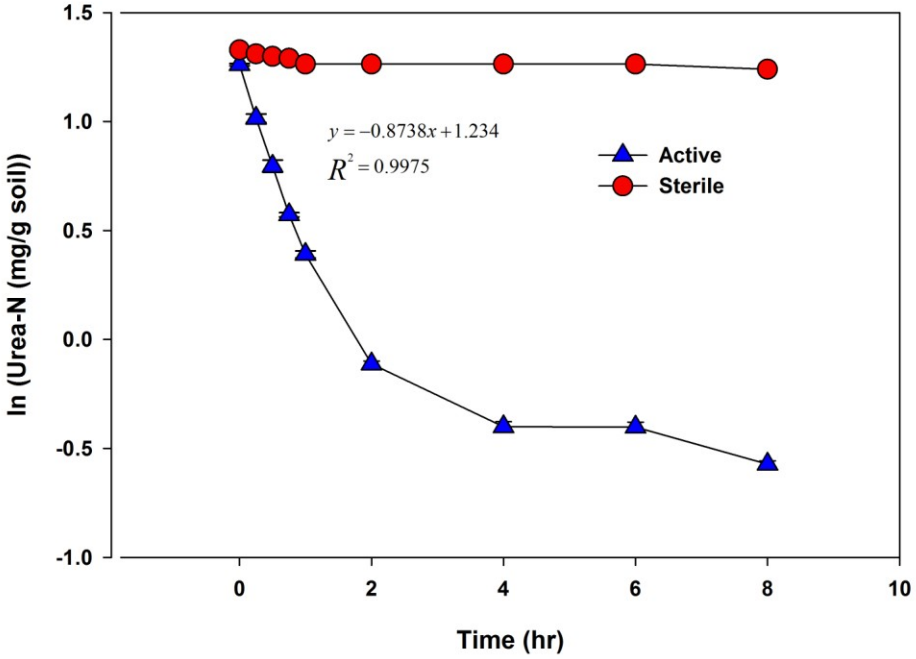

Figure 5.3. Pseudo first order decay of urea (blue) in animal waste from dairy cows at 25 °C. Linear correlation was performed on the first five data points. Controls (red) in which Agrotain was used to inhibit urease activity.

The activation energy for urea hydrolysis was determined to be 54 (σ = 4) kJ/mol using the pseudo first order approximation (Figure 5.4). Larger variations in k were measured at 6 °C and were believed to be created by frequent opening and closing of the incubator shaker. Michaelis-Menten experiments were conducted at 25 °C in both dairy and beef waste. Line-weaver Burk plots demonstrated that the maximum urea hydrolysis rates were not significantly different in beef waste (8.4 ± 2.7 mg urea-N/g waste hr^{-1}) and dairy waste (6.6 ± 9.8 mg urea-N/g waste hr^{-1}) (Figure 5.5).

5.4. Discussion

Agrotain was capable of inhibiting urease activity at 3.45 $x10^3$ nL/mg urea-N and did not interfere with colorimetric determination of urea. Phenyl mercuric acetate was not capable of inhibiting urease activity even within a 2 hours reaction time. Phenyl mercuric acetate likely inhibited the enzyme, however, heavy metals exhibit lower inhibition factors than other inhibitors such as Agrotain (*182*). Phosphoramide compounds (Agrotain) inhibiting plant derived urease better than heavy metals. The enzyme concentration was not determined, thus sufficient PMA may have not been added to inhibit the reaction. If the enzyme concentration is large, increase in addition of PMA would not be advised due to the toxicity of mercury. Likewise, other sterilization methods (e.g. sodium azide, etc) would result in the limited inhibition or no inhibition in the case of sodium azide. Agrotain was a robust urease inhibitor at 2 hours and continued up to a 24 hour interval.

The calculated activation energy (54 kJ/mol) for urea hydrolysis was within experimental error of previous fecal/urine mixtures studies in which an activation energy of 51.88 kJ/ mol was reported (*104*). This fecal/urine study used an Michaelis-Menten approach

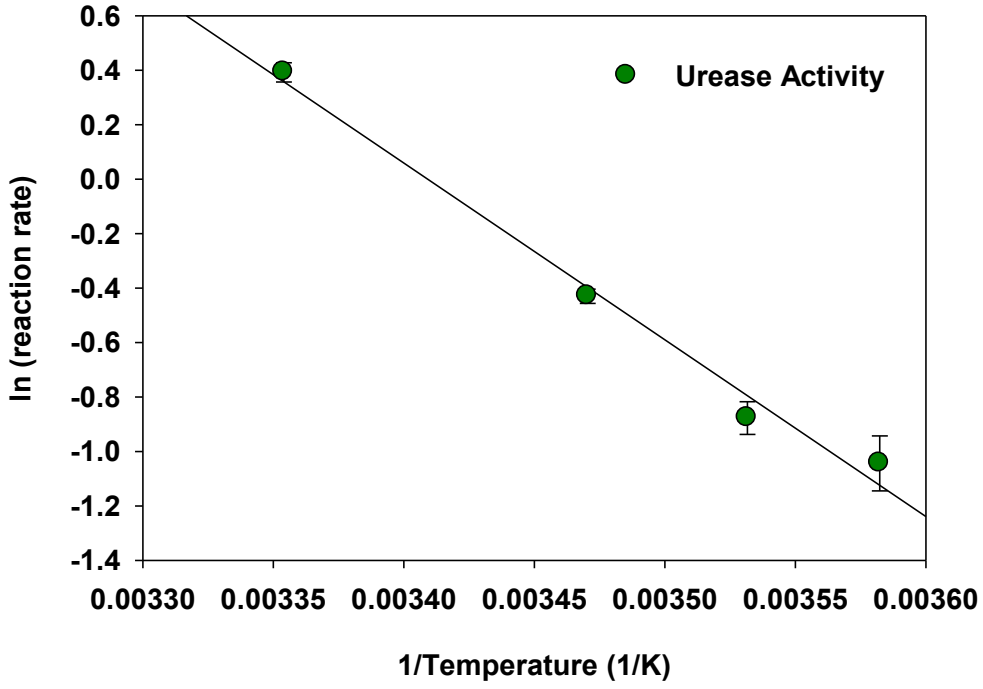

Figure 5.4. Arrhenius plot of urease activity measured in dairy waste. Activation energy of urea hydrolysis in dairy operation waste was determined at 6, 10, 15, 25 °C.

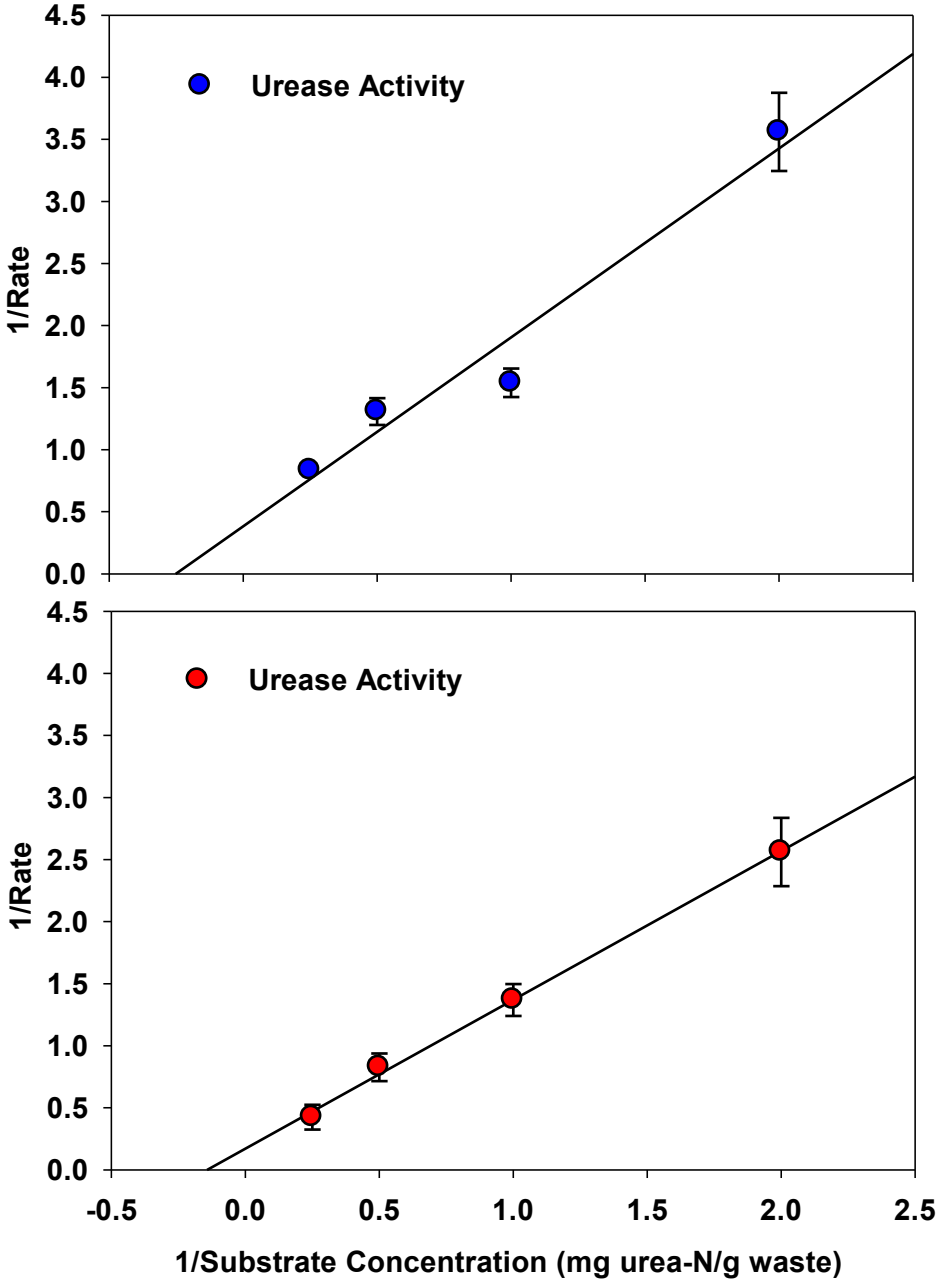

Figure 5.5. Line-weaver Burk approximation of maximum urea hydrolysis rates at 25 °C in dairy (top) and beef (bottom) dry pen waste. Error bars represent one standard deviation (n=3).

where an initial pseudo first order kinetic model was used in this study to calculate the activation energy E_a (*104*). Minimal difference between pseudo first order and Michaelis-Menten exist at low substrate concentrations compared to enzyme concentrations. The activation energy obtained in this study was nearly double of results reported for natural soils (24.4 kJ/mol at 20 °C) (*103*). Although higher amount of urease are most likely present in animal waste in comparison to natural soils; pH affects the rate of urea hydrolysis (*104*). Optimal pH ranges for urea hydrolysis are 6.8 to 7.5. The studies conducted in soils were in this range, however our pH ranges from 8.2 to 8.5 in dairy waste (Table 4.1). Reductions in urea hydrolysis up to 40% have been reported at pH 8.2-8.5 (*104*).

All calculated half-lives were shorter than 30 minutes at 25 °C and shorter than 2 hours at 6 °C. Other studies conducted in animal waste have suggested complete breakdown of urea within 2 to 24 hours between 10 and 25 °C (*17, 20, 103, 104, 108*). These studies refer to breakdown in dairy waste on a concrete surface while this work was studied on feedlot dry pen surfaces. If we assume five half-lives constitute complete breakdown (>96%), our study supports compete breakdown of urea within 8.4 and 2.4 hours at 10 and 25 °C, respectively. Although, Michaelis-Menten experiments were not conducted for all temperatures, the reaction rates obtained at 25 °C for dairy and beef feedlot waste were not significantly different ($p = 0.571$, $p = 0.693$) than previous calculations based on urine/fecal/water mixtures (8.9 ± 1.6 mg N/g dry feces hr^{-1}) (*104*). This result supports the application of urea hydrolysis reaction rates to other CAFO systems; however, this would need to be substantiated.

5.5. Conclusion

Agrotain was a suitable urease inhibitor that allowed for monitoring urea hydrolysis kinetics in feedlot waste. The activation energies for the observed urea hydrolysis in dairy and beef feedlot dry pen waste were in good agreement with values reported in previous fecal-like studies but about two times higher than activation energies derived from studies in natural soils. Moreover, maximum urea hydrolysis rates using the Michaelis-Menten approach were not significantly different from previous studies in animal waste. Interestingly, the observed urea hydrolysis half-lives were resulted in complete turnover ($5t_{1/2}$) in roughly 2 to 8 hours. Thus, turnover of urea may be much faster than originally thought at even low temperatures (6 °C). Thus production of ammonia in feedlots is not strongly inhibited by low temperatures (6-10 °C) as anticipated. Thus, it is highly unlikely that urea increase on feedlot surfaces during the winter. While temperatures below 5 °C in northern Colorado are commonplace, there are sufficient days of temperatures over 5 °C and allow for rapid conversion of urea to ammonium. Feedlot pens are exposed to radiation during the day and can exceed air temperatures by 10 to 15 °C (*188*). These data suggest that NH_3 losses from feedlots could be reduced by slowing or suppressing urea hydrolysis. Unfortunately, additions of urease inhibitors such as Agrotain have shown temporary results (*189*) and require weekly applications which is currently prohibitive by high costs.

5.6. Future Work

Future studies should conduct a complete comparison of the pseudo first order kinetic model approximation to ensure the observed values in a feedlot system compare to an empirical maximum rate calculated from the Michaelis-Menten methodology. Additionally, testing various

feedlot systems with different soil types (sandy, clay, silt) should be compared to confirm the application of this data to various feedlot soil types.

CHAPTER SIX

Summary

Atmospheric deposition of ammonia and ammonium contribute to negative ecosystem responses within sensitive sub-alpine ecosystems of Rocky Mountains, USA. The work presented here describes processes controlling ammonia emission (Chapter 4, 5), magnitude of ammonia emissions (Chapter 3, Appendix 1), impact of ammonium deposition on ammonia emission from native soils (Chapter 3), and the use of N isotopes as a tool for tracing ammonia pollution through atmospheric transport and deposition (Chapter 2). The isotope-based ammonia source tracking results showed that δ^{15}N-NH_3 isotopes were distinguishable ($p < 0.05$) among certain emission sites (e.g., beef cattle, dairy cattle, and waste water treatment). However, the average δ^{15}N value of ammonia gas (-29.9‰) and ammonium wet deposition measured at a receptor location within RMNP could not be used to directly categorize the primary ammonia sources. Use of weekly integrated samples of gaseous and particulate reduced nitrogen, oxidized nitrogen, and sulfur measurements and HYSPLIT modeling indicated post emission physical and chemical processes, such as source mixing, isotopic fractionation, and dry deposition, as the most likely reasons for why δ^{15}N values measured at the receptor site did not reflect the original sources. However, δ^{15}N values may be able to provide evidence of chemical processing and demonstrated the potential to be used as an indicator of secondary reactions such as extent of aerosol formation and ammonia scavenging. The use of δ^{15}N values as an indicator of environmental impact still needs to be supplemented with modeling or other chemical information.

This work applied a dynamic (flow through) laboratory chamber apparatus to measure native ammonia emissions under semi-realistic conditions (Chapter 3). This work provides new

information on the magnitude of ammonia emissions from native sub-alpine soils, indicating that natural emissions are not, as previously suggested, major sources of reduced nitrogen in the RMNP airshed. This work demonstrated that ammonia emissions from sub-alpine grassland and forest within RMNP were significantly different. Moreover, the average quantifiable ammonia emissions from sub-alpine grassland and forest soil cores were low in comparison to other lowland grasslands and forest ecosystems. The use of emission models to estimate the influence of temperature on ammonia emissions from sub-alpine soils supported soil emissions minimal contribution to observed wet deposition. Furthermore, using an $\delta^{15}N$ labeled ammonium solution, it was shown that wet deposition of ammonium did not enhance short term loss of ammonia from grassland and forest soil.

Wet deposition was monitored at the sampling location since it is the primary pathway for nitrogen deposition. The wet nitrogen deposition was found to be higher than the estimated critical load (1.5 kg N ha^{-1} yr^{-1}) of RMNP and is thus likely to have an adverse effect on the ecosystem. This study found that large nitrogen deposition events can occur throughout the spring and summer period. The largest weekly deposition accounted for one-third of the ecosystem's critical load. With the addition of HYSLIT modeling, wet deposition of potassium and organic nitrogen supported the importance of nitrogen sources such as biomass burning.

Livestock production is the largest contributor to ammonia emissions in the US, and the world. However, accurate measurements and estimates had proven difficult in the past due to poor census and ammonia characterization. This work described an approach to measure the Henry and acid dissociation constants in complex matrices with various solid contents (animal waste) and high ionic strengths. This work suggested the use of porous tubing as a more appropriate and robust approach to headspace ammonia measurements used for calculation of K_H

and K_a. The Henry constants reported here for animal waste systems were in agreement with previous published work in water and high salinity solutions. The K_a values determined here were not as robust as the K_H values, and should be further investigated with the approach suggested in Chapter 4. Our results support previous studies that have indicated that microbially produced CO_2 can change the surface pH by 0.5 units during degassing resulting in alteration of the speciation of ammonium and ammonia in animal waste-based systems and thus complicate the determinations of K_H and K_a.

Production of ammonia through urea hydrolysis in feedlot animal waste was briefly investigated using a commercially available urease inhibitor, Agrotain (Chapter 5). Both a pseudo first order kinetic model and Michaelis-Menten approaches were used in order to determine the activation energy and temperature dependency of urea hydrolysis. The activation energy determined for urea hydrolysis supported previous work conducted in fecal-urine mixtures. The urea hydrolysis rate was found to be insensitive to temperature variations typical for Colorado feedlots. Turnover of urea to ammonia was found to be fast (2-10 hours) and is not expected to be a limiting aspect of ammonia emission from feedlots in Colorado.

This work has provided useful information for the production, speciation, and emission of ammonia from natural and intensively managed soil and animal waste systems. This information can be used to better quantify ammonia cycling and verify current nitrogen models for both native and agricultural land. This information will help land managers, farmers and regulators by providing a set of tools and results that can be used to limit emissions of reduced nitrogen from major sources in order to prevent further eutrophication of sensitive ecosystems.

REFERENCES

1. M. Pidwirny, in *Fundamentals of Physical Geography*. (2006).

2. V. P. Aneja, W. H. Schlesinger, J. W. Erisman, Farming pollution. *Nature Geoscience* **1**, 409 (2008).

3. Malm W. *et al.*, "RoMANS: Rocky Mountain atmospheric nitrogen and sulfur study report" *0737-5352-84* (2009).

4. K. B. Benedict *et al.*, A seasonal nitrogen deposition budget for Rocky Mountain National Park. *Ecological Applications* **23**, 1156 (2013/07/01, 2013).

5. R. M. Holmes, J. W. McClelland, D. M. Sigman, B. Fry, B. J. Peterson, Measuring ^{15}N-NH_4^+ in marine, estuarine and fresh waters: An adaptation of the ammonia diffusion method for samples with low ammonium concentrations. *Marine Chemistry* **60**, 235 (Apr, 1998).

6. D. M. Sigman *et al.*, Natural abundance-level measurement of the nitrogen isotopic composition of oceanic nitrate: an adaptation of the ammonia diffusion method. *Marine Chemistry* **57**, 227 (1997).

7. H. D. Freyer, Seasonal trends of NH_4^+ and NO_3^- nitrogen isotope composition in rain collected at Julich, Germany. *Tellus* **30**, 83 (1978).

8. H. Moore, The isotopic composition of ammonia, nitrogen dioxide and nitrate in the atmosphere. *Atmospheric Environment (1967)* **11**, 1239 (1977).

9. H. Moore, Isotopic measurement of atmospheric nitrogen compounds. *Tellus* **26**, 169 (1974).

10. T. H. E. Heaton, Isotopic studies of nitrogen pollution in the hydrosphere and atmosphere: A review. *Chemical Geology: Isotope Geoscience section* **59**, 87 (1986).

11. T. H. E. Heaton, $^{15}N/^{14}N$ ratios of nitrate and ammonium in rain at Pretoria, South Africa. *Atmospheric Environment* **21**, 10 (1987).

12. L. Vitòria, N. Otero, A. Soler, À. Canals, Fertilizer characterization: Isotopic data (N, S, O, C, and Sr). *Environmental Science & Technology* **38**, 3254 (2004).

13. A. N. Hristov *et al.*, Review: Ammonia emissions from dairy farms and beef feedlots 1. *Canadian Journal of Animal Science* **91**, 1 (2011/03/01, 2011).

14. K. M. Russell, J. N. Galloway, S. A. Macko, J. L. Moody, J. R. Scudlark, Sources of nitrogen in wet deposition to the Chesapeake Bay region. *Atmospheric Environment* **32**, 2453 (1998).

15. H.-W. Xiao, H.-Y. Xiao, A.-m. Long, Y.-L. Wang, Who controls the monthly variations of NH_4^+ nitrogen isotope composition in precipitation? *Atmospheric Environment* **54**, 201 (2012).

16. S. G. Yeatman, L. J. Spokes, P. F. Dennis, T. D. Jickells, Comparisons of aerosol nitrogen isotopic composition at two polluted coastal sites. *Atmospheric Environment* **35**, 1307 (2001).

17. F. Montes, C. A. Rotz, H. Chaoui, Process modeling of ammonia volatilization from ammonium solution and manure surfaces: A review with recommended models. *Trans. ASABE* **52**, 1707 (Sep-Oct, 2009).

18. D. C. Harris, *Quantitative chemical analysis*. (Macmillan, 2010).

19. P. K. Dasgupta, S. Dong, Solubility of ammonia in liquid water and generation of trace levels of standard gaseous ammonia. *Atmospheric Environment (1967)* **20**, 565 (1986).

20. G. J. Monteny, D. D. Schulte, A. Elzing, E. J. J. Lamaker, *A conceptual mechanistic model for the ammonia emissions from free stall cubicle dairy cow houses*. (American Society of Agricultural Engineers, St. Joseph, MI, ETATS-UNIS, 1998), vol. 41.

21. J. Ni, Mechanistic models of ammonia release from liquid manure: a review. *Journal of Agricultural Engineering Research* **72**, 1 (1999).

22. A. G. Hashimoto, *Ammonia desorption from concentrated chicken manure slurries*. (Cornell Univ., 1972).

23. R. Zhang, University of Illinois at Urbana-Champaign (1992).

24. J. E. Girard, *Principles of environmental chemistry*. (Jones & Bartlett Publishers, 2012).

25. J. W. Erisman, A. Bleeker, J. Galloway, M. S. Sutton, Reduced nitrogen in ecology and the environment. *Environmental Pollution* **150**, 140 (2007).

26. J. N. Galloway *et al.*, Nitrogen cycles: Past, present, and future. *Biogeochemistry* **70**, 153 (2004).

27. J. N. Galloway *et al.*, Transformation of the nitrogen cycle: Recent trends, questions, and potential solutions. *Science* **320**, 889 (May, 2008).

28. M. Prud'homme, Global fertilizers and raw materials supply and demand outlook. *Demand Balances*, 2007 (2007).

29. V. Smil, Nitrogen and food production: proteins for human diets. *AMBIO: A Journal of the Human Environment* **31**, 126 (2002).

30. B. J. Finlayson-Pitts, J. N. Pitts, *Chemistry of the upper and lower atmosphere*. (Academic Press, New York, 1999).

31. M. A. Sutton, U. Dragosits, Y. S. Tang, D. Fowler, Ammonia emissions from non-agricultural sources in the UK. *Atmospheric Environment* **34**, 855 (2000).

32. D. A. Hegg, L. F. Radke, P. V. Hobbs, R. A. Rasmussen, P. J. Riggan, Emissions of some trace gases from biomass fires. *Journal of Geophysical Research: Atmospheres* **95**, 5669 (1990).

33. D. A. Hegg, L. F. Radke, P. V. Hobbs, P. J. Riggan, Ammonia emissions from biomass burning. *Geophysical research letters* **15**, 335 (1988).

34. S. Reis, R. Pinder, M. Zhang, G. Lijie, M. Sutton, Reactive nitrogen in atmospheric emission inventories. *Atmos. Chem. Phys.* **9**, 7657 (2009).

35. J. T. Houghton *et al.*, *Climate change 2001: the scientific basis*. (Cambridge University Press Cambridge, 2001), vol. 881.

36. J. G. Irwin, M. L. Williams, Acid-Rain - Chemistry and Transport. *Environmental Pollution* **50**, 29 (1988).

37. V. P. Aneja, G. Murray, and J. Southerland, Atmospheric nitrogen compounds: Emissions, transport, transformation, deposition, and assessment. *Environ. Man*, 4 (1998).

38. W. A. H. Asman, M. A. Sutton, J. K. Schjorring, Ammonia: Emission, Atmospheric Transport and Deposition. *New Phytologist* **139**, 27 (1998).

39. A. Stelson, J. Seinfeld, Relative humidity and temperature dependence of the ammonium nitrate dissociation constant. *Atmospheric Environment (1967)* **16**, 983 (1982).

40. T. B. Onasch *et al.*, Infrared spectroscopic study of the deliquescence and efflorescence of ammonium sulfate aerosol as a function of temperature. *Journal of Geophysical Research: Atmospheres (1984–2012)* **104**, 21317 (1999).

41. M. E. Fenn *et al.*, Nitrogen emissions, deposition, and monitoring in the western United States. *Bioscience* **53**, 391 (Apr, 2003).

42. P. M. Vitousek, S. Hättenschwiler, L. Olander, S. Allison, Nitrogen and nature. *Ambio: A Journal of the Human Environment* **31**, 97 (2002).

43. P. M. Vitousek *et al.*, Human alteration of the global nitrogen cycle: Sources and consequences. *Ecological Applications* **7**, 737 (Aug, 1997).

44. J. S. Baron *et al.*, Ecosystem responses to nitrogen deposition in the Colorado front range. *Ecosystems* **3**, 352 (2000).

45. J. S. Baron, C. T. Driscoll, J. L. Stoddard, E. E. Richer, Empirical critical loads of atmospheric nitrogen deposition for nutrient enrichment and acidification of sensitive US lakes. *Bioscience* **61**, 602 (2011).

46. J. S. Baron, Hindcasting nitrogen deposition to determine an ecological critical load. *Ecological Applications* **16**, 433 (Apr, 2006).

47. D. Qin *et al.*, Climate change 2007: the physical science basis. *Contribution of Working Group I to the Fourth Assessment Report of the Intergovernmental Panel on Climate Change. Cambridge University Press, Cambridge, UK, New York, NY, USA* **996**, (2007).

48. United States Census Bureau, "2010 census redistricting data" (Census Bureau, 2010).

49. United States Census Bureau, "Population change in the 100 fastest growing metropolitan statistical areas: April 1, 2000 to July 1, 2006" (Census Bureau, 2007).

50. United States Department of Agriculture, "2007 census of agriculture: Weld county, CO" (National Agricultural Statistics Service, 2007).

51. D. A. Burns, Atmospheric nitrogen deposition in the Rocky Mountains of Colorado and southern Wyoming—a review and new analysis of past study results. *Atmospheric Environment* **37**, 921 (2003).

52. D. A. Burns, The effects of atmospheric nitrogen deposition in the Rocky Mountains of Colorado and southern Wyoming, USA - a critical review. *Environmental Pollution* **127**, 257 (2004).

53. K. R. Nydick, B. M. Lafrancois, J. S. Baron, B. M. Johnson, Nitrogen regulation of algal biomass, productivity, and composition in shallow mountain lakes, Snowy Range, Wyoming, USA. *Canadian Journal of Fisheries and Aquatic Sciences* **61**, 1256 (2004).

54. J. E. Korb, T. A. Ranker, Changes in stand composition and structure between 1981 and 1996 in four Front Range plant communities in Colorado. *Plant Ecology* **157**, 1 (2001).

55. M. Silverstein, C. Taipale. (Colorado Department of Public Health & Environment, 2006), vol. 2007.

56. K. B. Beem *et al.*, Deposition of reactive nitrogen during the Rocky Mountain Airborne Nitrogen and Sulfur (RoMANS) study. *Environmental Pollution* **158**, 862 (Mar, 2010).

57. K. B. Benedict *et al.*, Observations of atmospheric reactive nitrogen species in Rocky Mountain National Park and across northern Colorado. *Atmospheric Environment* **64**, 66 (2013).

58. C. Press, CRC handbook of chemistry and physics. *New York, New York*, (2003).

59. C. E. Kendall, E. M.; Wankel, Scott D., *Tracing anthropogenic inputs of nitrogen to ecosystems*. (2008).

60. C. Kendall, J. J. MacDonnell, *Isotope tracers in catchment hydrology*. (Access Online via Elsevier, 1998).

61. G. Junk, H. J. Svec, The absolute abundance of the nitrogen isotopes in the atmosphere and compressed gas from various sources. *Geochimica et Cosmochimica Acta* **14**, 234 (1958).

62. D. J. Felix, E. M. Elliott, T. J. Gish, L. L. McConnell, S. L. Shaw, Characterizing the isotopic composition of atmospheric ammonia emission sources using passive samplers and a combined oxidation-bacterial denitrifier approach. *Rapid Commun. Mass Spectrom.* **27**, 2239 (2013).

63. X.-Y. Yu *et al.*, Loss of fine particle ammonium from denuded nylon filters. *Atmospheric Environment* **40**, 4797 (2006).

64. T. H. E. Heaton, B. Spiro, S. M. C. Robertson, Potential canopy influences on the isotopic composition of nitrogen and sulphur in atmospheric deposition. *Oecologia* **109**, 600 (1997).

65. D. D. A. McQuarrie, J. J. D. Simon, *Physical chemistry: a molecular approach*. (University Science Books, 1997).

66. M. Wolfsberg, W. A. Van Hook, P. Paneth, in *Isotope Effects*. (Springer, 2009), pp. 77-137.

67. J. Bigeleisen, M. G. Mayer, Calculation of equilibrium constants for isotopic exchange reactions. *The Journal of Chemical Physics* **15**, 261 (1947).

68. R. A. Skinner, P. Ineson, H. Jones, D. Sleep, R. Rank, Using $\delta^{15}N$ values to characterise the nitrogen nutrient pathways from intensive animal units. *Rapid Commun. Mass Spectrom.* **20**, 2858 (2006).

69. K. Dittert, T. Goerges, B. Sattelmacher, Nitrogen turnover in soil after application of animal manure and slurry as studied by the stable isotope ^{15}N: A review. *Zeitschrift für Pflanzenernährung und Bodenkunde* **161**, 453 (1998).

70. D. M. Kool, J. Dolfing, N. Wrage, J. W. Van Groenigen, Nitrifier denitrification as a distinct and significant source of nitrous oxide from soil. *Soil Biology and Biochemistry* **43**, 174 (2011).

71. D. M. Kool *et al.*, Nitrifier denitrification can be a source of N_2O from soil: a revised approach to the dual-isotope labelling method. *European Journal of Soil Science* **61**, 759 (2010).

72. A. Mosier *et al.*, Closing the global N_2O budget: Nitrous oxide emissions through the agricultural nitrogen cycle. *Nutrient Cycling in Agroecosystems* **52**, 225 (1998/10/01, 1998).

73. E. Davidson, S. Hart, C. Shanks, M. Firestone, Measuring gross nitrogen mineralization, and nitrification by ^{15}N isotopic pool dilution in intact soil cores. *Journal of Soil Science* **42**, 335 (1991).

74. D. H. Kohl, G. B. Shearer, B. Commoner, Fertilizer nitrogen: Contribution to nitrate in surface water in a corn belt watershed. *Science* **174**, 1331 (1971).

75. R. D. Hauck *et al.*, Use of variations in natural nitrogen isotope abundance for environmental studies: A questionable approach. *Science* **177**, 453 (1972).

76. R. D. Hauck, Letter to the editor: Kohl, Shearer, and Commoner method. *Journal of Environmental Quality* **2**, 158 (1973).

77. R. D. Hauck, Nitrogen tracers in nitrogen cycle studies—Past use and future needs. *Journal of Environmental Quality* **2**, 317 (1973).

78. J. Bremner, M. Tabatabai, Nitrogen-15 enrichment of soils and soil-derived nitrate. *Journal of Environmental Quality* **2**, 363 (1973).

79. J. R. Gormly, R. F. Spalding, Sources and concentrations of nitrate-nitrogen in ground water of the central Platte Region, Nebraska. *Ground Water* **17**, 291 (1979).

80. E. M. Elliott *et al.*, Nitrogen isotopes as indicators of NO_x source contributions to atmospheric nitrate deposition across the midwestern and northeastern United States. *Environmental Science & Technology* **41**, 7661 (2007).

81. L. Nanus, M. W. Williams, D. H. Campbell, E. M. Elliott, C. Kendall, Evaluating regional patterns in nitrate sources to watersheds in national parks of the Rocky Mountains using nitrate isotopes. *Environmental Science & Technology* **42**, 6487 (2008/09/01, 2008).

82. J. D. Felix, E. M. Elliott, S. Shaw, The nitrogen isotopic composition of coal-fired power plant NO_x: The influence of emission controls and implications for global emission inventories. *Environmental Science & Technology*, (2012).

83. S. S. Kaushal *et al.*, Tracking nonpoint source nitrogen pollution in human-impacted watersheds. *Environmental Science & Technology* **45**, 8225 (2011/10/01, 2011).

84. E. Derse *et al.*, Identifying sources of nitrogen to Hanalei Bay, Kauai, utilizing the nitrogen isotope signature of macroalgae. *Environmental Science & Technology* **41**, 5217 (2007/08/01, 2007).

85. M. M. Savard, Tree-ring stable isotopes and historical perspectives on pollution – An overview. *Environmental Pollution* **158**, 2007 (2010).

86. T. H. E. Heaton, P. Wynn, A. M. Tye, Low $^{15}N/^{14}N$ ratios for nitrate in snow in the High Arctic (79 degrees N). *Atmospheric Environment* **38**, 5611 (Oct, 2004).

87. T. D. Jickells *et al.*, Isotopic evidence for a marine ammonia source. *Geophys. Res. Lett.* **30**, 1374 (2003).

88. S. G. Yeatman, L. J. Spokes, P. F. Dennis, T. D. Jickells, Can the study of nitrogen isotopic composition in size-segregated aerosol nitrate and ammonium be used to investigate atmospheric processing mechanisms? *Atmospheric Environment* **35**, 1337 (2001).

89. S. G. Yeatman, L. J. Spokes, T. D. Jickells, Comparisons of coarse-mode aerosol nitrate and ammonium at two polluted coastal sites. *Atmospheric Environment* **35**, 1321 (2001).

90. G. Jia, F. Chen, Monthly variations in nitrogen isotopes of ammonium and nitrate in wet deposition at Guangzhou, south China. *Atmospheric Environment* **44**, 2309 (2010).

91. C. Occhipinti, V. P. Aneja, W. Showers, D. Niyogi, Back-trajectory analysis and source-receptor relationships: Particulate matter and nitrogen isotopic composition in rainwater. *Journal of the Air & Waste Management Association* **58**, 1215 (Sep, 2008).

92. H. Y. Xiao, C. Q. Liu, Sources of nitrogen and sulfur in wet deposition at Guiyang, southwest China. *Atmospheric Environment* **36**, 5121 (2002).

93. Shah Sanjay B., W. P. W., A. Jactone, *Measuring ammonia concentrations and emissions from agricultural land and liquid surfaces : A review*. (Air & Waste Management Association, Pittsburgh, PA, ETATS-UNIS, 2006), vol. 56, pp. 16.

94. D. Parker *et al.*, in *Symposium of the State of the Science on Animal Manure and Waste Management. January 5e7. San Antonio, TX, USA*. (2005).

95. D. Parker *et al.*, Standardization of flux chamber and wind tunnel flux measurements for quantifying volatile organic compound and ammonia emissions from area sources at animal feeding operations. *Atmospheric Environment*, (2012).

96. B. Woodbury, D. Miller, R. Eigenberg, J. Nienaber, Technical note: An inexpensive laboratory and field chamber for manure volatile gas flux analysis. *Transactions of the ASAE* **49**, 767 (2006).

97. F. K. Teye, M. Hautala, A comparative assessment of four methods for estimating ammonia emissions at microclimatic locations in a dairy building. *International journal of biometeorology* **54**, 63 (2010).

98. Y. Shi, D. Parker, N. Cole, B. Auvermann, J. Mehlhorn, Surface amendments to minimize ammonia emissions from beef cattle feedlots. *Transactions of the ASAE* **44**, 677 (2001).

99. S. G. Sommer, S. McGinn, X. Hao, F. Larney, Techniques for measuring gas emissions from a composting stockpile of cattle manure. *Atmospheric Environment* **38**, 4643 (2004).

100. E. Le Cadre, S. Génermont, C. Decuq, S. Recous, P. Cellier, A laboratory system to estimate ammonia volatilization. *Agronomy for Sustainable Development* **25**, 101 (2005).

101. D. Kissel *et al.*, Rainfall timing and ammonia loss from urea in a loblolly pine plantation. *Soil Sci. Soc. Am. J.* **68**, 1744 (2004).

102. S. B. Shah, Ammonia adsorption in five types of flexible tubing materials. *Applied Engineering in Agriculture* **22**, 6 (2006).

103. V. Kumar, R. J. Wagenet, Urease activity and kinetics of urea transformation in soils. *Soil Sci.* **137**, 263 (1984).

104. R. E. Muck, Urease activity in bovine feces. *J. Dairy Sci.* **65**, 2157 (1982).

105. J. M. Hales, D. R. Drewes, Solubility of ammonia in water at low concentrations. *Atmospheric Environment* **13**, 1133 (1979).

106. J. Arogo, P. Westerman, Z. Liang, Comparing ammonium ion dissociation constant in swine anaerobic lagoon liquid and deionized water. *Transactions of the ASAE* **46**, 1415 (2003).

107. S. D. Hafner, J. J. Bisogni, W. J. Jewell, Measurement of un-ionized ammonia in complex mixtures. *Environmental Science & Technology* **40**, 1597 (2006/03/01, 2006).

108. H. Chaoui, F. Montes, C. A. Rotz, T. L. Richard, Volatile ammonia fraction and flux from thin layers of buffered ammonium solution and dairy cattle manure. *Trans. ASABE* **52**, 1695 (Sep-Oct, 2009).

109. G. A. Anderson, R. J. Smith, D. S. Bundy, E. G. Hammond, Model to predict gaseous contaminants in swine confinement buildings. *Journal of Agricultural Engineering Research* **37**, 235 (1987).

110. J. N. Galloway, W. H. Schlesinger, I. Hiram Levy, A. Michaels, J. L. Schnoor, Nitrogen fixation: anthropogenic enhancement-environmental response. *Global Biogeochemical Cycles* **9**, 235 (1995).

111. R. E. Baumgardner Jr, T. F. Lavery, C. M. Rogers, S. S. Isil, Estimates of the atmospheric deposition of sulfur and nitrogen species: Clean Air Status and Trends Network, 1990-2000. *Environmental Science & Technology* **36**, 2614 (2002).

112. V. P. Aneja, J. P. Chauhan, J. T. Walker, Characterization of atmospheric ammonia emissions from swine waste storage and treatment lagoons. *Journal of Geophysical Research* **105**, 11535 (2000).

113. V. P. Aneja *et al.*, Atmospheric nitrogen compounds II: emissions, transport, transformation, deposition and assessment. *Atmospheric Environment* **35**, 1903 (2001).

114. G. A. Dawson, in *Environmental Impact of Natural Emissions,* V. P. Aneja, Ed. (Air Pollution Control Association, Pittsburgh, PA, 1984), pp. 66–73.

115. J. W. Erisman, A. W. M. Vermetten, W. A. H. Asman, A. Waijersijpelaan, J. Slanina, Vertical-distribution of gases and aerosols - the behavior of ammonia and related components in the lower atmosphere. *Atmospheric Environment* **22**, 1153 (1988).

116. R. Ellis *et al.*, Present and future nitrogen deposition to national parks in the United States: critical load exceedances. *Atmospheric Chemistry and Physics Discussions* **13**, 9151 (2013).

117. J. Baron, A. S. Denning, The influence of mountain meteorology on precipitation chemistry at low and high elevations of the Colorado front range, USA. *Atmospheric Environment. Part A. General Topics* **27**, 2337 (1993).

118. M. A. Rodriguez *et al.*, Modeling the fate of atmospheric reduced nitrogen during the Rocky Mountain Atmospheric Nitrogen and Sulfur Study (RoMANS): Performance evaluation and diagnosis using integrated processes rate analysis. *Atmospheric Environment* **45**, 223 (2011).

119. K. A. Gebhart *et al.*, Back-trajectory-based source apportionment of airborne sulfur and nitrogen concentrations at Rocky Mountain National Park, Colorado, USA. *Atmospheric Environment* **45**, 621 (2011).

120. X. Y. Yu *et al.*, Particulate nitrate measurement using nylon filters. *Journal of the Air & Waste Management Association* **55**, 1100 (Aug, 2005).

121. M. A. Puchalski *et al.*, Passive ammonia monitoring in the United States: Comparing three different sampling devices. *Journal of Environmental Monitoring* **13**, 3156 (2011).

122. D. E. Day *et al.*, Spatial and temporal variability of ammonia and other inorganic aerosol species. *Atmospheric Environment* **61**, 490 (2012).

123. L. Zhang, M. A. Altabet, T. Wu, O. Hadas, Sensitive measurement of NH_4^+ $^{15}N/^{14}N$ ($\delta^{15}NH_4^+$) at natural abundance levels in fresh and saltwaters. *Analytical Chemistry* **79**, 5297 (2007/07/01, 2007).

124. D. M. Sigman *et al.*, A bacterial method for the nitrogen isotopic analysis of nitrate in seawater and freshwater. *Analytical Chemistry* **73**, 4145 (2001/09/01, 2001).

125. R. R. Draxler, G. Hess, An overview of the HYSPLIT_4 modelling system for trajectories. *Australian Meteorological Magazine* **47**, (1998).

126. R. R. Draxler, G. Hess, Description of the HYSPLIT4 modeling system. (1997).

127. R. R. Draxler, B. Stunder, G. Rolph, A. Taylor, HYSPLIT4 user's guide. *NOAA Technical Memorandum ERL ARL* **230**, 35 (1999).

128. R. R. Draxler, G. D. Rolph, HYSPLIT (HYbrid Single-Particle Lagrangian Integrated Trajectory) model access via NOAA ARL READY website (http://ready.arl.noaa.gov/HYSPLIT.php). (2013).

129. G. D. Rolph, Real-time environmental applications and display system (READY) website (http://ready.arl.noaa.gov). (2013).

130. K. A. Baum, J. M. Ham, Adaptation of a speciation sampling cartridge for measuring ammonia flux from cattle feedlots using relaxed eddy accumulation. *Atmospheric Environment* **43**, 1753 (2009).

131. G. Hutchinson, A. Mosier, C. Andre, Ammonia and amine emissions from a large cattle feedlot. *Journal of Environmental Quality* **11**, 288 (1982).

132. S. McGinn, H. Janzen, T. Coates, Atmospheric ammonia, volatile fatty acids, and other odorants near beef feedlots. *Journal of Environmental Quality* **32**, 1173 (2003).

133. R. Todd, N. Cole, L. Harper, T. Flesch, B. Baek, in *Proc. Symposium State of the Science: Animal Manure and Waste Management*. (2005).

134. M. B. Rhoades *et al.*, in *Proceedings of 2008 ASABE Annual International Meeting*. (2008).

135. R. J. W. Kruit *et al.*, Modeling the surface–atmosphere exchange of ammonia. *Atmospheric Environment* **44**, 945 (2010).

136. C. Perrino, M. Catrambone, A. Di Menno Di Bucchianico, I. Allegrini, Gaseous ammonia in the urban area of Rome, Italy and its relationship with traffic emissions. *Atmospheric Environment* **36**, 5385 (2002).

137. J. Whitehead, I. Longley, M. Gallagher, Seasonal and diurnal variation in atmospheric ammonia in an urban environment measured using a quantum cascade laser absorption spectrometer. *Water, Air, and Soil Pollution* **183**, 317 (2007).

138. R. D. Saylor, E. S. Edgerton, B. E. Hartsell, K. Baumann, D. A. Hansen, Continuous gaseous and total ammonia measurements from the southeastern aerosol research and characterization (SEARCH) study. *Atmospheric Environment* **44**, 4994 (2010).

139. E. J. T. Levin *et al.*, Aerosol physical, chemical and optical properties during the Rocky Mountain Airborne Nitrogen and Sulfur study. *Atmospheric Environment* **43**, 1932 (2009).

140. D. L. Phillips, J. W. Gregg, Uncertainty in source partitioning using stable isotopes. *Oecologia* **127**, 171 (2001).

141. J. H. Kroll, J. H. Seinfeld, Chemistry of secondary organic aerosol: Formation and evolution of low-volatility organics in the atmosphere. *Atmospheric Environment* **42**, 3593 (2008).

142. J. Cape, S. Cornell, T. Jickells, E. Nemitz, Organic nitrogen in the atmosphere—Where does it come from? A review of sources and methods. *Atmos. Res.* **102**, 30 (2011).

143. M. E. Fenn *et al.*, Ecological effects of nitrogen deposition in the western United States. *Bioscience* **53**, 404 (Apr, 2003).

144. W. D. Bowman, J. Murgel, T. Blett, E. Porter, Nitrogen critical loads for alpine vegetation and soils in Rocky Mountain National Park. *Journal of Environmental Management* **103**, 165 (2012).

145. Colorado Department of Public Health and Environment, "Rocky Mountain National Park deposition reduction plan" (Public Health and Environment, 2007).

146. M. Sutton *et al.*, Plant-Atmosphere Exchange of Ammonia [and Discussion]. *Philosophical Transactions of the Royal Society of London. Series A: Physical and Engineering Sciences* **351**, 261 (1995).

147. C. Potter, S. Klooster, C. Krauter, Regional modeling of ammonia emissions from native soil sources in California. *Earth Interactions* **7**, 1 (2003).

148. R. J. Wichink Kruit *et al.*, Ammonia fluxes and derived canopy compensation points over non-fertilized agricultural grassland in The Netherlands using the new gradient ammonia—high accuracy—monitor (GRAHAM). *Atmospheric Environment* **41**, 1275 (2007).

149. J. Neirynck, A. S. Kowalski, A. Carrara, R. Ceulemans, Driving forces for ammonia fluxes over mixed forest subjected to high deposition loads. *Atmospheric Environment* **39**, 5013 (2005).

150. J. Neirynck, R. Ceulemans, Bidirectional ammonia exchange above a mixed coniferous forest. *Environmental Pollution* **154**, 424 (2008).

151. S. C. Pryor, R. J. Barthelmie, L. L. Sørensen, B. Jensen, Ammonia concentrations and fluxes over a forest in the midwestern USA. *Atmospheric Environment* **35**, 5645 (2001).

152. K. Hansen *et al.*, Ammonia emissions from beech forest after leaf fall–measurements and modelling. *Biogeosciences discussions* **9**, 15633 (2012).

153. W. Battye, V. P. Aneja, P. A. Roelle, Evaluation and improvement of ammonia emissions inventories. *Atmospheric Environment* **37**, 3873 (2003).

154. A. Bouwman *et al.*, A global high-resolution emission inventory for ammonia. *Global Biogeochemical Cycles* **11**, 561 (1997).

155. C. M. Kim, Influence of vegetation types on the intensity of ammonia and nitrogen dioxide liberation from soil. *Soil Biology and Biochemistry* **5**, 163 (1973).

156. G. Sarwar *et al.*, Measurements of ammonia emissions from oak and pine forests and development of a non-industrial ammonia emissions inventory in texas. *Atmospheric Environment* **39**, 7137 (2005).

157. R. K. Peet, Forest vegetation of the Colorado front range. *Vegetatio* **45**, 3 (1981).

158. K. Galles *et al.*, Influence of reduced nitrogen diets on ammonia emissions from cattle feedlot pens. *Atmosphere* **2**, 655 (2011).

159. K. J. McInnes, J. L. Heilman, M. J. Savage, Aerodynamic conductances along a bare ridge-furrow tilled soil surface. *Agricultural and Forest Meteorology* **68**, 119 (1994).

160. J. M. Tarara, J. M. Ham, Measuring sensible heat flux in plastic mulch culture with aerodynamic conductance sensors. *Agricultural and Forest Meteorology* **95**, 1 (1999).

161. J. Ham, J. Heilman, Aerodynamic and surface resistances affecting energy transport in a sparse crop. *Agricultural and Forest Meteorology* **53**, 267 (1991).

162. J. Wu, D. L. Nofziger, J. G. Warren, J. A. Hattey, Modeling ammonia volatilization from surface-applied swine effluent. *Soil Sci. Soc. Am. J.* **67**, 1 (2003/1, 2003).

163. M. Sutton *et al.*, Dynamics of ammonia exchange with cut grassland: synthesis of results and conclusions of the GRAMINAE Integrated Experiment. *Biogeosciences discussions* **6**, 1121 (2009).

164. K. Morris, A. Mast, D. Clow, G. Wetherbee, J. Baron, C. Taipale, T. Blett, D. Gay, E. Richer, "2010 monitoring and tracking wet deposition at Rocky Mountain National Park: August 2012" (National Park Service, Denver, Colorado, 2012).

165. J. Reid, R. Koppmann, T. Eck, D. Eleuterio, A review of biomass burning emissions part II: intensive physical properties of biomass burning particles. *Atmos. Chem. Phys.* **5**, 799 (2005).

166. S. Gao *et al.*, Water-soluble organic components in aerosols associated with savanna fires in southern Africa: Identification, evolution, and distribution. *Journal of Geophysical Research* **108**, 8491 (2003).

167. K. Pratt *et al.*, Flight-based chemical characterization of biomass burning aerosols within two prescribed burn smoke plumes. *Atmospheric Chemistry Physics* **11**, 12549 (2011).

168. M. D. Zauscher, Y. Wang, M. J. K. Moore, C. J. Gaston, K. A. Prather, Air quality impact and physicochemical aging of biomass burning aerosols during the 2007 San Diego wildfires. *Environmental Science & Technology* **47**, 7633 (2013/07/16, 2013).

169. National Park Service, "The Las Conchas fire and Bandelier" *Bulletin* (National Park Service, 2012).

170. D. Salas, J. Stevens, K. Schulz, Rocky Mountain National Park, Colorado USGS-NPS vegetation mapping program. *US Department of the Interior, Bureau of Reclamation's Remote Sensing and GIS Group, Denver, CO*, (2005).

171. J.O. Bash, J.T. Walker, J.E. Pleim, Evaluation of a regional air-quality model with bi-directional NH_3 exchange coupled to an agro-ecosystem model. *Biogeosciences discussions* **9**, 11375 (2012).

172. J. Arogo, P. Westerman, A. Heber, W. Robarge, J. Classen, Ammonia emissions from animal feeding operations. *National Center for Manure and Animal Waste Management White Papers*, (2002).

173. R. E. Muck, B. K. Richards, Losses of manurial nitrogen in free-stall barns. *Agricultural Wastes* **7**, 65 (1983).

174. R. Muck, T. Steenhuis, Nitrogen losses in free stall dairy barns. *LivestockWastes: A Renewable Source. American Society of Agricultural Engineers, St. Joseph*, 406 (1981).

175. S. D. Hafner, J. J. Bisogni, Modeling of ammonia speciation in anaerobic digesters. *Water research* **43**, 4105 (2009).

176. S. D. Hafner, F. Montes, C. Alan Rotz, The role of carbon dioxide in emission of ammonia from manure. *Atmospheric Environment* **66**, 63 (2013).

177. V. L. Snoeyink, D. Jenkins, *Water chemistry*. (John Wiley, 1980).

178. F. Morel, J. G. Hering, *Principles and applications of aquatic chemistry*. (Wiley New York etc, 1993).

179. N. A. Cole, A. M. Mason, R. W. Todd, M. Rhoades, D. B. Parker, Chemical composition of pen surface layers of beef cattle feedyards. *The Professional Animal Scientist* **25**, 541 (October 1, 2009, 2009).

180. Y. Qin, J. Cabral, M.S., Review properties and applications of urease. *Biocatalysis and Biotransformation* **20**, 1 (2002).

181. M. I. Zantua, J. M. Bremner, Comparison of methods of assaying urease activity in soils. *Soil Biology and Biochemistry* **7**, 291 (1975).

182. L. S. B. Upadhyay, Urease inhibitors: A review. *Indian Journal of Biotechnology* **11**, 381 (2012).

183. X. Dong, Y. Li, Z. Li, Y. Cui, H. Zhu, Synthesis, structures and urease inhibition studies of copper(II) and nickel(II) complexes with bidentate N,O-donor Schiff base ligands. *Journal of Inorganic Biochemistry* **108**, 22 (2012).

184. J. T. Trevors, Sterilization and inhibition of microbial activity in soil. *Journal of Microbiological Methods* **26**, 53 (1996).

185. C. D. L. Rawluk, C. A. Grant, G. J. Racz, Ammonia volatilization from soils fertilized with urea and varying rates of urease inhibitor NBPT. *Canadian Journal of Soil Science* **81**, 239 (2001/05/01, 2001).

186. C. J. Watson, N. A. Akhonzada, J. T. G. Hamilton, D. I. Matthews, Rate and mode of application of the urease inhibitor N-(n-butyl) thiophosphoric triamide on ammonia volatilization from surface-applied urea. *Soil Use and Management* **24**, 246 (2008).

187. R. J. X. Z. Zawada, P. K. P. Kwan, K. L. O. K. L. Olszewski, M. L. M. Llinas, S. G. H. S. G. Huang, Quantitative determination of urea concentrations in cell culture medium. *Biochemistry and Cell Biology* **87**, 541 (2009).

188. J. Ham, personal communication.

189. D. B. Parker *et al.*, Rate and frequency of urease inhibitor application for minimizing ammonia emissions from beef cattle feedyards. *Transactions of the ASAE* **48**, 787 (2005).

190. G. C. Vaillant, Kansas State University (2007).

APPENDIX 1

Laboratory Chamber Apparatus

Motivation

Ammonia emissions from confined animal feeding operations (CAFOs) are important since they are among the top ammonia sources. Thus, our first objective was to characterize important sources of ammonia within a CAFO system. CAFO ammonia studies included a determination of emission differences between intact soil cores and loose duff material (non-compacted feces), effect of soil additives (water and synthetic urine), and investigations into effects of best management practices (BMPs), such as water application or scrapping. Scraping consists of mounding all waste materials into the center of a pen as a mound. The scrapped areas are the areas furthest from the center of the pen. The addition of synthetic urine was studied to investigate how quickly urea-N is converted into ammonia and emitted from feedlots. This was achieved by adding a known amount of urea and measuring the increase in emitted ammonia after application. Water application and scraping were important to study, because they may be viable BMPs for limiting ammonia volatilization.

Methods

Laboratory Chamber Apparatus

In general, refer to Vaillant 2007 for description of the laboratory chamber system (*190*). The chambers were mounted in a wooden rack that allowed tight clamping of chamber tops. (Figure A 1.1). Modifications from chamber described in chapter 2 are as follows: no ammonia

Figure A1.1. Picture of laboratory chamber system. A. Ventilation system B. Steel Manifold C. 10 L/min flow meter D. Sample Chamber E. Reinforcement using a 2x4 F. Acid Traps.

scrubber (Purafil: Puracarb AM Media, Doraville, GA), smaller chambers (Space Saver Vacuum Desiccator, Scienceware, 17 cm diameter), addition of ventilation system, lack of PFE coated walls, and use of bevaline tubing for all connections.

Summary of Chamber Design Modificaitons

- In place of PVC, steel manifolds were introduced to limit leaks which became problematic with use with PVC.
- Initially, saline solution (KCl, NaCl, etc.) were used to control dew point, however, this was replaced by a refridgerator bath to allow for finer control of dew point. Furthermore saline solutions caused flow blockages by precipitating within the tubing.
- In place of binder clips to seal the top and bottom half of the chamber, all threads, wing nuts, and a 2.54 cm x 10.2 cm board (including a centered beveled circle) were used to ensure a tight seal.
- The chamber system has been expanded to house up to twelve samples to enhance complexity of studies, as well as, throughput
- A ventilation system was installed to help control odor

Chamber Testing

First, incoming air was tested for ammonia using a Piccaro real time gas analyzer. Chamber blanks and mass balance experiments were performed to ensure a clean and closed system. Chamber blanks were conducted by running zero air through the system. This experiment was performed by flushing the chambers for 24 hours prior to the start of the experiment and collecting ammonia for 12, 24 and 48 hour integration periods. The limit of

detection (LOD) and quantification (LOQ) were calculated using three and ten times the standard deviation of the blank, respectively. For the mass balance study, the bottom of a Petri dish filled with glass beads was placed in the center of the chamber and 30 mL of 30 mM ammonium chloride solution was added into the Petri dish, 5 mL of 10 M NaOH was added, and the chamber was closed.

Effects of flow rate and humidity were tested on cores collected from Greely, CO. Flows were adjusted to 2, 5, and 8 L min^{-1} for four chambers. Emissions were monitored daily for seven days. A second test was performed with additional treatments of with two relative humidities (19, 52%) with 2.5 and 5.0 L min^{-1} flow rates. All future experiments were set at a dew point of 8 °C, resulting in roughly 35% relative humidity (RH.)

Soil Experiments

Soils samples were collected from a beef feedlot near Greely, CO, USA. Cores were collected on the same day as the experiments were conducted. Intact soils cores were collected as described in chapter 3, with the exception that the stainless steel rings were 5.08 cm in depth. Duff material was collected by gathering loose aggregates near or along the surface of a pen. Experiments were conducted following the conditions described previously (*158*). The soil chamber studies were conducted over a 5 to 14 day period in which the ammonia soil emission was integrated over 24 hour intervals. This chamber system was also used in other studies (*158*) looking at soil ammonia emissions from livestock systems.

The effects of duff material, water application, and scrapping on ammonia emission were investigated. Duff materials were packed into steel rings alongside soil cores and monitored for 5 days. To assess the effects of water and synthetic urine (484 mg urea-N $core^{-1}$), cores were run undisturbed for seven days and then treated with synthetic urine (n=4), water (n=4), or no

addition (n=4). To test the effecting of pen scrapping, cores were collected from the scrapped and mounded areas. Scrapping consists of mounding animal waste in the center of the pen creating a mound where the cattle can stay dry. Cores were gathered from the interior (mounded areas) and the exterior of the pen (scrapped areas) and tested at the same environmental conditions within the chamber system.

Results

Chamber Data

Incoming laboratory air showed a minimal ammonia concentration utilizing only the water bath as a trap (Figure A1.2). It was deemed unnecessary to use another ammonia scrub for feedlot studies, but a secondary ammonia scrub should be used where emission concentrations of ammonia are near 20 ppbv. The results of the chamber testing showed a closed system with a satisfactory LOD and LOQ allowing for potential investigations into native ammonia fluxes as discussed in Chapter 3. Since emission from feedlots can be over 1000x higher than native soils, it was deemed acceptable for CAFO comparisons (Figure A1.3). No significant difference was observed between 24 and 48 hour integrations. The lack of variability between ammonia mass collected at 12, 24, and 48 hours indicates ammonia collected in blanks were due to the operating procedure and not to air entering the chamber apparatus. Furthermore, the calculated LOD and LOQ are 0.0005 μg NH_3-N m^{-2} s^{-1} and 0.0016 μg NH_3-N m^{-2} s^{-1}, respectively. The average concentration entering the chamber was 0.13 μg NH_3 m^{-3}, which should be sufficiently low to stimulate emission. The results from the mass balance experiment showed 96.3% (+/-2.6%, n=6) recovery of ammonia.

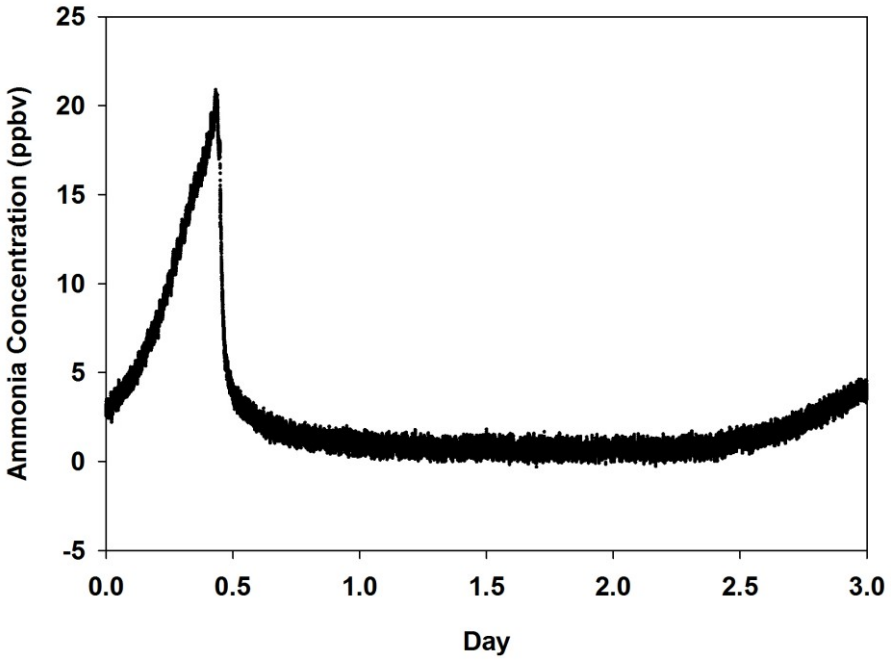

Figure A1.2 Ammonia concentration as a function of time utilizing a water bath as a trap for laboratory air. Water trap was changed at 0.37 days.

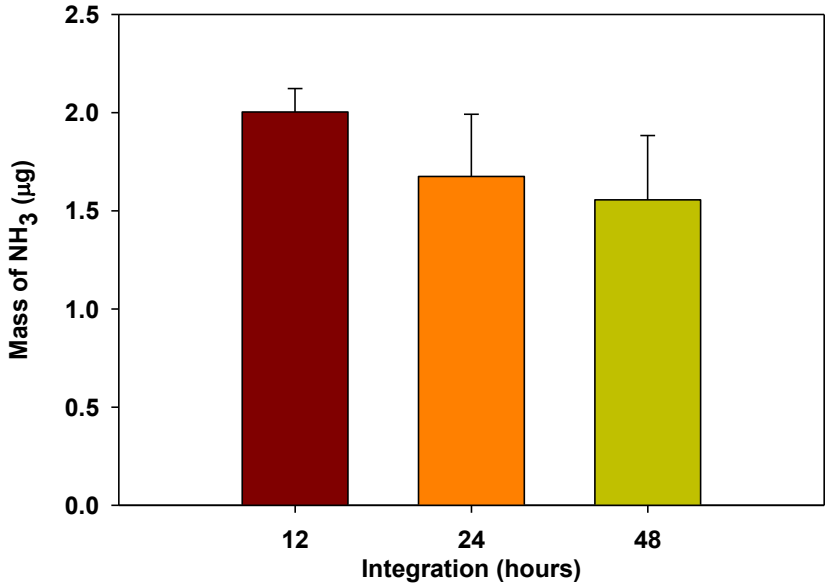

Figure A1.3. Mass of ammonia collected from zero air experiments at 12, 24, and 48 hours. Error bars represent one standard deviation (n=6).

The flow rate of atmospheric air over a soil surface should directly affect ammonia flux by increasing the mass transfer coefficient (Equation 3.1). The experiments here support this correlation (Figure A1.4) although the data are not significantly different. Usually, the first day has the highest emissions and most variability. Adjusting the RH along with flow rate was compounded by extensive cracking of the soil core surface (Figure A1.5). Ammonia emission did not exhibit pseudo first order results as previously observed. Attempts to normalize to other properties such as water loss could not account for the abnormal behavior, but visual inspection demonstrated extensive cracking of the soil surface. Surface cracking would change the surface area of the soil causing the behavior to deviate from pseudo first order. It should be noted that water loss did lower the deviation amongst each treatment and plays a role on ammonia emission. The surface crusting or cracking of the surface lowers ammonia emission, thus with higher relative humidities, surface crusting will be delayed allowing for a larger cumulative ammonia emissions.

CAFO Experiments

Certain soil chemical properties of soil cores and duff material are given in Table A1.1. Our findings show that intact CAFO soil cores have higher ammonia emissions (44.7%) than duff material (non-compacted feces) from CAFOs (Figure A1.6). Additionally, ammonia emissions from both soil cores and loose material followed pseudo-first order kinetics. We found that 42.1% of the added urea-N in the synthetic urine was converted to NH_4^+ and volatilized as NH_3 within seven days from CAFO soil cores (Figure A1.7). This confirms that urine plays a large role in ammonia emission from CAFOs, and future investigations are important to better understand how to control N emissions from CAFOs. Lastly, both application of water and

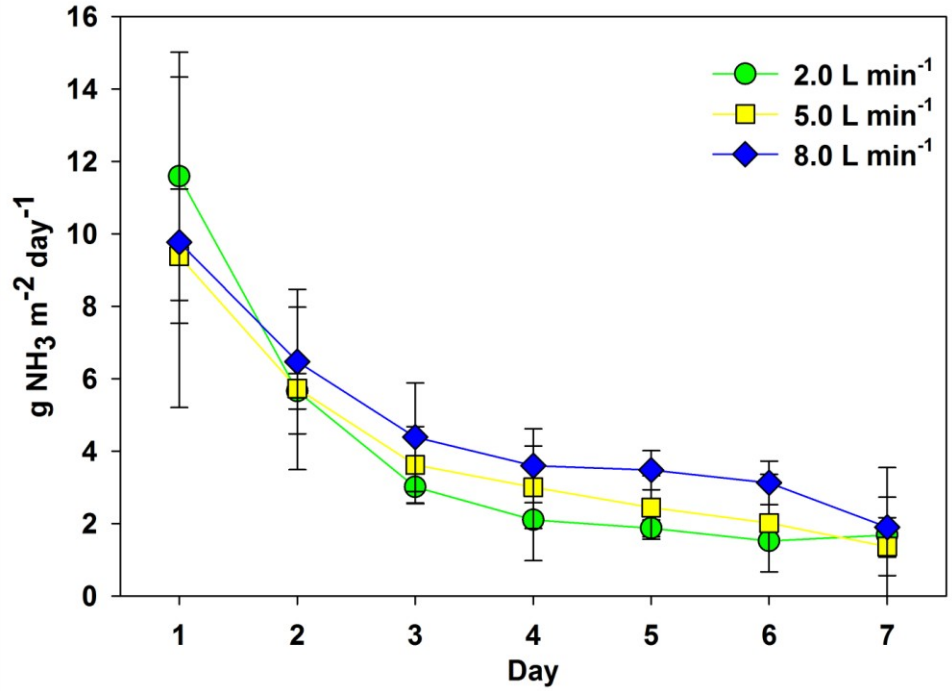

Figure A1.4. Effect of air flow on ammonia emissions from intact soil cores from a beef feedlot pen surface. 2.0 L min^{-1}, 5.0 L min^{-1}, 8.0 L min^{-1} treatments are shown in green, yellow, and blue, respectively. Error bars represent one standard deviation (n=4).

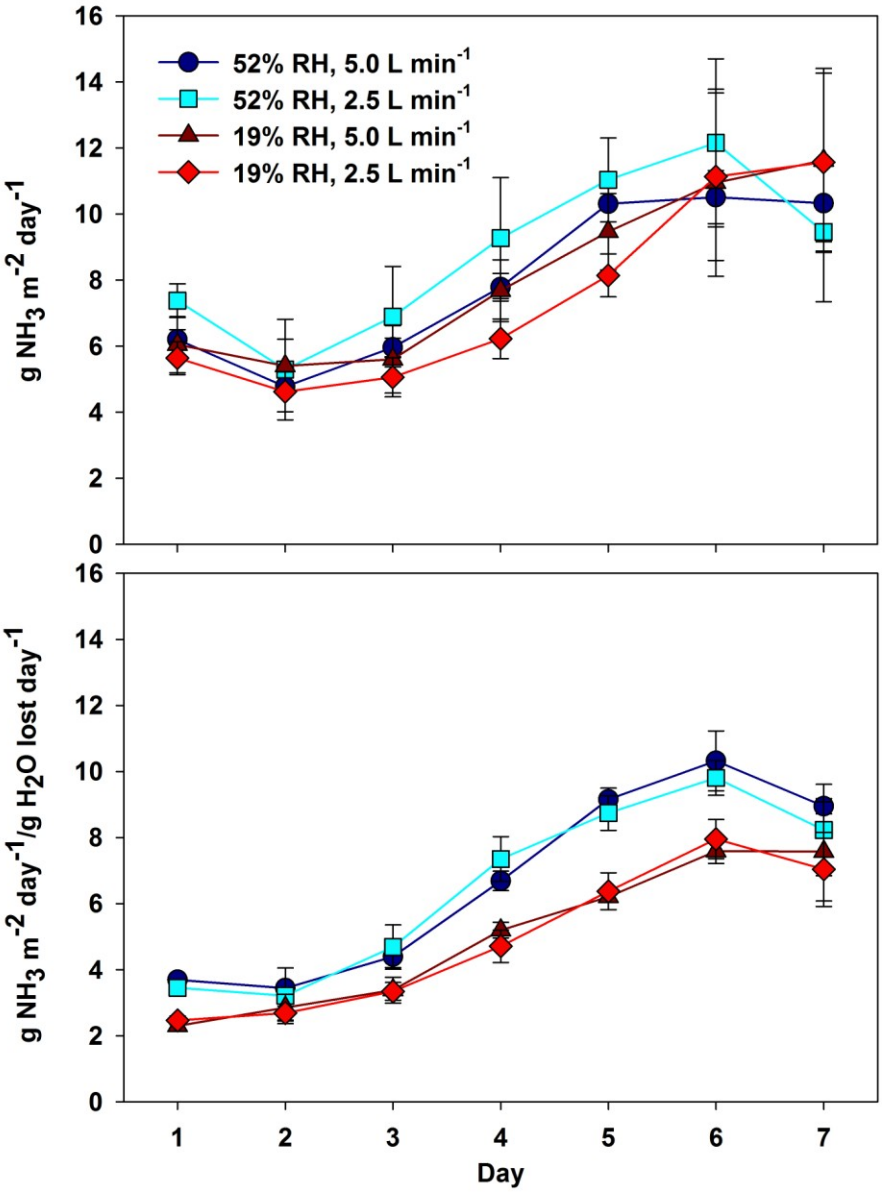

Figure A1.5. Effect of flow rate (2.5, 5.0 L min^{-1}) and relative humidity (19, 52%) on ammonia emission (top). Treatments normalized by water lost per day (bottom). Error bars represent one standard deviation (n=3).

scraping can lower (8.3%, 40.4%, respectively) ammonia volatilization; however, the n value (number of replicates) in these preliminary experiments is not adequate to assess effectiveness. These results show that both water application and scraping (Figure A1.8) can be viable management practices to help limit ammonia emissions.

Conclusions

The laboratory system described in this appendix was shown capable of measuring differences in ammonia emissions from different soil/animal waste types and from animal waste/soil that has undergone different treatments relevant for manure management within feedlots. Sufficient mass balance and limits of detection and quantification were achieved to study feed lots and even native soils. We found that duff material play a minor role compared to soil cores on ammonia emission from feedlots surfaces. Also, we found that water application and scrapping resulted in short term (<5 days) reductions of ammonia emission. Lastly, we found that nearly 50% of urea-N is rapidly converted and re-volatilized as ammonia from soil cores under aerodynamic conditions similar to the field conditions.

Table A1.1. Chemical properties of duff and soil cores

	TOC (%)	Total N (%)	Organic N (%)	NH4-N (mg/kg)	NO3-N (mg/kg)	Dry Matter (%)
Soil Core	58.2	2.68	2.59	857.2	6.2	88.4
Duff	78.7	2.89	2.77	1134	20.1	83.5

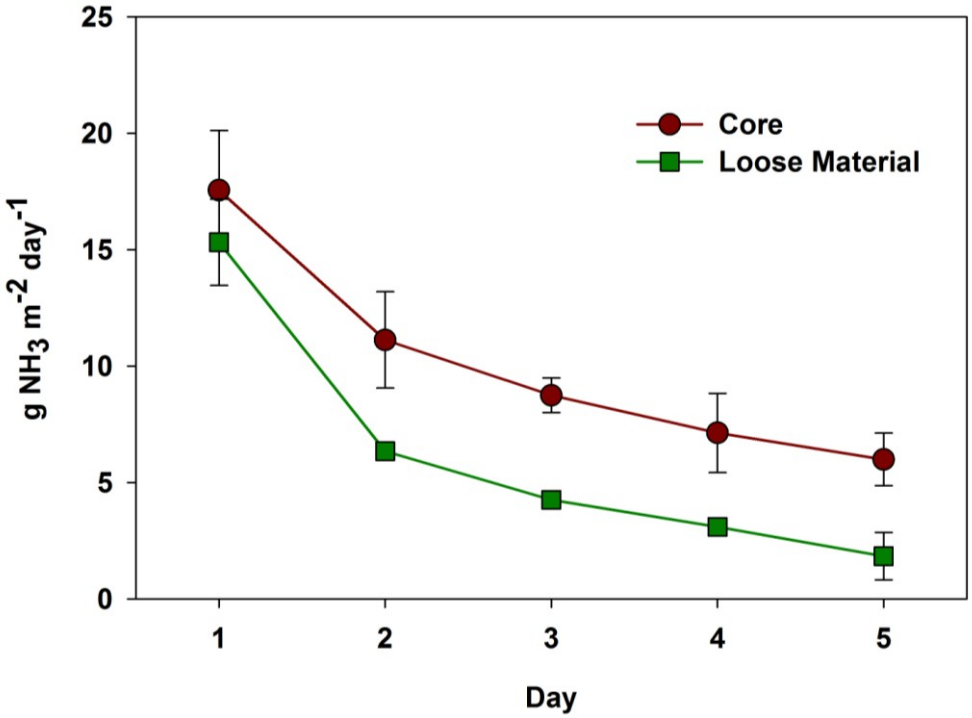

Figure A1.6: Graph of ammonia emission in grams of ammonia (NH_3) per meter squared. Core represents intact samples while loose material represents compiled materials. Error bars represent on standard deviation (n=6)

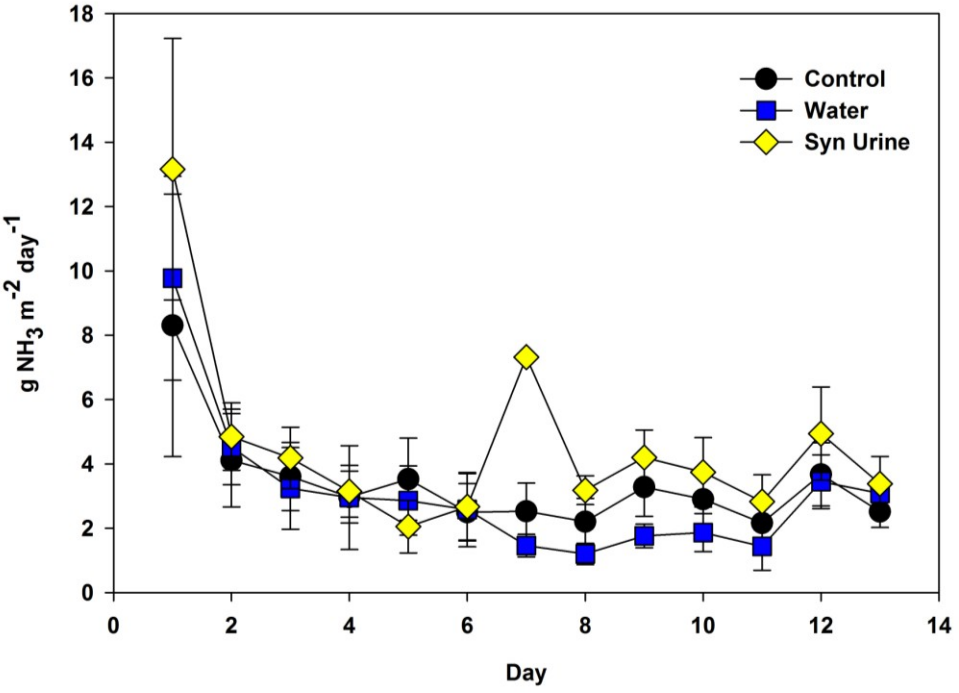

Figure A1.7. Graph of ammonia flux in grams of ammonia (NH_3) per meter squared. The first six days were undisturbed with no additives (n=12). On day seven synthetic urine (yellow) and water (blue) were added to four cores respectively, while the remaining four cores were given no additives (black) were considered controls. Error bars represent one standard deviation (n=4).

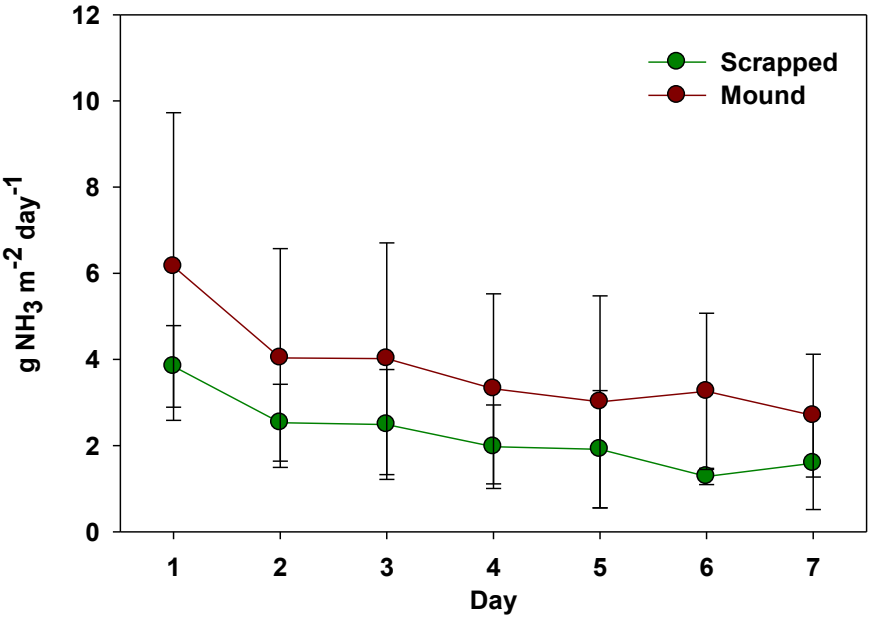

Figure A1.8: Graph of ammonia flux in grams of ammonia (NH_3) per meter squared. Error bars represent on standard deviation. Scraped areas (n=3) and mounded samples (n=9) are samples from the exterior (scrapped) and interior (mound) areas of the feedlot pen surface.

APPENDIX 2

Active Conditional Ammonia Sampling

Motivation

Due to the difficulty in sampling low ammonia emission areas and to prevent mixing of undesired emission sources (i.e. urban mixing with agricultural air); an active conditional sampler was designed and constructed. This ammonia sampler design will help prevent mixing between neighboring sources, such as waste water treatment and mobile sources, to allow identification of the isotopic signature from a single source.To enhance our ability to sample sites with lower ammonia emissions and prevent possible source mixing, or both, three active conditional samplers were constructed (Figure A2.1). These samplers were capable of turning on/off based on the environmental conditions (wind speed and direction).

Design

The sampler consists of five basic aspects: the ammonia sampler, basic met station, data logger, pump, and power. All mechanical (pump, etc) and electrical (power supply, data logger, etc.) are placed inside a plastic container (Figure A2.2) to prevent tampering from persons and animals, prevent water and snow from affecting electrical performance, and ease of use. The ammonia sampler used here is a Honeycomb denuder and casing. In short, air is pulled into the sampler by the pump and encounters an impaction plate to remove coarse particles (>10 μm). Air passes through the annular tubes of the phosphorous acid coated honeycomb denuder(s) and converts ammonia gas to ammonium phosphate. The back end of the denuder consists of up to 4 filters contained in a filter pack. Particles are collected on a phosphorous acid impregnated

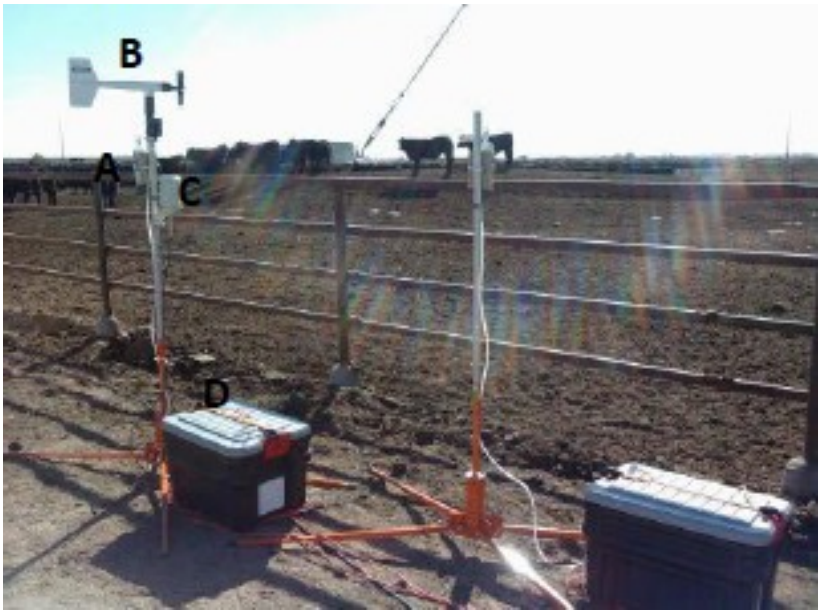

Figure A2.1. Conditional samplers deployed at a beef cattle feedlot. A is the denuder used for sampling, B is an anemometer used to monitor wind direction and speed, C is used to monitor temperature and humidity, and D is an enclosure for the pump and electronics.

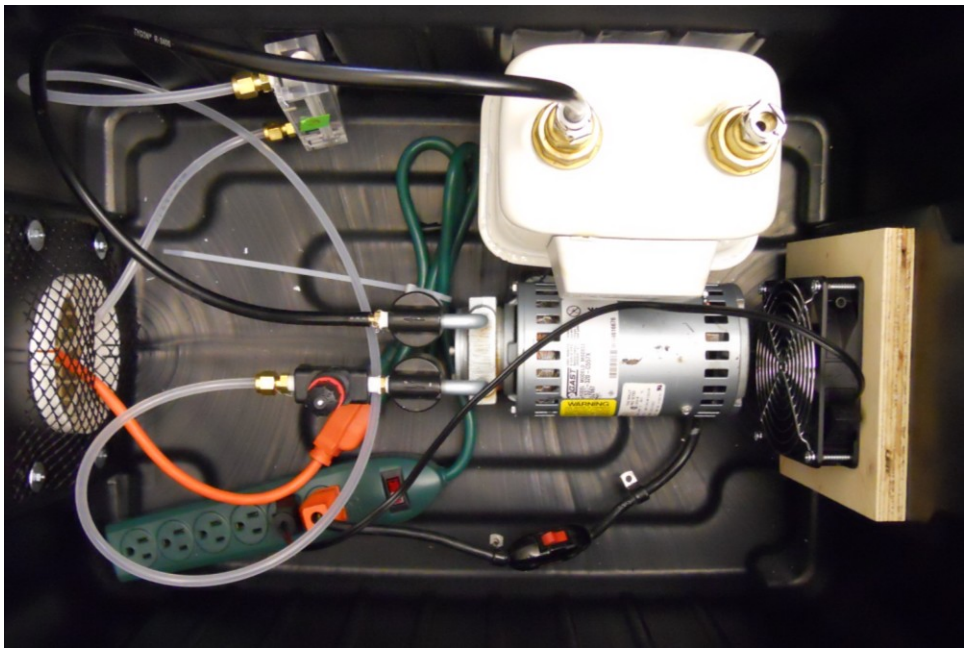

Figure A2.2. Schematic of active sampler chest consisting of air pump, dry air meter, flow meter, power strip, fan, and power relay (not shown).

Whatman 42 filter. Honeycomb samples were transported to and from the field within plastic cases. The samples were extracted in 18.2 MΩ water and analyzed on an ion chromatograph as described in chapter 2.

The meteorological station consists of an anemometer and a temperature and humidity sensor. The anemometer is used to monitor wind speed and direction. This met station is interfaced to a data logger (Campbell Scientific). The data logger is programmed to compile ten minute averages of wind direction and speed along with logging temperature and humidity information. Prior to deployment of sampler, meteorological requirements, such as wind speed and direction, were determined to ensure site specific sampling; this was performed by setting threshold wind speeds and upper and lower bounds on wind direction (0-360°) If the ten minute average for both wind direction and wind speed were met, the pump is set to "on" through a power switch attached to the data logger. Lastly, a sampling duration maximum was set to ensure the honeycomb samplers would not become saturated. Multiple samplers were setup with one meteorological station when possible.

Calibration of Flow

Flow rates were calibrated for all samplers in the laboratory using a dry air meter (Table A2.1). While field sampling, a dry air meter was placed in with the three samplers for quality assurance. Samples were run in the lab at 10 L min^{-1} according to the ball flow meters and adjusted accordingly to achieve 10 L min^{-1}. Pressure and temperature corrections were made following equation A2.1. Q is the flow rate at standard conditions (1 atm, 25 °C). P is pressure and T is absolute temperature at standard conditions and operating conditions (measured).

$$Q_{Corrected} = Q_{Standard} \sqrt{\frac{P_{Standard}\, T_{measured}}{P_{measured}\, T_{Standard}}} \qquad \text{Eq A2.1}$$

Proof of Concept

Active conditional samplers were deployed on the edge of a beef cattle feedlot in CO, USA. Two samplers were deployed and setup to sample air directly from feedlot, while the third was placed on the opposite side to assess air moving into the feedlot (Upwind). The meteorological requirements for both the samplers and background samplers are shown in Table A2.2. Samplers were deployed for up to two weeks or less if the maximum sampling was achieved.

Sampling was conducted from October 2010 to January 2011. Most of these periods experienced meteorological conditions allowing for downwind (feedlot) and upwind (background) sampling. The hourly averages of wind direction, speed, directional boundaries, and minimum wind speed for the source sampler during late October are shown in Figure A2.3. Meteorological conditions were similar for both background and feedlot samplers. Sampling occurred on October 30th, 2010 from 12:00 to 16:00 and completed the 2 hour maxim mum sampling duration within these 4 hours.

The system was verified to operate correctly based on meteorological conditions and did terminate sampling once the maximum duration was achieved. Next, average ammonia concentrations were compared to asses if the meteorological conditions used were adequate to separate a known source (downwind), the feed yard, from the background. Comparison of upwind and downwind (feedlot) ammonia concentrations from early December (Figure A2.4) demonstrated adequate meteorological requirements to distinguish upwind (41.77 ppbv) from feedlot sources (1660, 1710 ppbv).

Table A2.1 Percent error in flow meters compared to dry air meter used for active conditional samplers.

	Flow Meter 1	Flow Meter 2	Flow Meter 3
Percent Error at 10 L min^{-1}	3.28%	-1.19%	-4.71%

Table A2.2. Meteorological requirements for ammonia sampling at a beef feedlot in late 2010 to early 2011.

	Lower Directional Boundary	Upper Directional Boundary	Minimum Wind Speed	Maximum Sampling Duration
Feedlot	105°	255°	2.5 m s^{-1}	240 min
Background	285°	75°	2.5 m s^{-1}	240 min

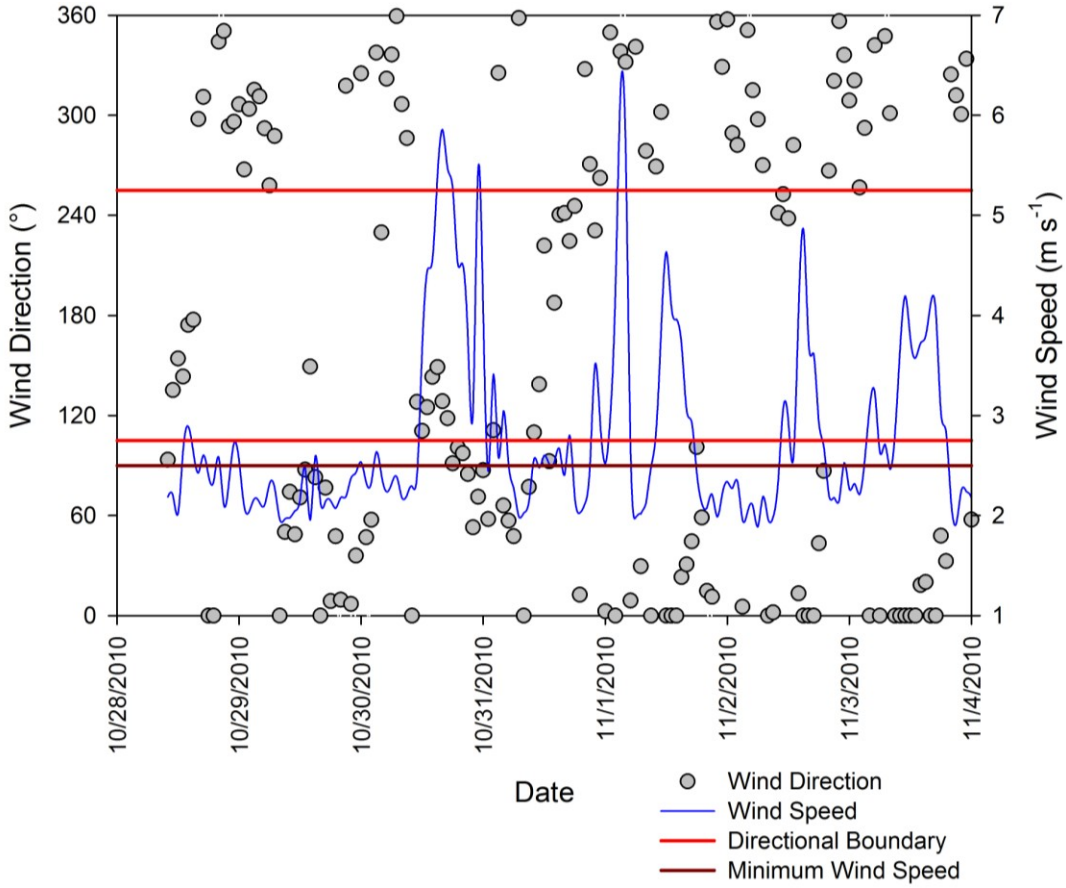

Figure A2.3. Hourly meteorological conditions measured at a beef feed yard from October 2010 to November 2011. Circles represent average wind direction; blue line represents average wind speed. Red lines represent the upper and lower boundaries of the meteorological requirements. The dark red line represents the minimum wind speed requirement.

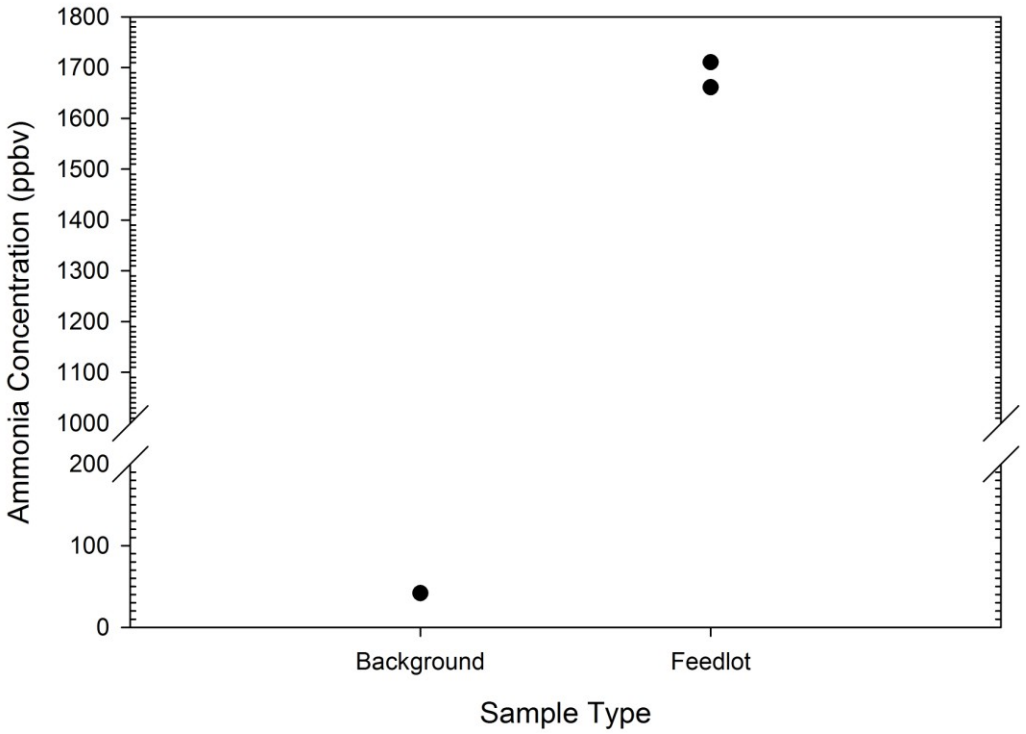

Figure A2.4. Comparison of integrated ammonia concentrations from active conditional samplers for background and feedlot samplers near a beef cattle feedlot in CO, USA.

Preliminary Sampling Results

Preliminary ammonia sampling continued throughout the winter period (Figure A2.5). Ammonia concentrations were shown to vary greatly (658.9 – 1710 ppbv) over the study period. However, environmental conditions such as inversion layer can affect the observed ammonia concentrations. Inversion layers can compress the available air above the feedlot. With continued ammonia emissions from the feedlot surface, the ammonia gas concentrations can greatly increase. Regardless, this sampler demonstrated the ability to sample a single source area based on meteorological conditions.

Conclusions

The conditional samplers described here were able to successfully sample air from a desired source (beef feedlot) versus background sources. The system was rather robust and capable of enduring conditions in the Colorado Front Range during the winter months. The use of this sampler was limited by labor, cost, and power for ammonia measurements. Future modifications and adaptations should address the concerns of labor, cost and power if widespread adoption for ammonia monitoring is desired. Passive samplers will limit labor, cost, and power requirements, but the passive sampler needs to be interfaced to a meteorological sensor.

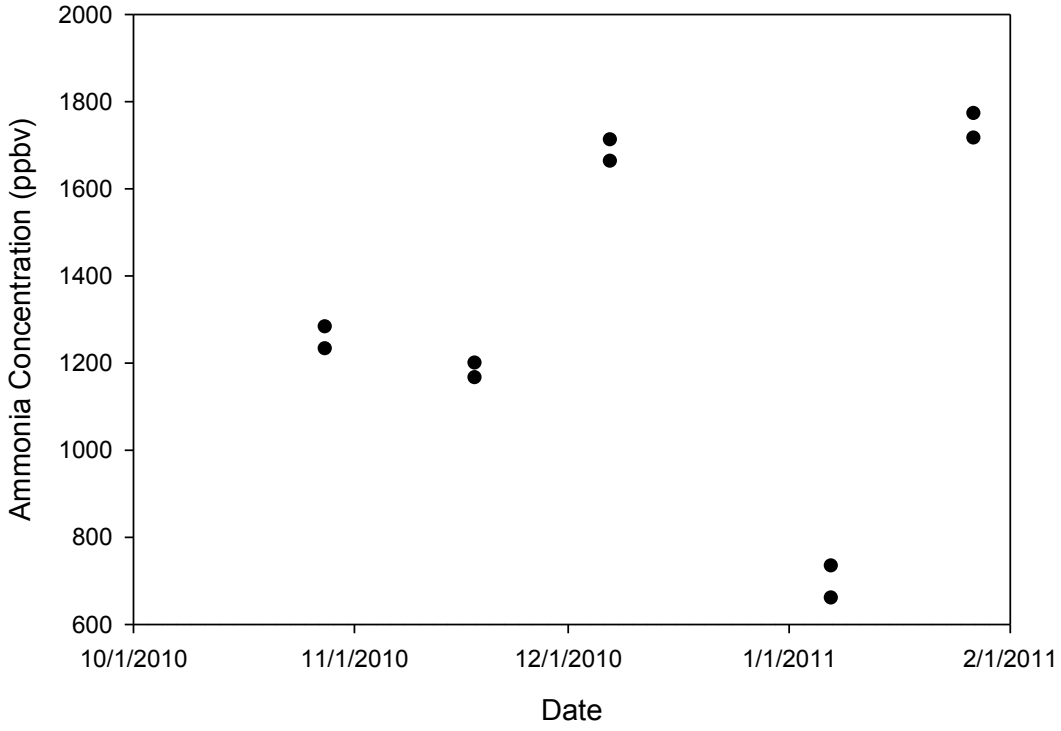

Figure A2.5 Integrated ammonia concentrations over the winter at a beef cattle feedlot near Greeley, CO.